UNIVERSITY OF OKLAHOMA

GRADUATE COLLEGE

MODELING RELAXATION EFFECTS ON MULTIPHASE FLUID TRANSPORT IN WELLS AND PIPELINES

A DISSERTATION

SUBMITTED TO THE GRADUATE FACULTY

in partial fulfillment of the requirements for the

Degree of

DOCTOR OF PHILOSOPHY

By

GUILLERMO GERMAN MICHEL VILLAZÓN
Norman, Oklahoma
2012

MODELING RELAXATION EFFECTS ON MULTIPHASE FLUID TRANSPORT IN WELLS AND PIPELINES

A DISSERTATION APPROVED FOR THE
MEWBOURNE SCHOOL OF PETROLEUM AND GEOLOGICAL ENGINEERING

BY

Dr. Faruk Civan, Chair

Dr. Deepak Devegowda

Dr. Jeffrey Callard

Dr. Yucel Akkutlu

Dr. Dimitrios Papavassiliou

“Science without religion is lame, religion without science is blind”

Albert Einstein (1879 - 1955)

"Science, Philosophy and Religion: a Symposium", 1941

To my lovely wife, Alejandra, for her infinite love and unlimited kindness and care.

To my parents, Ricardo and Stina, for their unconditional support and faith.

ACKNOWLEDGMENTS

I wish to acknowledge and thank many people for their cooperation during the course of my studies at the University of Oklahoma.

In particular, I would like to express my most sincere gratitude to Dr. Faruk Civan, chairman of my committee, for his advice and assistance in completing the present work, for his patience and guidance, and for the trust he put in my work.

I acknowledge the time and dedication given by the members of my committee Dr. Deepak Devegowda, Dr. Jeffrey Callard, Dr. Yucel Akkutlu and Dr. Dimitrios Papavassiliou.

I would like to thank to the ConocoPhillips Company for providing a fellowship during my graduate studies.

I am grateful to our Creator, for all the blessings received in the path that he has chosen for me.

TABLE OF CONTENTS

LIST OF TABLES

LIST OF FIGURES

ABSTRACT

The effect of relaxation in processes involving phase transition during flow of reservoir fluids in pipelines and wells is investigated and formulated. Applications concerning the steady-state flow of producing wells, waxy-oil rheology during transient cooling, and wax gelation of shut-in submarine pipes are studied by the means of numerical simulation.

This is accomplished by description of the transport of reservoir fluids flowing through pipes in terms of spatially-averaged phase properties. Several homogeneous models are developed by introducing the spatially-averaged properties into the equations describing the concurrent transport of phases, referred to as multi-fluid model. Thus, the number of unknown variables is decreased from several sets of properties corresponding to each phase in the multi-fluid model to one set of properties corresponding to a single pseudo-phase in the homogenous model.

First, flow of reservoir fluids in oil production wells is described by a three-phase model. Relaxation phenomenon concerning dissolved-gas separation from the oil and water phases is elaborated. Two numerical procedures are presented for simulating the gas/oil/brine flow in production pipes with heat transfer at steady state: one based on liquid holdup estimation and the other based on relaxation of gas separation. Deviation of actual fluid conditions from equilibrium is characterized by a new constitutive equation. Effect of relaxation time and holdup of liquids involving in typical field

scenarios is demonstrated for reservoir fluids containing oil, water, and gas phases. It is observed that the liquid holdup phenomenon at steady-state conditions can be described as a metastable state characterized by an incomplete separation of the gas phase. Also, the gas separation from the oil and water phases constitutes two different non-equilibrium processes and, therefore, these phases should not be lumped into one liquid phase.

Second, a description of the more relevant characteristics of crystalline growth for waxy-oils is presented. Relative crystallinity subject to different final temperatures is modeled and correlated for two types of waxy-oils. Laboratory measurements of the rheology for two samples of waxy oil taken at different temperatures are analyzed successfully. Constitutive equations are provided for modeling the viscoelastic behavior, gelation kinetics, and rheology of waxy-oils. The effect of cooling rate on relaxation of waxy-oil gel strength and apparent viscosity is described by three theoretical approaches which relate the relaxed viscoelastic behavior of waxy-oils to their plastic nature based on relaxation in wax crystallization. It is demonstrated by the means of numerical methods that the effect of relaxation phenomenon on wax rheology is significant for cooling rates in the order of units of degrees Rankine per minute.

Third, a modeling of wax solidification in submarine oil pipelines undergoing a cooling process after shut-in is presented. Transport models for transient cooling in a circular pipe cross-section and along vertical pipelines are developed. The wax/oil mixtures are modeled as a multiphase system. A correlation applicable to the fraction of wax precipitated is validated using experimental data. Accurate correlation of pressure

dependence of the Wax Appearance Temperature is developed. Relevant mechanisms of wax gelation without forced convection are described in detail. Two finite difference methods are presented for simulating the wax gelation: one applicable over a cross-section without involving force convection and the other applicable to a shut-in submarine pipe. The effects of pressurization and relaxation of wax precipitation on wax gelation are investigated. The simulation results show that the experimental temperature profile of solidifying wax/oil mixture can be explained better by adopting an effective liquid thermal conductivity higher than the actual thermal conductivity. Also, the pressurization effect on solidification of wax is shown to be very significant whereas the effect of relaxation in wax crystallization is negligible.

The information presented in this work may help accomplish effective mitigation of the flow assurance problems in pipelines and wells involving multiphase flow and gelation problems.

CHAPTER 1

INTRODUCTION

1.1. OVERVIEW

The scope of the present study is established in this chapter. This dissertation is focused on describing the kinetics of phase transition in pipelines and wells concerning the gas separation during steady-state flow, thermal effect on wax rheology and transient gelation without force convection of reservoir fluids, which are amongst the important issues concerning flow assurance. The fluids are described as homogeneous multiphase systems. A homogenous system is characterized by having its properties defined as the spatial averaging of the properties of each phase in the system. Descriptions about upward flow with geothermal heat transfer in wells, effect of gelation kinetics on wax

rheology, and transient gelation in shut-in submarine pipes are presented. Then, the main objective of the present study is defined. Specific objectives are set in order to accomplish the solution of the main objective. The organization of this study towards the fulfillment of the objectives is delineated at the end.

1.2. DESCRIPTION OF THE PROBLEM

Description of the transport of multiphase-fluids involving phase transition requires a set of conservation laws applied to each phase complemented with adequate constitutive relationships. However, the multi-fluid model describing the flow of a multiphase system usually involves a number of unknown variables exceeding the number of equations to be solved in flow simulations. Consequently, several auxiliary relationships are required for obtaining a well posed problem. In order to reduce the number of unknown variables, the multi-fluid model can be simplified in the form of a homogenous model. A model for homogeneous multiphase fluids can be derived by performing a spatial averaging of the various properties of all phases. Then, modeling of the transport of this multiphase system usually involves the spatially-averaged mass, momentum, and energy conservation equations and few auxiliary equations, such as the equation of state and other constitutive relationships.

Modeling a reservoir multiphase-fluid system as a homogenous system reduces the load of calculations significantly so that the efforts can be focused on consideration of other relevant phenomena in addition to transport. In particular, the kinetics of phase transition is of special interest and considered in this study. In common practice, a usual

simplification in solving engineering problems associated with pipeline and well flow is to assume the phase transition is an instantaneous process. However, the retardation or relaxation in phase transition may play an important role in processes involving reservoir fluids under certain conditions of practical importance. Certainly, a gradual o relaxed phase transition has a significant effect in attaining flow assurance for pipelines and wells. For instance, the retardation in gas separation from oil and phases due to the pressure drop during fluid flow may increase the pressure drop because less gas concentration implies a higher density. Moreover, retardation in waxy crystal precipitation from waxy-oils during cooled transport inside pipelines may lower viscous resistance to flow because less solid concentration implies a lower viscosity. Furthermore, a gradual and incomplete precipitation of waxy crystals during shut-in conditions in a cold environment may decrease the restriction to flow after flow restart because less solid precipitation implies less volume unavailable to fluid flow.

For instance, the steady-state flow inside production pipes experiencing liquid holdup can be modeled as a homogeneous multiphase system where relaxation in phase transition can adequately describe the holdup. Liquid holdup occurs when the liquid phases exhibit slippage past the gas phase during multiphase fluid flow. The steady-state flow with liquid holdup is often modeled by the means of a two-phase model, that is gas and liquids, where the phases are assumed to be at the same temperature and pressure conditions but having different flowing velocities (Brill & Mukherjee, 1999). This approach is also known as the Separated Flow Model (Faghri & Zhang, 2006). When liquid holdup occurs, the gas-liquid ratio is less than the ratio given by

thermodynamic equilibrium. Thus, liquid holdup can be attributed to kinetics or relaxation of gas separation from the liquids. Moreover, the holdup leads to a higher local density of the reservoir fluid along the pipe length. However, the conventional approach infers for the gas-liquid ratio depending on the local spatial arrangements of the gas and liquids. It was observed experimentally that the concurrent flow of the gas and liquids phases will induce different spatial arrangements, known as flow patterns, depending on the flowing conditions. These flow patterns can be grouped into various categories like: uniformly dispersed, such as bubbly and mist flow; orderly separated, such as slug, wavy, and annular flow; and chaotic, such as churn and wispy flow. Although the conventional approach considers different empirical correlations for calculating the mixture density depending on the flow pattern, a more direct approach to obtain the density would be to apply a relaxation in gas separation from the liquids. A relaxation in gas separation during the flow of a multiphase fluid would induce a metastable state where liquid mobilization or slippage is necessary for accounting of the increase in liquid mass fraction or holdup and the degree of slippage may indicate the resulting flow pattern. Thus, the liquid holdup and the resulting flow pattern can be both explained by the relaxation phenomenon. On the contrary, the conventional approach bases the description of the holdup by predicting the flow pattern.

Another example where the importance of phase transition kinetics becomes evident is the crystallization or gelation of wax from cooled crude oil. The crystallization kinetics affects all properties of a waxy-oil because the solid concentration is experiencing relaxation in wax precipitation. Specifically, change in the rheology due to thermal

stress of a gelled wax is not instantaneous but known to be time dependent where equilibrium is achieved in the order of minutes. Gelling of wax requires a sufficiently long time. Aging implies the gelled wax has attained it maximum hardness. This means that the apparent viscosity of waxy-oil subject to cooling increases in time until a maximum is reached. Then, the gelation process is assumed complete. This time dependency can be attributed to a gradual precipitation of wax crystals. Essentially, a gradual precipitation of wax crystals implies a continuous increase of solid concentration which leads to a progressive increase in apparent viscosity. The time dependency of the viscoelastic property known as the storage modulus can be described by a model for crystallization kinetics (Ekweribe, Civan, Lee, & Singh, 2009); (Lopez-Da-Silva & Couthino, 2007). Similarly, the gelation kinetics can be related to the plastic response of waxy-oils subject to stress and cooling. Altogether, aging can be modeled as the effect of relaxation in wax crystals precipitation on the rheological behavior of a gelled wax.

The effect of crystallization kinetics on gradual wax gelation inside shut-in submarine pipes is yet to be determined. In order to investigate this effect, a model describing the gelation inside pipes needs to be adopted first. A well-known approach for modeling wax gelation occurring inside pipes is describe to the wax precipitation as an instantaneously-forming moving front with a piston-like separation of phases (Mehrotra & Bhat, 2007); (Edmonds, Moorwood, Szczepanski, & Zhang, 2008); (Bhat & Mehrotra, 2008); (Mehrotra & Bhat, 2010); (Lindeloff & Kerjbjerg, 2002); (Tiwary & Mehrotra, 2009). The reservoir fluid is modeled as two separate substances at any cross-

section of the pipe: oil with dissolved wax and oil having fully precipitated wax. Thus, there is no continuous wax concentration but a step change in the radial concentration profile. However, there is an underlying inconsistency in such modeling approach. The radial temperature profile is allowed to be continuous for a given pipe cross-section in this approach although the thermodynamics of wax precipitation yield a binary profile of wax concentration implying a binary temperature profile. In order to facilitate a continuous wax precipitation during wax gelation, the reservoir fluid should be modeled as two-phase homogenous system, meaning a mixture of oil phase with dissolved wax and a gelled waxy-oil phase. Moreover, homogenous modeling of wax precipitation allows the coupling with crystallization kinetics. This allows the execution of simulations that provide valuable insights on the importance of considering gelation kinetics in shut-in pipes.

1.3. PRESENT STUDY

The scope of the present study is describing kinetics of phase transition in homogenous multiphase systems applied to steady-state flow and transient solidification of reservoir fluids at non-adiabatic and non-isothermal conditions. The reservoir fluid is described as a single multiphase fluid system where the fundamental laws of conservation can be applied in order to describe the prevailing transport conditions.

The fundamental laws of conservation are formulated in their differential forms. All the properties of the multiphase fluid system are spatially averaged properties leading to a

homogenous model. Numerical techniques are developed for solving the differential equations given by the conservation laws. These techniques are described in detail.

Then, the effect of retardation or relaxation in phase transition is investigated for processes concerning the transport and rheology of reservoir fluids. The transport processes are studied as homogenous systems undergoing relaxed phase transition with heat transfer. These are, steady-state flow of gas/oil/water systems occurring in production pipes with geothermal heat transfer, and, transient wax gelation occurring in shut-in submarine pipes undergoing a cooling heat transfer process. Additionally, the change in rheological behavior during the cooling of waxy-oil is studied at non-isothermal and non-equilibrium conditions.

For the flow of gas/oil/water systems, the reservoir fluid is modeled as a mixture of these three phases, whereas the conventional approach combines the liquid phases into one. Also, the effect of liquid holdup is considered along the flow throughout the production pipe. The driving mechanism for this flow is pressure drop but the geothermal heat transfer plays also an important role in determining the flow conditions. The pressure drop is set mainly by the mixture density. However, the reservoir fluid density cannot be obtained by flash calculations alone when liquid holdup occurs because the holdup has an intrinsic nature of not being at thermodynamic equilibrium conditions. The conventional approach applies empirical correlations which are not related to the non-equilibrium nature of liquid holdup. Instead, the density property needs to be estimated by means of non-equilibrium models. For this purpose, a backward modeling based on the ratio of gas phase velocity to the liquid phase velocity,

known as slip ratio, is presented for estimating the density during the flow of reservoir fluids experiencing liquid holdup. The data generated by this backward modeling facilitates the development of a forward modeling which is based on kinetics of gas separation from liquid phases. In the separation kinetics modeling, the holdup is attributed to the non-equilibrium mass transfer across the interface between the liquid phases and the gas phase. This forward modeling is validated by the means of study cases generated from published data for producing vertical wells.

For modeling of transient wax gelation without force convection occurring in shut-in wells, the reservoir fluid is modeled as a mixture of oil phase with dissolved wax and gelled waxy-oil phase. The relevant properties of the wax-free and waxy-oil phases are assumed constant but the mixture properties may vary because they constitute volume-averaged properties of the properties of each phase. The driving mechanism of wax gelation in submarine pipes is the heat loss towards the sea environment. At shut-in conditions, the pressure is set by the pressure head alone at any location. A waxy-oil gelation model applied to a cross-section with constant surroundings temperature is developed first. This model is validated with experimental data corresponding to wax gelation inside a thin cylinder. The waxy-oil gelation model is extended so that it can be applied to a vertical pipe with varying surroundings temperature. A procedure is introduced for estimating the initial conditions of a shut-in submarine pipe. Simulations are executed for comparison of the effect of pressure change and retardation of crystallization.

The effect of phase transition during cooling of waxy-oils on its rheology is modeled by directly relating the crystallization kinetics to the rheological properties. The precipitation of waxy crystals during cooling is not an instantaneous process but retardation to achieve equilibrium has been experimentally observed to happen gradually. The observed retardation in crystallization is associated with the viscoelastic behavior of waxy-oils. The similarities between the viscoelastic and plastic responses to stress stimulus are demonstrated theoretically here. Several approaches are introduced for modeling the effect of crystallization kinetics or relaxation of waxy-oil rheology. Study cases delineate the effect of cooling rate on the relaxation of waxy-oil rheology. Relatively high cooling rates are necessary to induce a significant relaxation effect on the wax-oil viscosity and gel strength.

1.4. OBJECTIVES

The main objective of the present study is to model and simulate the effect of phase transition kinetics of reservoir fluids during the steady-state flow of producing wells, waxy-oil rheology during transient state cooling, and waxy-oil gelation in shut-in submarine pipes. These threefold main objectives are accomplished by means of the following groups of specific objectives, which are essential issues of relevance for flow assurance in pipelines.

The specific objectives of the present work are:

- Development of a homogenous model describing the transport phenomena of reservoir fluids in one dimensional space for the steady-state flow of producing

wells and in cylindrical coordinates for waxy-oil gelation in shut-in submarine pipes.

- Development of effective techniques for solving numerically the equations which describe the transport during steady-state flow in producing wells, wax gelation in thin cylindrical vessels, and wax gelation in shut-in submarine pipes.

The objectives for steady-state flow of producing wells are:

- Data generation of fluid properties during upward flow inside pipes with heat transfer for predicting liquid holdup.
- Formulation of a new model for estimating the liquid holdup at thermodynamic non-equilibrium for gas separation from liquid phases.

The objectives for kinetics of wax rheology are:

- Development of a model for describing the kinetics of wax crystallization as a fractal growth process.
- Demonstration of the theoretical equivalency of viscoelastic and plastic responses to shear stress.
- Description of wax aging or hardening by applying the crystallization kinetics to wax rheology.

The objectives for wax gelation in shut-in pipes are:

- Development of the correlation models for approximating the fraction of

precipitated wax as a function of temperature and pressure.

- Development of a model for describing transient wax gelation for a circular cross-section without force convection.
- Development of a model for describing transient wax gelation for a submarine vertical pipe at shut-in conditions.

1.5. ORGANIZATION OF THE DISSERTATION

The contents of this dissertation are organized and reported in six chapters and one appendix as described in the following.

The current Chapter One provides an overview of the problem of interest and the scope of the present study. Also, the main and specific objectives are presented for the present study.

Chapter Two provides the multi-fluid and homogenous fluid approaches for describing the transport of multiphase systems. Volume-averaging and area-averaging formulations of the properties involved in the transport of homogenous multiphase systems are presented. A homogeneous model characterizing the transport without convection in cylindrical coordinates is elaborated, which is required for the modeling of wax gelation in shut-in submerged pipes. Also, homogenous area-averaged models representing the transport with and without liquid holdup in one-dimensional space are presented, which support the modeling of multiphase flow in upward oil wells.

Chapter Three describes the homogenous modeling of the upward motion in production wells where the liquid holdup phenomenon is explained as a non-equilibrium separation of the gas phase from the liquids. Data is generated by adjusting the gas velocity to liquid velocity ratio in order to match the measured pressure and temperature in the field. The generated data constitutes all properties involved in the transport of the multiphase system. Then, this data is analyzed for developing an empirical model. The empirical model estimates the rate governing the kinetics of gas separation. This empirical model coupled with the area-averaged model with liquid holdup facilitates the prediction of pressure drop in production wells of gas/oil and gas/oil/brine systems.

Chapter Four elaborates upon the effect of crystallization kinetics of a cooling waxy-oil on the rheological behavior. The crystallization is described as a fractal growth process. An empirical correlation is developed for the kinetics of waxy-crystal growth. It is demonstrated that the viscoelastic nature of gelled waxy-oil is intrinsically related to the plastic response to shear stress. The crystallization kinetics is coupled with a wax rheological model for delineating the effect of non-equilibrium wax precipitation on viscosity and gel strength,

Chapter Five describes the homogeneous modeling of transient gelation of shut-in submarine pipes. A critical review of the relevant mechanisms is provided. Empirical correlations are developed for the dependency of wax precipitation to temperature and wax appearance temperature to pressure. The transient gelation of waxy-oil is first modeled and validated for a pipe cross-section subject to cooling by heat transfer. Next, the model is extended for applications to vertical pipes subject to cooling by heat loss

towards the sea environment. Then, the effects of pressurization and wax precipitation kinetics on waxy-oil gelation are investigated in order to determine which is more significant.

Chapter Six presents the discussion and conclusions after analyzing the results obtained in the various case studies conducted in Chapters Three, Four, and Five.

Appendix A presents a collection of definitions and correlations required for estimating the properties of the gas, oil, and water phases as well as the wall surface properties of the pipe.

Appendix B elaborates on a numerical scheme for computational thermodynamics of wax gelation inside a cross-section of a pipe at cooled conditions.

Appendix C describes a numerical procedure for estimation the temperature profile of flowing cooled oil inside a submarine vertical pipe at the shut-in time.

Appendix D elaborates on a numerical scheme for computational thermodynamics of wax gelation inside a submarine vertical pipe at shut-in and cooled conditions.

CHAPTER 2

FORMULATION OF TRANSPORT PHENOMENA FOR MULTIPHASE SYSTEMS IN PIPES AND WELLS

2.1. OVERVIEW

A multiphase system is distinguished from a single-phase system by the presence of one or more interfaces separating the various phases (Faghri & Zhang, 2006). It can be considered as a mixture of single-phase regions separated by the interfaces. In this chapter, the transport of a multiphase system in pipelines and wells is described by performing Eulerian spatial averaging of the phase properties. The models presented here are specific cases of the multi-fluid and homogenous model. The multi-fluid model is expressed in general coordinates while the homogenous model is defined in cylindrical coordinates without force convection in one-dimensional coordinates for two

cases. In the first case, the phases flow at the same velocity; and, in the second case, the phase velocities are different from each other. Also, definitions of relevant multiphase system properties are provided.

2.2. MICROSCOPIC FORMULATION OF TRANSPORT

The microscopic formulation of transport phenomena, also known as the differential form, applies the control volume and control surface over a representative elemental volume of a fluid. The fluid transport presented here is considered inviscid, isotropic and flowing upwards inside a pipe with constant cross-sectional area. Also, the fluid transport experiences wall shear stress (τ_w) and wall heat transfer ($\dot{Q}_w$).

Then, the laws of conservation can be expressed as (Bird, Stewart, & Lightfoot, 1965):

$$\frac{\partial \rho}{\partial t} + \nabla \cdot \left(\rho \vec{v} \right) = 0 \quad \text{(2-1)}$$

$$\frac{\partial}{\partial t}\left(\rho \vec{v} \right) + \nabla \cdot \left(\rho \vec{v} \vec{v} \right) = -\nabla P - \rho \vec{g} - \tau_w \quad \text{(2-2)}$$

$$\frac{\partial}{\partial t}\left(\rho h \right) + \nabla \cdot \left(\rho h \vec{v} \right) - \frac{\partial P}{\partial t} - \vec{v} \cdot \nabla P = \nabla \cdot \left(k \nabla T \right) + \vec{v} \cdot \tau_w - \dot{Q}_w \quad \text{(2-3)}$$

where ρ is density, $\vec{v}$ is the velocity vector, P is pressure, T is temperature, $\vec{g}$ is the gravity vector, h is enthalpy, k is the heat conductivity coefficient.

2.3. VOLUME-AVERAGED MULTI-FLUID MODEL

The volume-averaged multi-fluid model can be adopted when the system control volume has fixed position in time. The Eulerian time and volume averaging, however, applies to processes having a moving control volume. The volume-averaged multi-fluid model treats the various phases as independent fluids where the spatial averaging of properties is performed for each individual phase, referred to as phase-averaging. This means that a phase-averaged property constitutes the mean value of that property taken over the entire phase volume. Consequently, the conservation of mass, momentum, and energy of the phase *i* having its properties phase-averaged over a representative element are given, respectively, by (Faghri & Zhang, 2006):

$$\frac{\partial}{\partial t}\left(\rho_i H_i\right)+\nabla\cdot\left(\rho_i H_i \vec{v}_i\right)=\Gamma_i \quad \text{(2-4)}$$

$$\frac{\partial}{\partial t}\left(\rho_i H_i \vec{v}_i\right)+\nabla\cdot\left(\rho_i H_i \vec{v}_i \vec{v}_i\right)=-\nabla\left(P_i H_i\right)-\rho_i H_i \vec{g}+\Psi_i \quad \text{(2-5)}$$

$$\frac{\partial}{\partial t}\left(\rho_i H_i h_i\right)-H_i\frac{\partial P}{\partial t}+\nabla\cdot\left(\rho_i H_i h_i \vec{v}_i\right)-H_i \vec{v}_i\cdot\nabla P_i=\nabla\cdot\left(k_i H_i \nabla T_i\right)+\Omega_i \quad \text{(2-6)}$$

Here, H_i is the volumetric fraction of phase *i* which represents the ratio of volume of phase *i* to the total volume of the multiphase system. The volumetric fraction is also referred to as volume concentration. The term Γ_i represents the net mass transfer of phase *i* from all other phases. Similarly, the terms Ψ_i and Ω_i represent the net momentum and net energy transfer of phase i from all other phases, respectively. The

term Ψ_i is comprised of the force of interaction and exchange of momentum between phase *i* and any other phase. The term Ω_i is comprised of the chemical energy exchange, the enthalpy exchange, and the heat transfer between phase *i* and any other phase.

2.4. HOMOGENOUS FLUID MODEL

A multiphase fluid is defined as being homogenous when some or all of its properties are obtained by spatial averaging of the corresponding phase-averaged property for each phase. This means that a multiphase system property constitutes the mean value of that property taken over the entire control volume.

2.4.1 HOMOGENOUS FLUID DESCRIPTION OF MULTIPHASE SYSTEMS

Because the multiphase system is comprised of various phases, each phase have a mass fraction (χ_i) and a volumetric fraction. By definition, the sum of the fractions of the various phases is equal to the unity.

$$\sum_i \chi_i = 1 \quad \text{(2-7)}$$

$$\sum_i H_i = 1 \quad \text{(2-8)}$$

The fundamental relationship between the volumetric and mass fraction of phase *i* is given by two definitions of the mass concentration of phase *i* in the multi-phase mixture.

$$\xi_i = \rho\chi_i = \rho_i H_i \quad \text{(2-9)}$$

$$\chi_i = \frac{\rho_i H_i}{\rho} \quad (2\text{-}10)$$

The specific volume a multiphase system is defined as the mass-averaged specific volume of all phases.

$$\frac{1}{\rho} = \sum_i \frac{\chi_i}{\rho_i} \quad (2\text{-}11)$$

The mass-averaged vector velocity, specific heat capacity (c_p) and the product between specific heat capacity and the Joule-Thompson coefficient (η) are defined, respectively, by:

$$\vec{v} = \sum_i \chi_i \vec{v}_i \quad (2\text{-}12)$$

$$c_p = \sum_i \chi_i c_{pi} \quad (2\text{-}13)$$

$$c_p \eta = \sum_i \chi_i c_{pi} \eta_i \quad (2\text{-}14)$$

The vector volumetric flux ($\vec{u}$) and the thermal conductivity (k) are defined directly by spatial averaging as:

$$\vec{u} = \sum_i H_i \vec{v}_i \quad (2\text{-}15)$$

$$k = \sum_i k_i H_i \quad (2\text{-}16)$$

The enthalpy can be formulated in its differential form as follows:

$$dh = c_p dT - c_p \eta \, dP \quad (2\text{-}17)$$

Likewise, the enthalpy of a phase is defined:

$$dh_i = c_{pi} dT - c_{pi} \eta_i dP \quad (2\text{-}18)$$

Therefore, enthalpy of a multiphase system is defined as:

$$dh = \sum_i \chi_i dh_i \quad (2\text{-}19)$$

The validity of equation 2-19 can be verified by introducing equations 2-13, 2-14, 2-17 and 2-18.

Further, equations 2-20, 2-21 and 2-22 can be written by combining equation 2-10 into equations 2-7, 2-12 and 2-19, respectively.

$$\rho = \sum_i \rho_i H_i \quad (2\text{-}20)$$

$$\rho \vec{v} = \sum_i \rho_i H_i \vec{v}_i \quad (2\text{-}21)$$

$$\rho dh = \sum_i \rho_i H_i dh_i \quad (2\text{-}22)$$

2.4.2. TRANSPORT OF MULTIPHASE FLUID SYSTEMS AS HOMOGENOUS FLUID

In this section, the various homogenous models are presented where pressure and temperature of all phases set are equal. Therefore, only the phase velocities are allowed to vary from each other. Also, all internal interactions among phases are considered to cancel out with each other. This means, the net mass, momentum, and energy exchanges among various phases vanish.

$$\sum_i \Gamma_i = 0 \quad \text{(2-23)}$$

$$\sum_i \Psi_i = 0 \quad \text{(2-24)}$$

$$\sum_i \Omega_i = 0 \quad \text{(2-25)}$$

A volume-averaged homogenous model is obtained by adding mass, momentum and energy conservation stated by equations 2-4, 2-5 and 2-6 for all phases. Consequently, the mass, momentum, and energy conservation laws take the form of equations 2-26, 2-27 and 2-28, respectively, in view of equations 2-23, 2-24 and 2-25.

$$\frac{\partial}{\partial t}\left(\sum_i \rho_i H_i\right) + \nabla \cdot \left(\sum_i \rho_i H_i \vec{v}_i\right) = 0 \quad \text{(2-26)}$$

$$\frac{\partial}{\partial t}\left(\sum_i \rho_i H_i \vec{v}_i\right) + \nabla \cdot \left(\sum_i \rho_i H_i \vec{v}_i \vec{v}_i\right) = -\nabla\left(P\sum_i H_i\right) - \sum_i \rho_i H_i \vec{g} \quad \text{(2-27)}$$

$$\frac{\partial}{\partial t}\left(\sum_i \rho_i H_i h_i\right) - \sum_i H_i \frac{\partial P}{\partial t} + \nabla \cdot \left(\sum_i \rho_i H_i h_i \vec{v}_i\right) - \sum_i H_i \vec{v}_i \cdot \nabla P = \nabla \cdot \left(\sum_i k_i H_i \nabla T\right) \quad (2\text{-}28)$$

Note that equations 2-26, 2-27 and 2-28 do not account for the wall interactions but account for all internal interactions occurring inside the multiphase system.

For convenience, equation 2-28 is rearranged and equation 2-26 is introduced in order to express the energy conservation law in the form:

$$\sum_i \rho_i H_i \frac{\partial h_i}{\partial t} - \sum_i H_i \frac{\partial P}{\partial t} + \sum_i \rho_i H_i \vec{v}_i \cdot \nabla h_i - \sum_i H_i \vec{v}_i \cdot \nabla P + \sum_i h_i \Gamma_i = \nabla \cdot \left(\sum_i k_i H_i \nabla T\right) \quad (2\text{-}29)$$

By introducing equations 2-20, 2-21 and 2-22 into equations 2-26, 2-27, 2-29, the following convenient form of the above homogenous model is obtained:

$$\frac{\partial \rho}{\partial t} + \nabla \cdot \left(\rho \vec{v}\right) = 0 \quad (2\text{-}30)$$

$$\frac{\partial}{\partial t}\left(\rho \vec{v}\right) + \nabla \cdot \left(\sum_i \rho_i H_i \vec{v}_i \vec{v}_i\right) = -\nabla P - \rho \vec{g} \quad (2\text{-}31)$$

$$\rho \frac{\partial h}{\partial t} - \frac{\partial P}{\partial t} + \sum_i \rho_i H_i \vec{v}_i \cdot \nabla h_i - \sum_i H_i \vec{v}_i \cdot \nabla P = \nabla \cdot \left(k \nabla T\right) \quad (2\text{-}32)$$

Note that the term $\Sigma_i \; h_i \Gamma_i$ is vanishes in the energy conservation law because it constitutes the net enthalpy exchange among all phases, as stipulated in equation 2-25.

There are some similitudes between the transport of a single phase fluid, which is given by equations 2-1, 2-2 and 2-3, and the transport of the homogenous model defined by equations 2-30, 2-31 and 2-32. Therefore, a multiphase system can be treated as a pseudo-single phase under the above provided necessary conditions and simplifications.

2.5. HOMOGENOUES MODEL APPLIED TO MULTIPHASE FLUID SYSTEM IN PIPES

Because a pipe is characterized by its circular cross-sectional area, the multiphase homogeneous model described in this section is derived in cylindrical coordinates. For simplicity, all volume-averaged properties are considered constant in the azimuthal direction. Thus, the resulting model constitutes a two-dimensional homogenous model where the spatial directions are axial and radial. This type of model still falls into the category of volume-averaged homogenous model (Faghri & Zhang, 2006). Moreover, the multiphase system involves no force convection.

2.5.1. FORMULATION IN CYLINDRICAL COORDINATES

A two-dimensional model for pipes can be obtained by expressing equations 2-30, 2-31 and 2-32 in cylindrical coordinates where the azimuthal direction has been disregarded.

$$\frac{\partial \rho}{\partial t} + \frac{1}{r}\frac{\partial}{\partial r}\left(r\rho v^{r}\right) + \frac{\partial}{\partial l}\left(r\rho v^{l}\right) = 0 \qquad (2\text{-}33)$$

$$\frac{\partial}{\partial t}\left(\rho v^{r}\right) + \frac{1}{r}\frac{\partial}{\partial r}\left(r\sum_{i}\rho_{i}H_{i}v_{i}^{r}v_{i}^{r}\right) + \frac{\partial}{\partial l}\left(\sum_{i}\rho_{i}H_{i}v_{i}^{l}v_{i}^{r}\right) = -\frac{\partial P}{\partial r} \qquad (2\text{-}34)$$

$$\frac{\partial}{\partial t}\left(\rho v^{l}\right)+\frac{1}{r}\frac{\partial}{\partial r}\left(r\sum_{i}\rho_{i}H_{i}v_{i}^{r}v_{i}^{l}\right)+\frac{\partial}{\partial l}\left(\sum_{i}\rho_{i}H_{i}v_{i}^{l}v_{i}^{l}\right)=-\frac{\partial P}{\partial l}-\rho g \quad \text{(2-35)}$$

$$\begin{aligned}\rho\frac{\partial h}{\partial t}-\frac{\partial P}{\partial t}+\sum_{i}\rho_{i}H_{i}v_{i}^{r}\frac{\partial h_{i}}{\partial r}+\sum_{i}\rho_{i}H_{i}v_{i}^{l}\frac{\partial h_{i}}{\partial l}-\sum_{i}H_{i}v_{i}^{r}\frac{\partial P}{\partial r}\\ -\sum_{i}H_{i}v_{i}^{l}\frac{\partial P}{\partial l}=\frac{1}{r}\frac{\partial}{\partial r}\left(r\,k\frac{\partial T}{\partial r}\right)+\frac{\partial}{\partial l}\left(k\frac{\partial T}{\partial l}\right)\end{aligned} \quad \text{(2-36)}$$

Then, without force convection, the model is reduced to:

$$\frac{\partial \rho}{\partial t}=0 \quad \text{(2-37)}$$

$$\frac{\partial P}{\partial l}=-\rho g \quad \text{(2-38)}$$

$$\rho\frac{\partial h}{\partial t}-\frac{\partial P}{\partial t}=\frac{1}{r}\frac{\partial}{\partial r}\left(r\,k\frac{\partial T}{\partial r}\right)+\frac{\partial}{\partial l}\left(k\frac{\partial T}{\partial l}\right) \quad \text{(2-39)}$$

Note that pressure becomes a function of longitudinal distance alone, because there is no force convection, but density is still a function of radius and longitudinal distance. Hence, an auxiliary definition of density is required; and, therefore, provided later in this work.

Equations 2-1, 2-2 and 2-3, the mass, momentum and energy conservation laws for a single phase fluid, become similar to equations 2-37, 2-38, 2-39 when expressed in cylindrical coordinates without force convection and wall interactions. Thus, the

transport of a multiphase system exhibiting these characteristics can be described as a single phase fluid.

2.5.2. CROSS-SECTIONAL AREA-AVERAGED FORMULATION

All properties are averaged over its cross-sectional area in an area-averaged model applied to any conduit or channel. Consequently, the resulting model constitutes a one-dimensional homogenous model where the only spatial direction is the axial direction. Additionally, the heat convection is assumed much greater than heat conduction. Thus, the heat conduction is neglected. Considering the afore-mentioned conditions, the general homogenous model specified by equations 2-30, 2-31 and 2-32 is simplified into the following equations, respectively.

$$\frac{\partial \rho}{\partial t} + \frac{\partial}{\partial l}(\rho v) = 0 \quad \text{(2-40)}$$

$$\frac{\partial}{\partial t}(\rho v) + \frac{\partial}{\partial l}\left(\sum_i \rho_i H_i v_i^{\,2}\right) = -\frac{\partial P}{\partial l} - \rho g \sin\varphi \quad \text{(2-41)}$$

$$\rho \frac{\partial h}{\partial t} - \frac{\partial P}{\partial t} + \sum_i \rho_i H_i v_i \frac{\partial h_i}{\partial l} - \sum_i H_i v_i \frac{\partial P}{\partial l} = 0 \quad \text{(2-42)}$$

In the classic area-averaged model, the velocities, pressures, and temperatures of all phases are equal; thus, all phases flow at the same velocity as the multiphase system.

$$v = v_i \quad \text{(2-43)}$$

By introducing equation 2-43 into equations 2-41 and 2-42, the momentum and energy conservation can be expressed as:

$$\frac{\partial}{\partial t}(\rho v)+\frac{\partial}{\partial l}(\rho v^2)=-\frac{\partial P}{\partial l}-\rho g\sin\varphi \quad \text{(2-44)}$$

$$\rho\frac{\partial h}{\partial t}-\frac{\partial P}{\partial t}+\rho v\frac{\partial h}{\partial l}-v\frac{\partial P}{\partial l}=0 \quad \text{(2-45)}$$

Equations 2-40, 2-44 and 2-45 are similar to the one-dimensional Cartesian form of equations 2-1, 2-2 and 2-3, for to the mass, momentum and energy conservation of a single phase fluid, provided that the heat conduction and wall interactions are not considered. Consequently, the conventional area-averaged model describes the transport of a multiphase system like a single phase fluid.

2.5.3 CROSS-SECTIONAL AREA-AVERAGED FORMULATION INCLUDING LIQUID HOLDUP EFFECT

The phase velocities are allowed to differ from each other in the area-averaged homogenous model with liquid holdup. Also, the heat conduction is assumed negligible compared to the heat convection. Thus, equations 2-40, 2-41 and 2-42 are suitable to describe the transport. The following simplification can be applied assuming each phase of the multiphase is flowing at a very low velocity compared to its local speed of sound:

$$\frac{\partial}{\partial l}\left(\sum_i \rho_i H_i v_i^{\,2}\right)\cong 0 \quad \text{(2-46)}$$

This simplification is based on the observation that the pressure gradient is much larger than the differential term in equation 2-46 at very low Mach numbers. The following additional approximation is introduced to obtain a condensed form:

$$\rho u \frac{\partial h}{\partial l} \cong \sum_i \rho_i H_i v_i \frac{\partial h_i}{\partial l} \quad \text{(2-47)}$$

The momentum and energy conservation are reduced to the following form by substituting equation 2-46 into equation 2-41 and equations 2-15 and 2-47 into equation 2-42:

$$\frac{\partial}{\partial t}(\rho v) = -\frac{\partial P}{\partial l} - \rho g \sin\varphi \quad \text{(2-48)}$$

$$\rho \frac{\partial h}{\partial t} - \frac{\partial P}{\partial t} + \rho u \frac{\partial h}{\partial l} - u \frac{\partial P}{\partial l} = 0 \quad \text{(2-49)}$$

Equations 2-40, 2-48 and 2-49 are similar to the one-dimensional Cartesian form of the mass, momentum and energy conservation for a single phase fluid neglecting the effects of heat conduction and wall interactions. However, the model differs in that the flow rate is given by the mixture volumetric flux instead of the mixture velocity in energy law, as stipulated by equation 2-3. Thus, the transport of an area-averaged model can be described as a pseudo-single phase fluid provided that the transfer rate over the control surface is given by the volumetric flux.

CHAPTER 3

MODELING LIQUID HOLDUP IN PRODUCTION WELLS AS A RELAXED GAS SEPARATION

3.1. OVERVIEW

Flow of reservoir fluids in oil production wells is described by an improved three-phase model. Relaxation phenomenon concerning the gradual dissolved-gas separation from the oil and water phases is elaborated by two approaches and the results are compared. Rigorous formulations for holdup of the liquid phases and the associated relaxation times are presented. Deviation of actual fluid conditions from equilibrium is characterized by a new constitutive equation. Tendency of faster gas phase flow relative to liquid phases is shown to be the primary driving force for the liquid holdup in wells. Effect of relaxation time and holdup of liquids involving in typical field scenarios is

demonstrated for reservoir fluids containing oil, water, and gas phases. The three-phase model developed in this study is proven to be more rigorous and accurate than the previous two-phase models which group the oil and water phases into one pseudo-liquid phase for convenient description of the gas/oil/water systems.

3.2. LITERATURE REVIEW

Liquid holdup occurs when the liquid phase slip past the gas phase. The slippage of the liquids indicates a higher liquid fraction than that predicted by flash calculations is being experienced. This implies the gas separation occurs under non-equilibrium thermodynamic conditions. The effect of liquid holdup on pressure drop during the multiphase flow inside pipes is an important issue in pipeline flow of hydrocarbons. The pressure drop in single phase flow has been successfully explained for both turbulent and laminar flow cases by estimating the momentum losses due to gravitational and friction forces. Some of the attempts in describing the liquid holdup phenomena are reviewed in the following.

For two-phase flow, developed models for calculating pressure drop are characterized by:

- Considering the multiphase system either as one mixture fluid or as two completely separated substances sharing the cross-sectional area of the pipe (Faghri & Zhang, 2006)
- Correcting the gravitational momentum losses and/or the frictional momentum losses with correlations (Brill & Mukherjee, 1999)

- Predicting flow patterns and applying customized correlations for correcting the momentum losses various flow patterns (Brill & Mukherjee, 1999)

The Hagedorn and Brown method (Hagedorn & Brown, 1965) considers the gas/oil systems as one single mixture and corrects its density and the friction loss according to the flowing conditions. The liquid holdup and the friction losses are estimated by a single correlation in order to obtain a correction on the mixture density. Then, the corrected mixture density is calculated by performing an area-averaging of each phase density having the liquid holdup as a weighting factor. The uncorrected density is obtained by using liquid fractional flow, which is the ratio of phase flow rate to the total flow rate, as the weighing factor. However, the frictional loss remains uncorrected, and it is calculated by applying the uncorrected density. This method is one of most widely used approach for oil wells and several modifications have improved its accuracy.

The Gray method (Gray, 1978) predicts the liquid holdup and corrects friction losses by a single correlation each for gas/condensate or gas /water mixtures. The system is modeled as a mixture so that mixture density is calculated by performing an area-averaging using the liquid holdup as a weighting factor. Nevertheless, both the mixture density and friction losses remain uncorrected when the liquid flow rate is locally low, which implies a low gas/liquid ratio. This method is widely used for gas/condensate and gas/brine producing wells.

The Beggs and Brill method (Beggs & Brill, 1973) applies different correlation parameters depending on the predicted flow patterns in order to estimate the liquid

holdup and, hence, correct the frictional losses. The pattern prediction is based on various correlations using both the liquid fractional flow and the Froude Number. The flow patterns are classified as segregated, intermittent, and distributed. Then, the liquid holdup estimation is adjusted according to the angle of inclination and the multi-phase fluid system density is calculated using the liquid holdup as a weighting factor. The gas/liquid system is modeled as a mixture. Both the mixture density and friction losses remain uncorrected when the gas flow rate is locally low. This method is widely used for oil and gas transmission pipelines because these pipelines exhibit variable angle of inclination due to the irregular shape of the ground terrain features.

The Ansari et al. method (Ansari, Sylvester, Sarica, Shoham, & Brill, 1994) considers different correlation models for predicting the liquid holdup and frictional losses. The appropriate correlation is selected according to the predicted flow pattern. The pattern prediction is based on various correlations using both the liquid and gas fractional flow. The flow patterns are classified as bubbly, dispersed bubble, slug, and annular. The gas/liquid system is modeled as a mixture when the flow pattern is predicted to be bubbly or dispersed bubble types and as separated flowing phases when the flow pattern is predicted as slug or annular types. Both the mixture density and friction losses remain uncorrected when the gas flow rate is locally low. This method is well-known among the models based on the separated flow approach.

The Michel and Civan approach (Michel & Civan, 2008a) incorporates the effect of non-isothermal and non-adiabatic flow to the Asheim method (Asheim, 1986). It is not a predictive method but an optimized matching of the field production data. There are

three fitting parameters in the calculation of pressure drop and these parameters are completely unrelated to the flow pattern. The gas velocity is set as being linearly dependent to the liquid velocity where the slope and intercept are the first two fitting parameters. The liquid holdup is formulated using these two fitting parameters and constitute as the weighting factor in the calculation of the mixture density. The third parameter is a correction factor for the frictional losses. The gas/liquid system is modeled as a homogenous mixture where the mass, momentum, and energy balance are given in their differential forms. A correlation model is given for predicting not liquid holdup but the quality or dryness of the system based on the optimization in the matching of pressure and temperature drop corresponding to several wells. Then, the mixture density is calculated using the predicted quality.

Applying correlations in the prediction of liquid holdup and the flow patterns may introduce some inconsistencies into the transport modeling. There are several most common inconsistencies. First, the mixture density may be over- or under-estimated when either the gas or liquid flow rate is locally low because the required correction has been observed experimentally to be negligible. Second, discontinuities may be introduced in the liquid holdup profile when a change in flow pattern is predicted because the correlations corresponding to various flow patterns do not insure continuity. Finally, the mixture velocity must be corrected accordingly when the mixture density is corrected to account for liquid holdup in order to keep the mass flow rate constant as stated by the mass balance at steady-state flow conditions. All of these considerations are taken in account in the revised Michel and Civan approach (Michel & Civan,

2008b) which formulates the liquid holdup in terms of the slip ratio, a ratio of gas velocity to the liquid velocity. A slip ratio equal to the unity indicates no correction. The slip ratio is formulated using a quadratic relationship with the quality or dryness such that zero and unity dryness yields a slip ratio equal to the unity. Thus, the only fitting parameter for matching pressure and temperature drop is the slip ratio at the well-head.

3.3. LIQUID HOLDUP PHENOMENA

Usually, density of reservoir fluids flowing in oil and gas wells exceeds that of predicted by thermodynamic equilibrium because the liquid-holdup phenomenon increases the amount of liquids present per elemental unit, such as length, area or volume. This indicates an incomplete separation of the dissolved gas from the liquid phases (oil and brine) when flow through wells is sufficiently rapid so that equilibrium cannot be attained inside the elemental unit at local conditions. Hence, the concentration of dissolved gas remaining in the liquid phases may be different than the concentration dictated by the equilibrium conditions. Consequently, non-equilibrium conditions may induce the holdup of liquids. Liquid holdup observed at steady-state conditions indicates that a meta-stable state prevails so that an apparent incomplete separation of gas has been established along the well permanently (Civan, 2006); (Michel & Civan, 2008a). Proper characterization of liquid holdup is a paramount issue because inaccurate estimation of density leads to an inaccurate prediction of the pressure drop from the bottom-hole to the wellhead. In spite of vast amounts of efforts, however, the

nature and mechanism of the liquid holding-up process for vapor/liquid mixtures flowing in close channels is not well-understood.

A gas-transfer takes place from the liquid phases to the gas phase as the reservoir fluid flows along a producing well. Because the liquid and gas phases are flowing in a closed environment, retardation in the gas-transfer may induce a holdup of the liquids. Retardation in the process of gas-exchange between the liquid phases, such as oil and water, and the gas phase occurs as a result of the relatively slow diffusion of the dissolved gas molecules (Rasmussen & Civan, 2009) or flashing of vapors which leads to an incomplete gas separation. Rapid flow conditions do not allow sufficient time for complete separation of gas from liquids to their equilibrium amounts.

Further, it was observed experimentally that immiscible flow of vapor and liquid also yields a holdup of liquid under favorable conditions (Faghri & Zhang, 2006); (Rasmussen & Civan, 2009). Thus, holdup in oil wells is not necessarily caused by the gas-transfer process alone.

Another means for inducing liquid holdup is the pull effect exerted by the gravity on the liquids in which case droplets fall through the gas phase. Liquid holdup may also occur because of raising bubbles driven upward by the buoyancy effect through the liquid phase. All methods of liquid holdup prediction describing these phenomena are based on empirical correlations that breaks the flow to different flow regimes (Ansari, Sylvester, Sarica, Shoham, & Brill, 1994); (Asheim, 1986); (Ayala & Adewumi, 2003) (Aziz, Govier, & Fogarasi, 1972); (Cazaraez-Candia & Vásquez-Cruz, 2005);

(Chierici, Ciucci, & Sclocchi, 1974); (Hagedorn & Brown, 1965); (Ros, 1961); (Beggs & Brill, 1973); (Gray, 1978).

The conventional approach alleviates the difficulty of working with two liquid phases in the wellbore hydraulics modeling by grouping the oil and brine phases into one pseudo-liquid phase. Moreover, empirical correlations are applied to the gas and liquids fractional flow for predicting the prevailing flow pattern so that the corresponding empirical correlation is applied for estimating liquid holdup. Conversely, this study attempts at modeling of the individual gas separation processes associated with the oil and water phases, and their relevant parameters, such as the relaxation time and liquid holdup. Additionally, the three-phase flow model developed here adequately avoids the need to break the flow to different flow regimes.

3.4. MODELING WELLBORE HYDRAULICS IN WELLS FOR HOMOGENEOUS FLUIDS

The present modeling approach has been developed in various previous studies (Michel, 2007) ; (Michel & Civan, 2008a); (Michel & Civan, 2009a). This modeling considers the reservoir fluid as a homogenous mixture of its constituent phases. This means that the properties of reservoir fluids, such as pressure, temperature and density, are averaged over the wellbore cross-sectional area. Consequently, the reservoir fluid is treated as a one single multiphase pseudo-fluid and all its other properties are determined using the well-known correlations (Brill & Mukherjee, 1999); (Lee & Wattenbarger, 2004) by knowing pressure, temperature and other relevant properties.

Hence, the species contained inside the reservoir fluid are referred to as the gas, oil, and water pseudo-components.

Consider the flow of reservoir fluids occurring at the steady-state regime in wells operating under prescribed production conditions. When retardation in gas transfer causes the various phases to flow at different velocities, the fluid transport can be modeled by equations 2-40, 2-48 and 2-49. However, all time derivatives are dismissed due to the steady-state condition. The wall shear stress and the wall heat transfer are included as sink/source terms in order to take in account the effect of the surroundings. Summarizing the recommendations of the studies given in the literature review, the conservation laws can be formulated as:

$$\frac{\partial}{\partial l}(\rho v) = 0 \qquad (3\text{-}1)$$

$$0 = -\frac{\partial P}{\partial l} - \rho g \sin\varphi - \tau_w \qquad (3\text{-}2)$$

$$\rho u \frac{\partial h}{\partial l} - u \frac{\partial P}{\partial l} = u\tau_w - Q_w \qquad (3\text{-}3)$$

In this conventional approach, the wall shear stress, wall heat transfer and Joule-Thompson coefficient are determined by equations 3-4, 3-5 and 3-6, respectively:

$$\tau_w = \frac{1}{2}\frac{f_M}{D}\rho v^2 \qquad (3\text{-}4)$$

$$Q_w = \frac{4U}{D}(T - T_s) \quad \text{(3-5)}$$

$$\eta = -\frac{1}{c_p}\left[\frac{1}{\rho} + \frac{T}{\rho^2}\left(\frac{\partial \rho}{\partial T}\right)_P\right] \quad \text{(3-6)}$$

where D is constant internal diameter, f_M is Moody's friction factor, U is overall heat-transfer coefficient and T_s is surroundings temperature. The surroundings medium temperature is assumed to vary along the vertical direction (gravity direction) with a constant gradient, referred to as geothermal gradient (α_G).

$$T_s = T_{s0} + \alpha_G l \quad \text{(3-7)}$$

Here, T_{s0} is the surroundings temperature at zero depth (surface). It extends from the surrounding temperature at the wellhead to the reservoir temperature. Then, the geothermal gradient is approximated linearly by knowing the reservoir temperature (T_N) as:

$$\alpha_G = \frac{T_N - T_{s0}}{L} \quad \text{(3-8)}$$

Because steady-state conditions are assumed, the mass flow-rate $\dot{m}$ of the reservoir fluid remains constant along the pipe length and the mass flow rate is expressed by:

$$\dot{m} = \dot{V}_g^s \rho_g^s + \dot{V}_o^s \rho_o^s + \dot{V}_w^s \rho_w^s \quad \text{(3-9)}$$

where is ρ_g the gas density, ρ_o is the oil density, ρ_w is the brine density and $\dot{V}_g$ is gas flow rate, $\dot{V}_o$ is oil flow rate, $\dot{V}_w$ is brine flow rate. The superscript *s* denotes these properties are taken at standard conditions.

By introducing equations 2-17, 3-4, 3-5, 3-6 and 3-9 into equations 3-1, 3-2, 3-3, the following set of equations describes the flow conditions for a pipe with constant diameter and cross-sectional area *A*.

$$\rho v = \frac{\dot{m}}{A} \qquad (3\text{-}10)$$

$$\frac{dP}{dl} = -\frac{1}{2}\frac{f_M}{D}\rho v^2 - \rho g \sin\varphi \qquad (3\text{-}11)$$

$$\frac{dT}{dl} = -\frac{T}{\rho}\left(\frac{\partial \rho}{\partial T}\right)_P \frac{dP}{dl} + \frac{1}{2}\frac{f_M}{c_p D}v^2 - \frac{v}{u}\frac{U\pi D}{\dot{m} c_p}(T - T_s) \qquad (3\text{-}12)$$

subject to the following surface fluid conditions:

$$\rho = \rho_0 \qquad l = 0 \qquad (3\text{-}13)$$

$$P = P_0 \qquad l = 0 \qquad (3\text{-}14)$$

$$T = T_0 \qquad l = 0 \qquad (3\text{-}15)$$

where ρ_0, P_0 and T_0 are the density, pressure and temperature at the surface, respectively. The conservation laws of mass, momentum, and energy are represented by equations 3-10, 3-11, and 3-12, respectively. Then, the reservoir fluid pressure, temperature, and density become the unknown variables. The elemental unit of this model is the cross-sectional area of the pipe. For this reason, the change in pressure and temperature is described along the pipe length and not with respect to the vertical depth. In addition, the fluid pressure, temperature, velocity, and density are averaged across the elemental cross-sectional unit.

3.5. MODELING LIQUID HOLDUP FOR OIL/BRINE/GAS SYSTEMS

The homogenous model presented in the previous section is able to represent non-equilibrium conditions. Liquid holdup phenomenon is an indicator of non-equilibrium among various phases. In particular, the origin of the phase non-equilibrium is attributed in to the velocity difference among phases (Michel, 2007).

The set of equations 3-10, 3-11, 3-12 and 3-18 forms a closed system if the initial conditions are known. In such closed system, the various phases are assumed to have the same pressure and temperature as the mixture. However, the velocity of the phases and the mixture velocity are allowed to be different from each other since this phenomenon was observed experimentally. The velocities of the various phases differ significantly and the void fraction decreases when liquid holdup occurs. At liquid holdup conditions, mixture density is greater than the value expected using flash

calculations and the gas moves at a velocity much greater than the velocities of the liquid phases.

In order to facilitate the determination of the mixture density at liquid holdup conditions, a reservoir fluid is conventionally defined as a system of one single multiphase-fluid having the gas and liquids as the phases. In this study, gas, oil and water phases compound the multiphase system. Following the scheme presented in equation 2-20, the cross-sectional area-averaged density of a gas/oil/brine system is defined as:

$$\rho = \rho_g H_g + \rho_o H_o + \rho_w H_w \quad \text{(3-16)}$$

Similarly, the volumetric fractions adhere to equation 2-8:

$$H_g + H_o + H_w = 1 \quad \text{(3-17)}$$

Thus, the fluid density is expressed as a volume-fraction weighted average of the individual phase densities having the volumetric fractions of each phase acting as the weights. The volumetric fraction of the gas, oil and water phase are referred to as the void fraction (H_g), oil holdup (H_o) and brine holdup (H_w), respectively. Conversely, in the conventional approach, the multiphase system density is expresses in terms of void fraction and a liquid holdup where the liquid holdup lumps the oil and water holdup altogether.

Nevertheless, the equivalent area-averaged density stated by equation 2-11 is preferred in this study because the wellbore hydraulics is modeled in terms of the mass fraction of the phases in the current application.

$$\frac{1}{\rho} = \frac{X_g}{\rho_g} + \frac{X_o}{\rho_o} + \frac{X_w}{\rho_w} \quad \text{(3-18)}$$

where X_g is the gas mass fraction, X_o is the oil mass fraction and X_w is the water mass fraction. The mass fractions abide by equation 2-7:

$$X_g + X_o + X_w = 1 \quad \text{(3-19)}$$

Thus, the inverse of the fluid density is used as the weighted average of the inverse of the phase densities having the mass fraction of each phase as the weights.

The velocity of the various phases in expressed in a manner that the mass flow-rate of the mixture remains constant. Therefore, the velocity of a phase is defined as the ratio of the volumetric flow-rate of that phase to the cross-sectional area occupied by that phase. Thus, the following expressions can be written:

$$v_g = \frac{\dot{V}_g}{AH_g} \quad \text{(3-20)}$$

$$v_o = \frac{\dot{V}_o}{AH_o} \quad \text{(3-21)}$$

$$v_w = \frac{\dot{V}_w}{AH_w} \quad (3\text{-}22)$$

where v_g is gas velocity, v_o is oil velocity and v_w is brine velocity. The void fraction, oil holdup and brine holdup are related to the respective mass fraction as stated by equation 2-10:

$$H_g = \frac{\rho}{\rho_g} X_g \quad (3\text{-}23)$$

$$H_o = \frac{\rho}{\rho_o} X_o \quad (3\text{-}24)$$

$$H_w = \frac{\rho}{\rho_w} X_w \quad (3\text{-}25)$$

The density and volumetric flow-rate of the various phases can be estimated by applying proper correlations (Brill & Mukherjee, 1999); (Lee & Wattenbarger, 2004), when knowing the standard flow rate of each phase, local pressure, local temperature and other relevant constant properties, such as gas gravity, oil gravity, salinity (Michel, 2007).

3.6. CHARACTERIZATION OF THE EQUILIBRIUM STATE

The state of equilibrium for flowing multi-phase fluids implies that the velocities of the various phases are equal to the average mixture velocity (Michel & Civan, 2009a). Hence, this uniform velocity is the same as the volumetric flux. Under these

circumstances, neither liquid holdup nor retardation in gas transfer is expected (Michel, 2007). Consequently, the mixture density becomes equal to the ratio of the mass flow-rate to the volumetric flow-rate which can be obtained from flash calculations. Thus, the mixture density is calculated directly if the temperature and pressure are known. Therefore, the set of equations 3-10, 3-11 and 3-12 becomes a closed system of equations without the need of a liquid holdup model of equation or any other density formulation.

For the current application, the mass fraction of the various phases at equilibrium is formulated as the following:

$$X_g^E = \frac{\rho_g \dot{V}_g}{\dot{m}} \quad \text{(3-26)}$$

$$X_o^E = \frac{\rho_o \dot{V}_o}{\dot{m}} \quad \text{(3-27)}$$

$$X_w^E = \frac{\rho_w \dot{V}_w}{\dot{m}} \quad \text{(3-28)}$$

$$X_g^E + X_o^E + X_w^E = 1 \quad \text{(3-29)}$$

where the superscript *E* denotes the equilibrium state. Any mixture at meta-stable state will tend to attain this equilibrium state upon a change or disturbance induced on the meta-stable conditions.

3.7. ESTIMATING LIQUID HOLDUP FOR GAS/LIQUID SYSTEMS

In the conventional approach, the oil and brine phases are combined into one liquid phase. Therefore, the oil and brine phases are assumed to flow at the same area-averaged velocity v_L together as one liquid volumetric fraction H_L. For this type of system, the density can be defined as:

$$\rho = \rho_g (1 - H_L) + \rho_L H_L \quad \text{(3-30)}$$

$$v_L = \frac{\dot{V}_L}{A H_L} \quad \text{(3-31)}$$

where is $\dot{V}_L$ liquid flow rate.

Then, the closed system of equations given by the set of equations 3-10, 3-11, 3-12 and 3-30 can be solved if the liquid holdup can be determined. The liquid holdup can be calculated if the slip ratio is known (Michel, 2007); (Michel & Civan, 2008b); (Michel & Civan, 2008c):

$$H_L = \frac{\lambda f_L}{1 + (\lambda - 1) f_L} \quad \text{(3-32)}$$

where the slip ratio λ and liquid fractional flow f_L are defined as:

$$\lambda = \frac{v_g}{v_L} \quad \text{(3-33)}$$

$$f_L = \frac{\dot{V}_L}{\dot{V}} \quad (3\text{-}34)$$

and $\dot{V}$ is the total flow rate.

Non-equilibrium occurs when the gas and liquid velocities differ from each other (Michel, 2007). Consequently, the slip ratio is a good indicator of the degree of deviation from equilibrium conditions of the local metastable state. A system is said to be at non-equilibrium conditions when the local slip ratio is not equal to the unity.

In this study, theoretical basis is given to a previously proposed quadratic relationship between slip ratio and liquid fractional flow. This relationship is based on the fundamentals of entropy theory. Whether a fluid is in liquid state can be estimated from the basic definition of entropy based on the probability associated with the liquid state is the liquid fractional flow:

$$\Pi = -f_L \log_a f_L - (1 - f_L)\log_a (1 - f_L) \quad (3\text{-}35)$$

where *a* is the base of the logarithms and can take any positive value. If the uncertainty or level of disorganization is defined as the difference between the slip ratio and the unity, then the following relationship is obtained:

$$\lambda - 1 = -f_L \log_a f_L - (1 - f_L)\log_a (1 - f_L) \quad (3\text{-}36)$$

Therefore, a complete organized gas/liquid system is defined as a system in equilibrium where the slip ratio is equal to the unity. The relationship described in this equation can be approximated by the quadratic expression:

$$\lambda - 1 = f_L(1 - f_L)\log_a 16 \quad \text{(3-37)}$$

Based on the previous slip ratio formulation, an approximation in the form of a quadratic equation can be given empirically by (Michel & Civan, 2009a):

$$\lambda = 1 + \frac{\lambda_0 - 1}{f_{L0} - f_{L0}^2} f_L - \frac{\lambda_0 - 1}{f_{L0} - f_{L0}^2} f_L^2 \quad \text{(3-38)}$$

where λ_0 and f_{L0} represent the slip ratio and the liquid fractional flow at some reference state, respectively. Here, the chosen reference state is the well-head conditions because measurements are usually taken at this location.

3.8. A TECHNIQUE FOR SIMULATION OF LIQUID HOLDUP

An iterative backward scheme that was previously developed elsewhere (Michel, 2007); (Michel & Civan, 2008a) is applied for executing the simulation of liquid holdup. The upward flow of reservoir fluids inside a production pipe at steady-state conditions is considered. In this scheme, the production pipe is segmented into several partitions so that finite difference methods can be applied.

The fluid properties are calculated segment by segment and counter-flow, from outlet (surface) to the inlet (bottom-hole). The algorithm of this scheme is detailed in figure 3-1. The main procedures are elaborated in the following paragraphs.

Input Data. A set of known properties are necessary in order to calculate the gas, oil and brine individual properties, such as density, viscosity, compressibility, z-factor, bubble-point pressure, gas solubility, etc., as well as other relevant properties, such as Moody friction factor, over-heat transfer coefficient, etc. Also, additional data is needed only for the purpose of executing the simulation. All of the required data is listed as follows:

- Flow rate at standard conditions: gas, oil and brine
- Compositional: Gas gravity, oil gravity and brine Salinity
- Pipeline: length, diameter, roughness and inclination
- At the wellhead: surface pressure and temperature
- At the bottom-hole: flowing pressure and reservoir temperature
- Incremental length

Local properties. The input data and the constants facilitate the calculation of the local properties for each segment of the partitioned production pipe. Depending on the local pressure, the properties are calculated either below bubble-point or above bubble-point. Above the bubble-point, the liquid holdup is set equal to the unity since there is no gas phase.

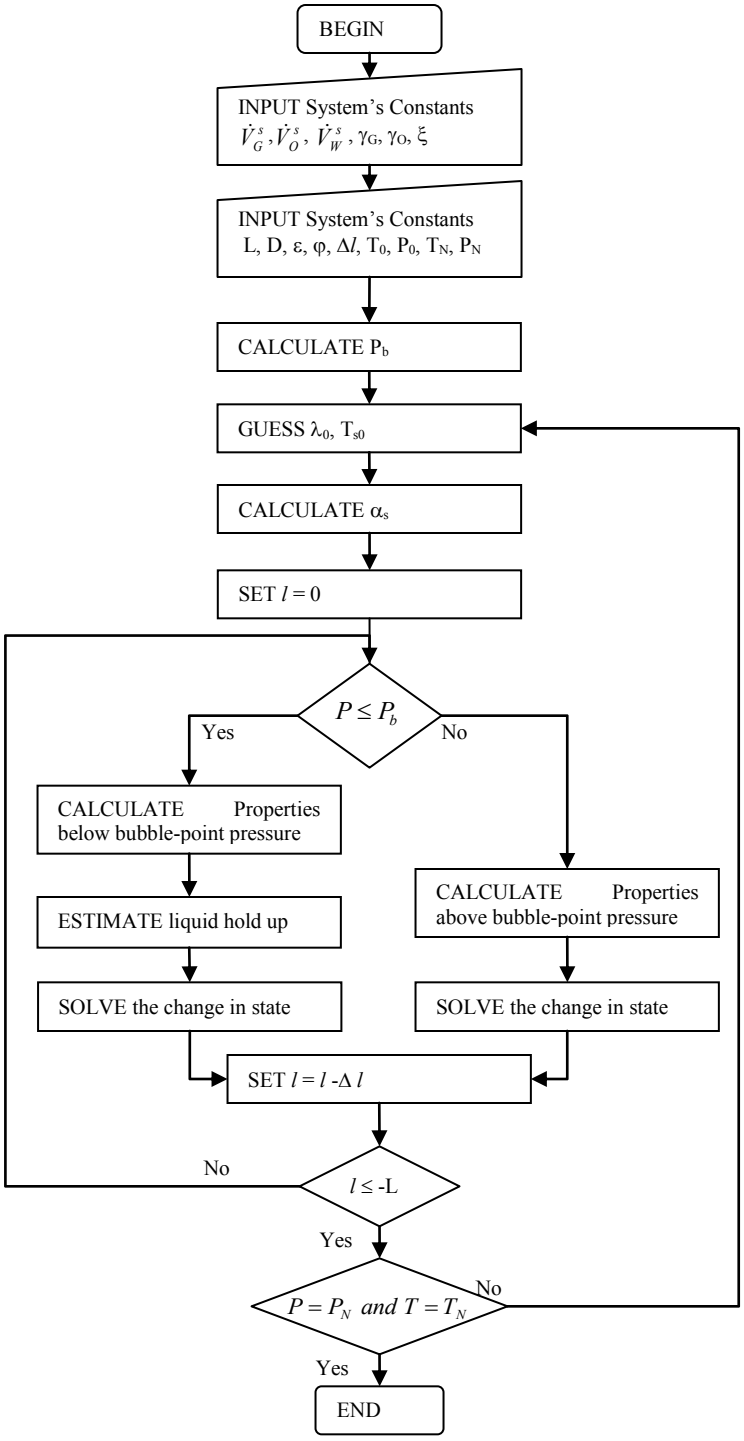

Figure 3-1: Flowchart for liquid holdup simulation

Relevant Constants. The simulation procedure demands the calculation of two constants: the bubble-point pressure and the geothermal gradient.

Change of state. The local pressure and temperature of a segment is calculated in base of the local pressure and temperature of the previous segment. At steady-state conditions, equations 3-2 and 3-3 can be solved numerically by applying the fourth order of the Runge-Kutta methods (Chapra & Canale, 1998).

Guessed parameters. The surface pressure and temperature are input parameters. Nevertheless, the surface density of the mixture is also needed in order to solve the change of state. The mixture density is obtained by estimating the slip ratio as described in section 3.7. Consequently, the surface slip ratio is required as initial conditions besides the surface pressure and temperature. Moreover, the surface surroundings temperature is also required in order to estimate the geothermal gradient. The geothermal gradient is required for computing of the heat loss towards the surroundings. Thus, both the surface slip ratio and the surroundings temperature need to be guessed since their values are not commonly measured. A valid set of guesses is determined by satisfying the convergence criteria.

Convergence Criteria. An incorrect guess of the slip ratio at the wellhead and the surroundings temperature lead to an inlet fluid pressure and temperature different than the bottom-hole flowing pressure and reservoir temperature, respectively. A valid solution is accomplished when the absolute value of these differences are less than a tolerable error.

3.9. MODELING RELAXATION OF VAPOR (GAS) SEPARATION

In nature, the relaxation on vapor separation from liquid phases takes place by various mechanisms. Two forms of coexistence of vapor and liquid phase in meta-stable state are considered here as described in this section.

Rapid separation of a vapor phase from a flowing fluid (flashing) causes a meta-stable state where the liquid phase becomes a super-heated liquid. When the gas nucleation happens rapidly while the fluid flows inside a conduit, the interface mass-transfer is delayed by superficial tension and capillary force effects (Badur & Banaszkiewicz, 1998). Consequently, the liquid surrounding each gas bubble would have a mass fraction greater than the expected equilibrium value at the prevailing temperature.

A differential equation for flashing fluids through capillary tubes is shown next (Bilicki & Kestin, 1990). This equation is the result of combining the law of mass conservation applied to the gas phase with the expression of the rate of gas transfer from the liquid phase to the vapor phase:

$$v\frac{\partial X_g}{\partial l} = -\frac{X_g - X_g^E}{\theta} \qquad (3\text{-}39)$$

where the change in the gas mass fraction with respect to a conduit length is directly proportional to the deviation from equilibrium. Subsequently, a correlation was developed for the relaxation time θ applicable to water/steam mixtures (Downar-

Zapolski, Bilicki, Bolle, & Franco, 1996). This correlation uses various dimensionless parameters involving the mixture pressure and temperature.

However, it was demonstrated that the model stated by 3-39 is applicable only for isobaric processes, and, the following model was proposed (Feburie, Goit, Granger, & Seyhaeve, 1993):

$$\frac{\partial}{\partial l}\left(X_g - X_g^E\right) = -\frac{X_g - X_g^E}{\theta} \quad \text{.....(3-40)}$$

where the relaxation time θ is a function of various dimensionless parameters involving the mixture pressure and temperature.

Another means of relaxation on vapor separation in nature occurs by gas diffusion. When a flowing fluid at a meta-stable state is allowed to come to rest, the gas and liquid phases tend to attain an equilibrium state. However, the transition from meta-stable to equilibrium states is not an instantaneous process. Moreover, the relaxation effect on fluid hydraulics in oil and gas wells was demonstrated to be significant (Civan, 2006).

Gas diffusion is described by the Fick's law which states mass-transfer occurs in the direction from the higher to lower concentration media. the following differential equation was proposed (Walas, 1991) for a stagnant fluid undergoing an isothermal separation of a vapor phase:

$$\frac{\partial C_D}{\partial t} = D_f \frac{\partial^2 C_D}{\partial l^2} \quad \text{(3-41)}$$

$$C_D = \frac{C - C^E}{C^E - C^0} \quad \text{(3-42)}$$

where the dimensionless-concentration C_D is expressed as a function of the concentration of vapor species C dissolved in the liquid phase and the diffusion coefficient D_f is assumed constant. This model has been demonstrated to be applicable to reservoir fluids (Jawed, 2006); (Ogundare, 2004); (Rasmussen & Civan, 2009).

3.10. DISSOLVED GAS DIMENSIONLESS-CONCENTRATION MODEL FOR HOMOGENOUS OIL/GAS SYSTEMS

In this study, the oil holdup is modeled as an apparent deviation from equilibrium of the concentration of the gas pseudo-component dissolved in the oil phase for a Gas/Oil system. Because there is neither a water phase nor a water pseudo-component present, the actual (C_o) and equilibrium (C_o^E) concentrations of the gas pseudo-component dissolved in the oil phase can be described as:

$$C_o = \frac{\rho}{H_o}\left(X_g^0 - X_g\right) \quad \text{(3-43)}$$

$$C_o^E = \frac{\dot{m}}{\dot{V}_o}\left(X_g^0 - X_g^E\right) \quad \text{(3-44)}$$

$$X_g^0 = \frac{\rho_g^s \dot{V}_g^s}{\dot{m}} \quad \text{(3-45)}$$

where the reference condition X_g^0 is the same as the standard condition (1 atm and 60^{o}F or 15.5^{o}C). Thus, the above-described concentration C_o is equal to zero at the reference conditions because the measurements at standard conditions are taken upon complete separation of gas. Then, the dimensionless-concentration is expressed by combining equations 3-19, 3-24, 3-27, 3-29, 3-43, 3-44 and 3-45.

$$C_{oD} = \frac{\left(1 - X_g^E\right)\left(X_g^0 - X_g\right)}{\left(1 - X_g\right)\left(X_g^0 - X_g^E\right)} - 1 \quad \text{(3-46)}$$

3.11. A CONSTITUTIVE EQUATION FOR DISSOLVED GAS DIMENSIONLESS-CONCENTRATION

It is not clear if the holdup of the liquids for flowing reservoir fluids is due to mechanism of inducing non-equilibrium such as by gas diffusion, flashing, gravity pull, etc. Nevertheless, the formulations describing these mechanisms are approximated by correlations in the conventional approach for modeling the holdup phenomenon.

Most holdup models rely on the assumption that the gravity pull on the liquids is the driving mechanism. The flow is classified according to the magnitude of the volumetric flux of the gas and liquids. However, this type of modeling leads to discontinuities that renders this approach inconsistent. Therefore, the conventional approach is not adopted. In this section, the liquid holdup is described by a relaxation in the concentration of gas dissolved in liquid phases.

Table 3-1: Data of the vertical oil-wells

Case	γ_o	$\dot{V}_G^s$	$\dot{V}_W^s$	$\dot{V}_O^s$	P_0	D	T_0	T_N	γ_g	ξ	L	P_N
		[Mscf/day]	[stb/day]	[stb/day]	[psia]	[in.]	[ºF]	[ºF]		[wt%]	[ft.]	[psia]
8	0.9826	231.8	110.1	1100.7	589.3	5.0	107.6	226.4	1.268	3.00	10171	4546.8
22	0.8236	180.7	0.000	191.8	1370.3	2.875	92.1	167.0	0.750	0.0	8038	3568.5
23	0.8236	311.7	0.000	330.8	1341.9	2.875	89.6	167.0	0.750	0.0	8038	3503.1
24	0.8236	452.7	0.000	480.5	1306.4	2.875	89.4	167.0	0.750	0.0	8038	3430.7
25	0.8236	1060.7	0.000	1125.9	1171.5	2.875	98.6	167.0	0.750	0.0	8038	3222.0

Determining the mechanism of inducing liquid holdup for producing oil/gas wells requires an estimate of pressure, temperature and quality along the well by some appropriate techniques. Here, pressure, temperature and quality is generated by applying the procedure presented in section 3.8 using the data of reservoir fluid samples 22, 23, 24 and 25 reported in Table 3-1 (Chierici, Ciucci, & Sclocchi, 1974) as input data. These samples exhibit various flow conditions for the same well.

The dissolved gas dimensionless-concentration and its derivative with respect to the pipe length, oil velocity and temperature are computed using the generated data for reservoir fluid samples 22, 23, 24 and 25. When the calculated dimensionless-concentration is plotted against its derivative with respect to the pipe length, a direct proportionality between these two terms in a log-log chart is somewhat observed.

The flow behavior of all reservoir samples showed a slope close to 0.5 indicating a direct proportionality to the square-root of the dimensionless-concentration. The proportionality is improved by multiplying derivative times the velocity of the oil phase. This is consistent to the structure of the reviewed models for the relaxation time. The mixture velocity of the multiphase system was not selected because the dissolved gas is flowing inside the oil phase. Both the diffusivity coefficient and the relaxation time of the dissolved gas are affected by the temperature (Downar-Zapolski, Bilicki, Bolle, & Franco, 1996); (Jawed, 2006). Consequently, further improvement in achieving a linear proportionality is gained when the square root of the dimensionless-concentration is divided by a dimensionless temperature.

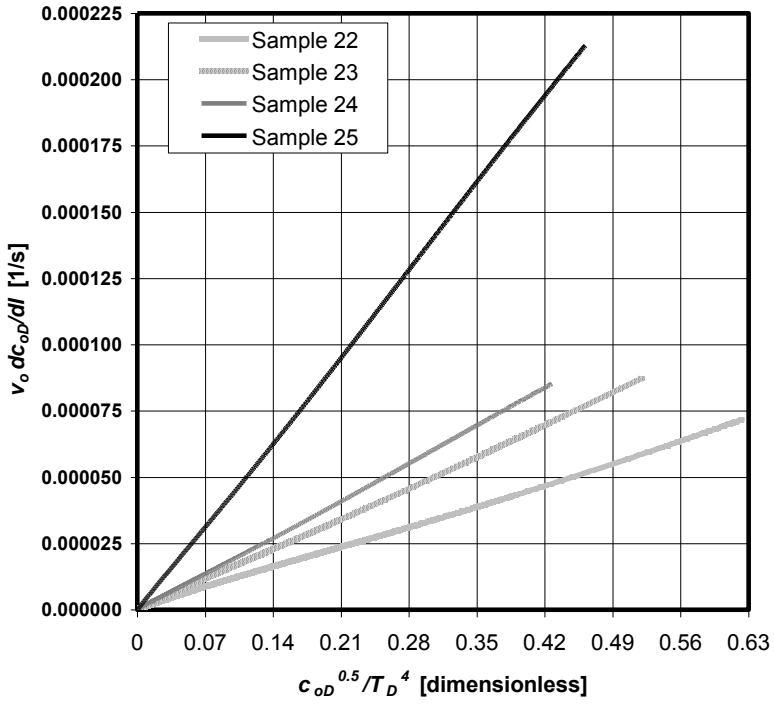

Figure 3-2: Relationship found for the terms of the constitutive equation describing the dimensionless-concentration using generated data based on field data (Chierici, Ciucci, & Sclocchi, 1974)

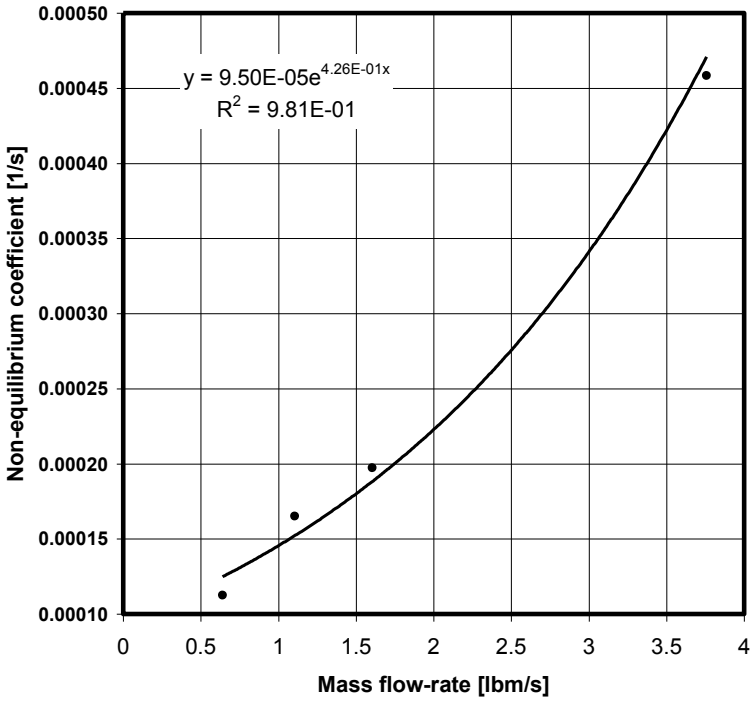

Figure 3-3: Correlation between the calculated non-equilibrium coefficients and the mass flow-rate of the solvent phase

Figure 3-2 shows a direct proportionality between the product of oil velocity times the derivative of dissolved gas dimensionless-concentration with respect length and the ratio of the square root of the dissolved gas dimensionless-concentration to the fourth power of the dimensionless temperature. The constant of proportionality is referred to as the non-equilibrium coefficient here. Thus, the following constitutive equation is proposed when liquid holdup is present:

$$v_o \frac{dC_{oD}}{dl} = \kappa \frac{\sqrt{C_{oD}}}{T_D{}^4} \qquad (3\text{-}47)$$

$$T_D = \frac{T}{T_{wh}} \qquad (3\text{-}48)$$

This constitutive equation applies the effect of relaxation to the dissolved gas concentration. Therefore, it can be defined as a combination of the diffusion model described by equation 3-41 and the relaxed model stated by equation 3-40.

A fairly good correlation is found between the non-equilibrium coefficient and the mass flow-rate of the solvent (oil pseudo-component) as shown in Figure 3-3. The resulting correlation is given as follows:

$$\kappa = 9.50 \times 10^{-5} e^{0.426 \dot{m}_L} \quad \text{.....(3-49)}$$

3.12. A TECHNIQUE FOR SIMULATING KINETICS OF GAS SEPARATION

An iterative forward scheme is presented for executing the simulation of the upward flow of reservoir fluids having gas, oil and brine as its phases. Here, the production pipe is segmented and finite difference methods are applied. The algorithm of this scheme is detailed in figure 3-4. For gas/oil systems the same scheme is applied by setting the brine dimensionless concentration equal to zero. The procedures *Input Data*, *Relevant Constants* and *Change of State* are the same as described in the previous section. The changes to the other procedures are detailed in the following.

Convergence Criteria. A valid solution is accomplished when the dissolved gas dimensionless-concentration of water and oil phases at the surface leads to zero dimensionless concentrations at the bubble-point conditions, and, the surface surroundings temperature leads to an inlet fluid temperature equal to the reservoir temperature.

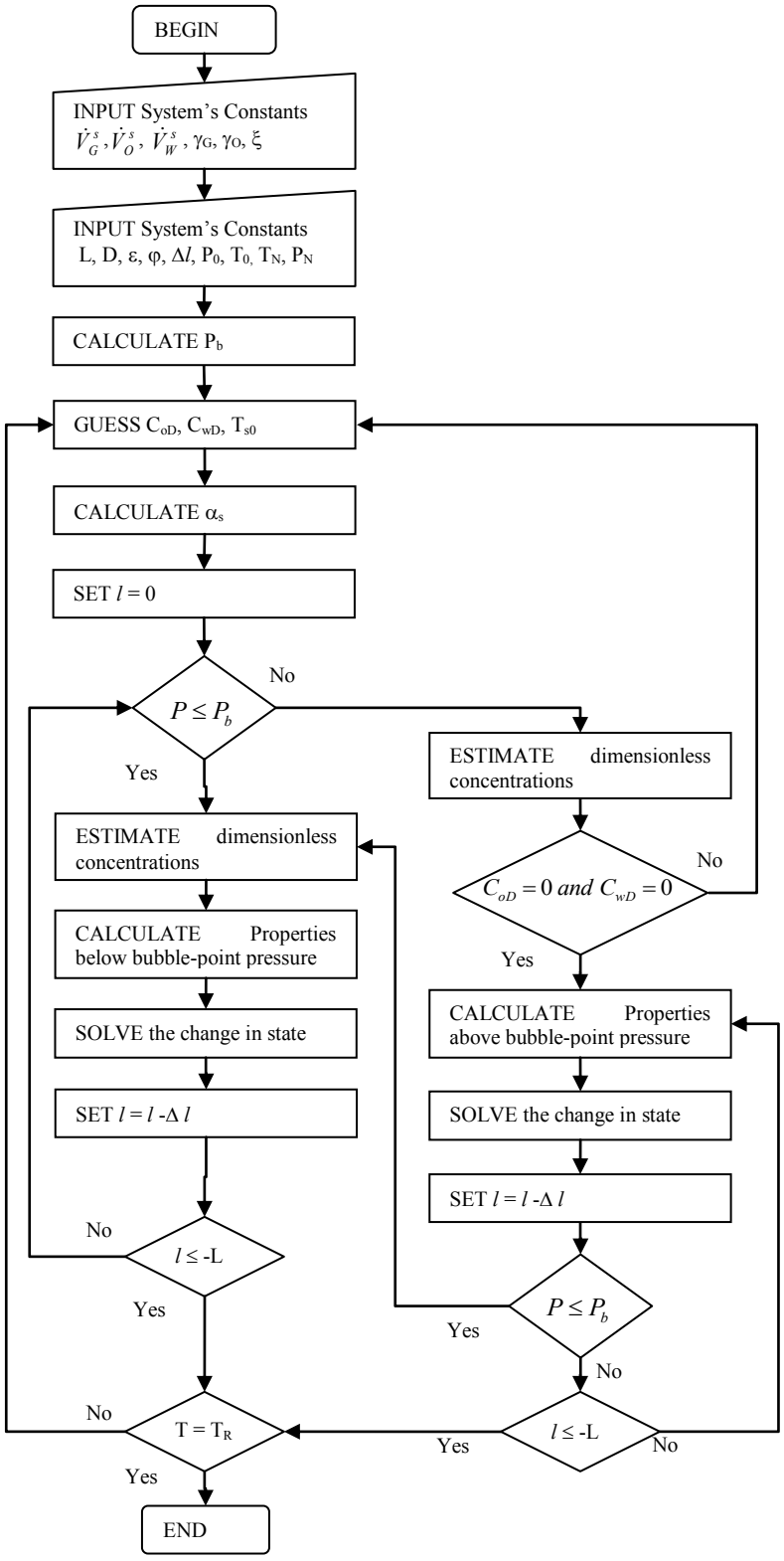

Figure 3-4: Flowchart for simulation of kinetics of gas separation

Local properties. Above the bubble-point, the dissolved gas concentrations are set equal to zero since there is no gas phase.

Guessed parameters. The mixture density is obtained by estimating the dissolved gas dimensionless-concentration of water and oil phases as described in section 3.10. Consequently, these concentrations at the surface are required as initial conditions besides the surface pressure and temperature. Thus, these concentrations at the surface and the surroundings temperature need to be guessed since their values are not commonly measured. A valid set of guesses is determined by satisfying the convergence criteria.

3.13. VALIDATION TO OIL/GAS SYSTEMS

The dimensionless-concentration model presented here for oil/gas systems consists on the set of equations 3-10, 3-11, 3-12 and 3-47. The bottom-hole pressure is estimated by applying this model to the fluid samples 22, 23, 24 and 25 in order to validate the proposed constitutive equation for the dissolved gas dimensionless-concentration.

A numerical scheme is devised for solving the resulting system of differential equations. This iterative procedure and its numerical-simulation flow chart are presented in section 3.12. The surroundings temperature and the dimensionless-concentration at the wellhead are adjusted until the convergence criteria are attained. These adjusted values are shown in Table 3-2. Note that the gas mass-fraction is determined if the dimensionless-concentration is known as stated in equation 3-46.

Consequently, the mixture density is determined with the definition given by equation 3-18. Thus, the model attains a closure under these conditions.

After convergence, the resulting bottom-hole pressure is accepted as a good estimation. The estimated pressure at the bottom-hole and the error in percentage for all four samples are reported in Table 3-2. The error of the model prediction is set as the ratio of the difference between the estimated pressures obtained using the dimensionless-concentration model and the actual pressure to the difference between the actual pressure and the estimated pressure assuming equilibrium in percentage where all three pressures are taken at the bottom-hole conditions. These properties are reported in Table 3-2 as well the calculated non-equilibrium coefficient.

Table 3-2: Data relevant to the Dimensionless-concentration model

Sample		22	23	24	25
A) Actual Pressure at Bottom-hole	[psia]	3569	3503	3431	3222
B) Estimated Pressure at Bottom-hole	[psia]	3581	3493	3428	3227
C) Equilibrium Pressure at Bottom-hole	[psia]	3481	3442	3389	3169
D) Percentage Error*	[%]	14.3	-17.1	-7.5	9.4
E) Non-equilibrium Coefficient	[s^{-1}]	1.248×10^{-4}	1.521×10^{-4}	1.882×10^{-4}	4.709×10^{-4}
F) Initial Surroundings Temperature	[°F]	79.3	72.5	68.2	67.8
D) Initial Gas Mass-Fraction	[%]	4.37	6.54	7.29	8.08

* $D = (B - A)/C$

3.14. DISSOLVED GAS DIMENSIONLESS-CONCENTRATION MODEL FOR HOMOGENEOUS OIL/BRINE/GAS SYSTEMS

For oil/brine/gas systems, the gas may be dissolved both in the oil and water phases, but at different amounts. Then, both the oil and the water phases will have the individual dimensionless-concentrations (C_{oD}, C_{wD}) expressed, respectively, by:

$$C_{oD} = \frac{1 - X_o^0 / X_o}{1 - X_o^0 / X_o^E} - 1 \quad \text{(3-50)}$$

$$C_{wD} = \frac{1 - X_w^0 / X_w}{1 - X_w^0 / X_w^E} - 1 \quad \text{(3-51)}$$

where the mass-fractions at the reference state are calculated by:

$$X_o^0 = \frac{\rho_o^s \dot{V}_o^s}{\dot{m}} \quad \text{(3-52)}$$

$$X_w^0 = \frac{\rho_w^s \dot{V}_w^s}{\dot{m}} \quad \text{(3-53)}$$

The constitutive equation for each dimensionless-concentration is defined as:

$$v_o \frac{dC_{oD}}{dl} = \frac{C_{oD}}{\theta_o} \quad \text{(3-54)}$$

$$v_w \frac{dC_{wD}}{dl} = \frac{C_{wD}}{\theta_w} \quad \text{(3-55)}$$

where the relaxation time for each phase (θ_o, θ_w) is formulated as:

$$\theta_o = \frac{1}{\kappa_o} \sqrt{C_{oD}} T_D^{\,4} \quad \text{(3-56)}$$

$$\theta_w = \frac{1}{\kappa_w}\sqrt{C_{wD}}T_D^{\,4} \qquad (3\text{-}57)$$

The non-equilibrium coefficient for the oil and water phases is obtained by designating the mass flow-rate of the oil pseudo-component and water pseudo-component in equation 3-49, respectively.

The model for oil/brine/gas systems consists of the set of equations 3-10, 3-11, 3-12, 3-54 and 3-55. The mass-fraction of each phase is obtained by knowing the dimensionless-concentrations of the oil and gas phases. Having the mass-fraction of the three phases, the mixture density is then determined. Hence, the model properly accomplishes a closure. A numerical scheme is required for solving the resulting system of differential equations. This iterative procedure and its numerical-simulation flow chart are presented in section 3.12.

3.15. VALIDATION TO OIL/BRINE/GAS SYSTEMS

An oil/brine/gas system can be represented as a two-phase system, where the oil and brine are combined either into one single liquid pseudo-phase or treated as a three-phase system, where each pseudo-component constitutes a phase. Typically, the oil and water phases are assumed to flow at the same velocity in all liquid holdup models in the previous studies. Here, we investigate the effect of modeling the oil/brine/gas system as a three-phase fluid in the estimation of the bottom-hole pressure. The fluid sample 8 (Chierici, Ciucci, & Sclocchi, 1974) is selected for simulation. The estimated pressure at the bottom-hole is 4531 psia if equilibrium is assumed.

Applying the two-phase model to this reservoir fluid, the simulation yielded an adjusted gas mass-fraction at the wellhead of 1.20%, an adjusted surroundings temperature at the wellhead of 56.6 °F, a non-equilibrium coefficient of 7.423×10^{-4} s^{-1} and an estimated bottom-hole pressure of 4557 psia. The error is obtained by dividing the difference between the measured and the estimated pressures at the bottom by the difference between the measured and the equilibrium pressures at the bottom. The error in this modeling approach is 63.7%, for example, which is indicates no much improvement from assuming no liquid holdup conditions along the pipe.

Applying the three-phase model to the sample 8, the simulation yielded an adjusted oil mass-fraction at the wellhead of 89.6%, an adjusted water mass-fraction at the wellhead of 8.78%, an adjusted surroundings temperature at the wellhead of 57.8 °F, a non-equilibrium coefficient for the oil phase of 6.146×10^{-4} s^{-1}, non-equilibrium coefficient for the water phase of 1.149×10^{-4} s^{-1} and an estimated bottom-hole pressure of 4548 psia. The error is calculated with the similar procedure as the previous paragraph. The error of this modeling is 5.7% in this case, which is indicates great improvement from assuming no liquid holdup conditions along the pipe. The pressure and temperature profiles corresponding to the two-phase and the three-phase modeling approaches overlaps as demonstrated in Figures 3-5 and 3-6, respectively. In contrast, however, the evolution of the gas phase along the pipe length differs from one modeling approach to the other. The starting mass-fraction and the position where the dissolution ends are also different as depicted in Figure 3-7.

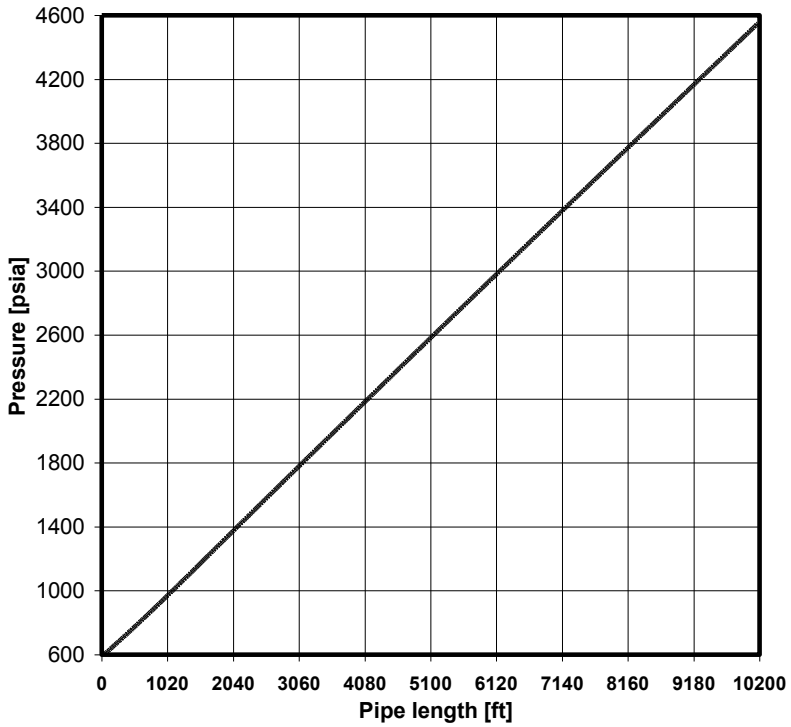

Figure 3-5: Pressure profile for the considered oil/brine/gas system

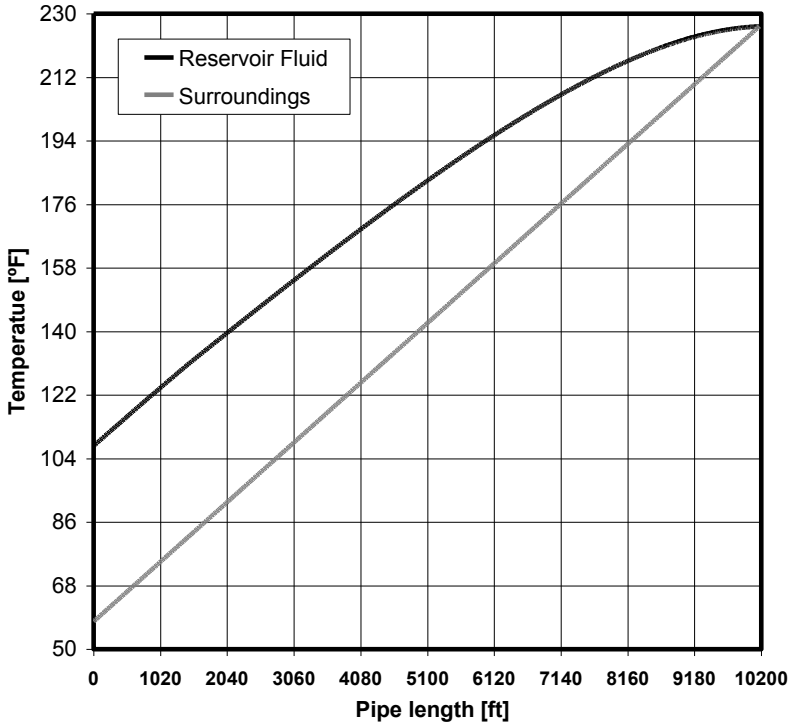

Figure 3-6: Temperature profile for the considered oil/brine/gas system

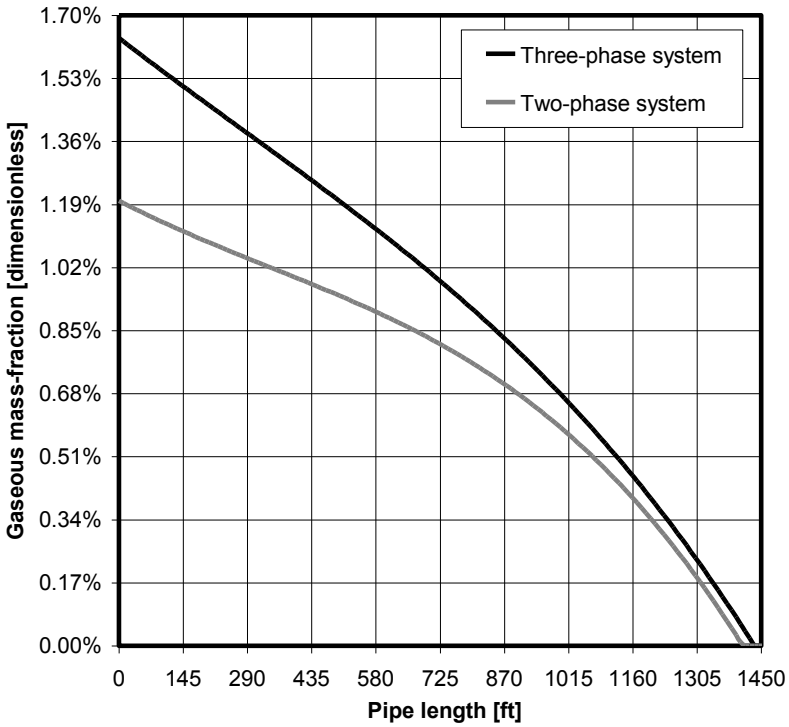

Figure 3-7: Mass-fraction profile of the gas phase for the considered oil/brine/gas system

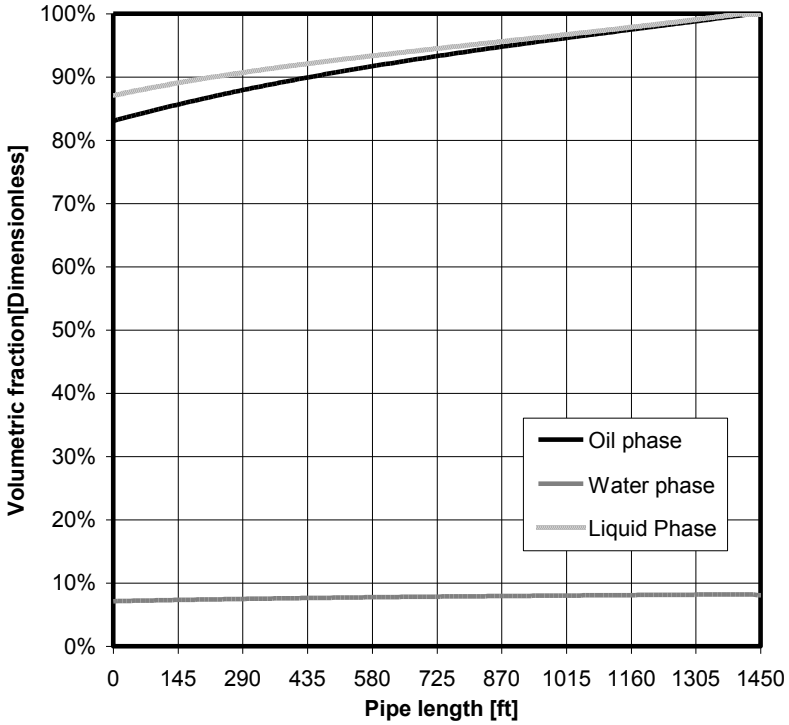

Figure 3-8: Volumetric-fraction profile for the considered oil/brine/gas system

It was expected that the liquid volumetric fraction of the two-phase model would be close to the sum of the oil and water volumetric fractions of three-phase model. However, this was not the case as demonstrated in Figure 3-8. Conceptually, the dissolved gas dimensionless-concentration of the two-phase model should be in between the oil and water dimensionless-concentrations in the three-phase model. However, the two-phase dimensionless-concentration is greater than the oil dimensionless-concentration as delineated in Figure 3-9. Similarly, the relaxation time of the two-phase model is expected to be in between the oil and water relaxation times of three-phase model. However, the two-phase relaxation time is less than the oil relaxation time as delineated in Figure 3-10. One possible explanation for these discrepancies is that oil and water phases are actually flowing at significantly different velocities in contrast to the assumption of equal velocities. The two-phase model lumps the oil and water phases in one pseudo-phase implying both phases are in equilibrium with each other. However, in the three-phase model, the oil and water velocities are almost equal to each other but the gas velocity differs significantly from these velocities. The gas velocity differs even more than the liquid velocity in the two-phase model. The corresponding velocity profiles for the three-phase model and the two-phase model are shown in Figures 3-11 and 3-12, respectively. Therefore, lumping the oil and liquid phases into a single phase fails to adequately describe the liquid holdup phenomenon, dimensionless-concentration, and relaxation time even though the assumption of equal liquid velocities is reasonably satisfied. Consequently, the relaxation in mass transfer from the oil and water phases to the gas phase cannot be represented as a transfer of a lumped phase.

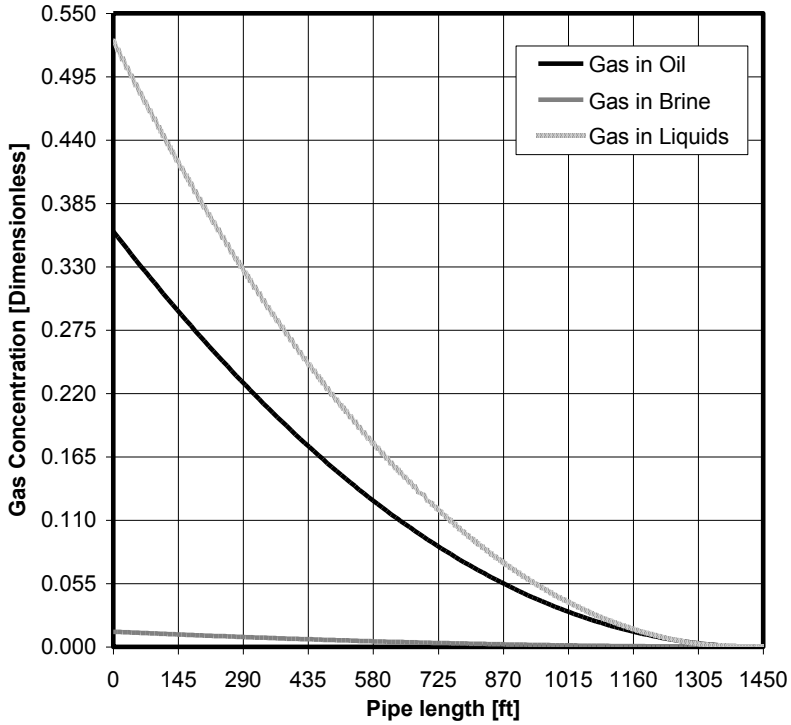

Figure 3-9: Dimensionless-concentration profile for the considered oil/brine/gas system

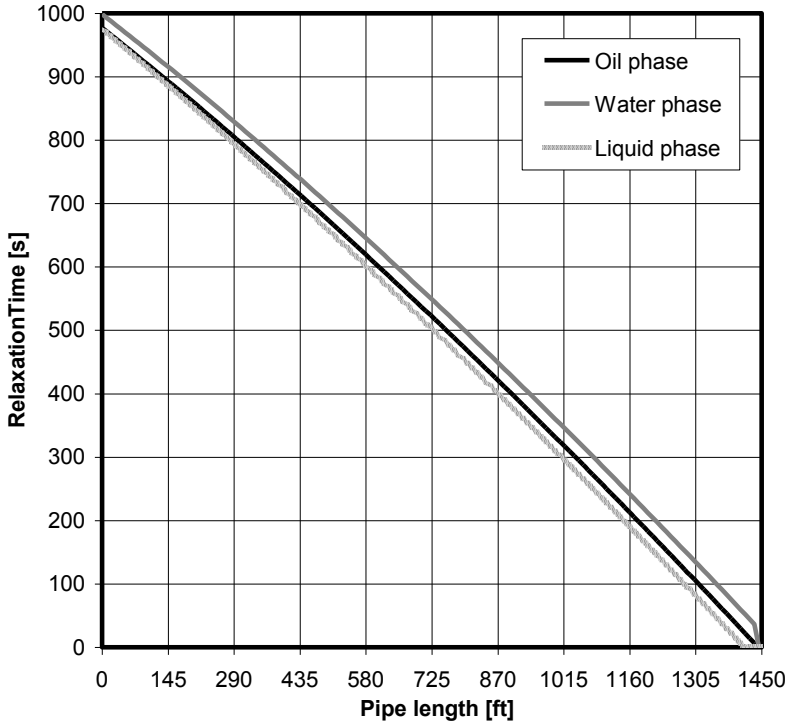

Figure 3-10: Relaxation profile for the considered oil/brine/gas system

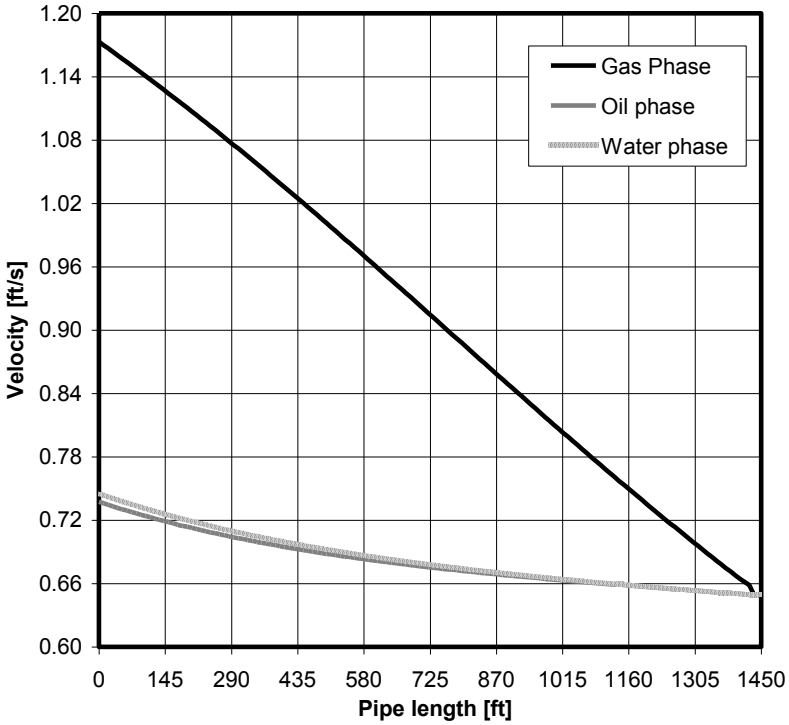

Figure 3-11: Velocity profile for the considered oil/brine/gas system as a three-phase mixture

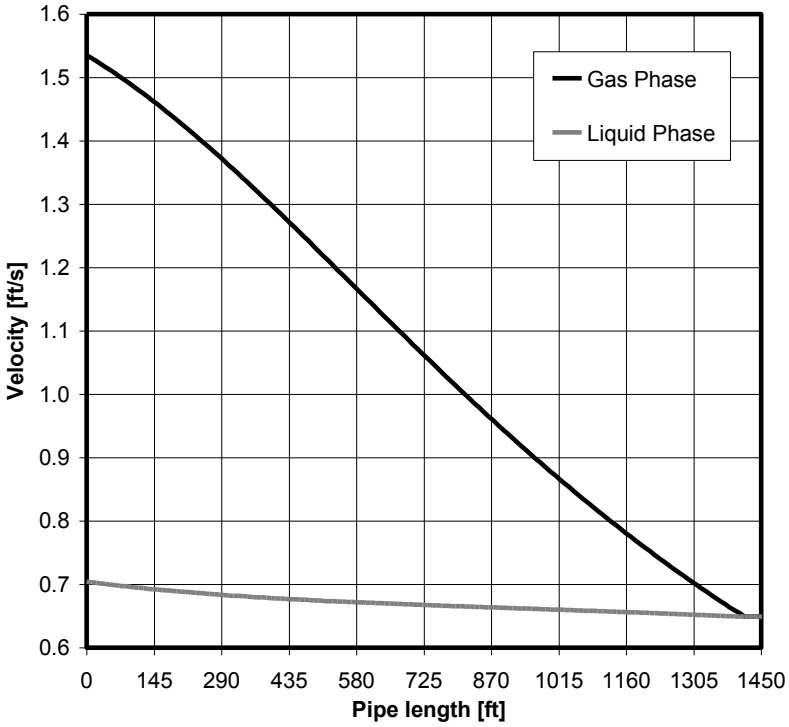

Figure 3-12: Velocity profile for the considered oil/brine/gas system as a two-phase mixture

CHAPTER 4

MODELING THE RHEOLOGY OF COOLING WAX DEPENDENT ON ITS CRISTALLIZATION KINETICS

4.1. OVERVIEW

A summary of the more relevant characteristics of crystalline growth for waxy-oils is provided based on studies presented elsewhere. The crystalline growth by evolution of lattices involving entrapment of oil droplets is considered. This growth behavior is shown to describe the viscoelastic nature of waxy oils which exhibit significant retardation in their strain-stress response to change in temperature. Hence, the dependency of the crystalline growth retardation to temperature can be correlated in a physically meaningful manner. Wax crystallization subject to different final temperatures is modeled and correlated for two types of waxy-oils. Laboratory

measurements of the rheology for two samples of waxy oil taken at different temperatures are analyzed successfully. This leads to the development of a temperature-dependent correlation which is applied for these oils using a generalized rheological model. Constitutive equations are provided for modeling of the viscoelastic behavior, gelation kinetics, and rheology of waxy-oils. The validity of the correlations are demonstrated by analyzing the various laboratory tests involving waxy-oil gelation under static cooling conditions without involving any forced convection effects. Then, the effect of cooling rate on the thermal history of waxy-oil gel strength and apparent viscosity until attaining equilibrium is described by three theoretical approaches. The interactive effects of the gelation kinetics and rheology of waxy oils exposed to low temperature are rigorously formulated. The kinetics is incorporated by relating the relaxation in the dynamic behavior of viscoelastic waxy-oils to its rheology. The effect of cooling rate and gelation kinetics on gel strength and viscosity is illustrated by a series of applications.

4.2. LITERATURE REVIEW

Wax precipitation occurs at a characteristic rate similar to rate processes of chemical reactions. The kinetic rate determines the pace at which the wax concentration approaches the thermodynamic equilibrium. Therefore, a certain amount of time is required for complete precipitation at a given temperature. This retarded crystallization affects the rheological parameters having the maximum strength at thermodynamic equilibrium. The wax is considered aged or hardened when the crystal growth attains an equilibrium concentration (thermodynamic equilibrium). Consequently, gradual

crystallization in time implies gradual increment of rheological properties, such as viscosity and gel strength. Some of the efforts in describing the kinetics of crystallization and its effect on rheological parameters are presented in the following.

The Avrami model (Avrami, 1940) for kinetics of crystallization applies to the relaxation in isothermal phase change of a pure substance. It is based on a probabilistic approach related to crystal growth as a rate process. The growth spreads from nuclei which are located randomly. According to the Avrami model, the fractal exponent in this model provides information about the shape of the crystals; a value of the exponent less than one corresponds to linear growth with low energy fluctuations, between one and two corresponds to linear growth with high energy fluctuations, between two and three corresponds to plate-like growth with low energy fluctuation, between three and four corresponds to plate-like growth with high energy fluctuation, and greater than four corresponds to polyhedral growth.

The Ozawa model (Ozawa, 1971) for kinetics of crystallization applies to the relaxation in phase change of a pure substance at constant cooling rate. This approach is based on calculating the crystal growth around nuclei as a function of temperature and cooling rate. The final form of the model for wax crystallization is dependent on time and cooling rate once the temperature is replaced by the product of time and cooling rate. For variable cooling rate, it was demonstrated that a step-wise computation in time of constant cooling rates can be adopted for describing the kinetics of crystallization.

The Ozawa model is generalized for waxy-oils compounded by various paraffin chains by Zougari and Sopkow (Zougari & Sopkow, 2007). The Ozawa model is applied to all paraffin components and all the resulting equations are combined into a generalized expression describing the crystallization kinetics for waxy-oils. Experimental measurements are conducted for various compositions of paraffinic waxes. The fraction of wax precipitated is normalized and the crystallization kinetics are compared at different constant rates of cooling. The comparisons show higher relaxation for higher cooling rates but less crystalline surfaces.

Lopez-Da-Silva and Couthino related the Avrami model to wax rheology by the means of the parameter known as the storage modulus (Lopez-Da-Silva & Couthino, 2007), which represents the elasticity. The progression in time of the storage modulus is experimentally measured at several temperatures for various paraffinic waxes. The Avrami model is demonstrated to describe this progression satisfactorily. The fractal exponent is shown to exhibit a power-law relationship with temperature, where higher temperature implies higher fractal dimension.

It was shown that the rate coefficient of the Avrami model is governed by the Arrhenius equation (Ekweribe, Civan, Lee, & Singh, 2009) where waxy-oils present unique activation energy for crystallization. Also, this study provides relevant definitions and measurements concerning wax gelation, such as Pour Point Temperature (PPT), Wax Appearance Temperature (WAT) and Gelation Time. The Pour Point Temperature is defined as the temperature at which waxy crystals begin to interlock. The region between Wax Appearance Temperature and Pour Point Temperature is characterized by

having all crystals as suspended particles. The Gelation Temperature is defined as the temperature at which the Storage Modulus profile and the Loss Modulus cross-over.

It was demonstrated that the stress-strain response is similar when measuring the rheology of waxy-oils by Control Stress Tests (CST) or Dynamic Oscillation Test (DOT) (Chang, Boger, & Nguyen, 2000). Viscoelastic and Plastic behaviors are experimentally observed for several waxes during crystallization at constant temperature and cooling rates. The measured gel strength exhibits a linear trend in the log-log space against cooling rate. The trends obtained by CST and DOT collapses to one when the gel strength is normalized.

Although there is no standard definition, the Pour Point Temperature (PPT) of waxy-oils can be defined as the critical temperature when a cooled waxy-oil changes its Newtonian rheological nature to Non-Newtonian plastic behavior. During experimental measurements, it has been observed the waxy-oil rheology changes its nature from Newtonian to Non-Newtonian when cooled (Ajienka & Ikoku, 1991). No gel strength is measured until the waxy-oil reaches certain critical temperature. Also, the waxy-oil behaves as a Newtonian fluid until attaining this critical temperature. The PPT has been evidenced to be the temperature at which cooled waxy-oils change its nature from Newtonian to Non-Newtonian is near the PPT (Oh, Gandhi, Magda, & Deo, 2009). Newtonian behavior is observed above the PPT and gel strength is measurable below the PPT. The Pour Point Temperature is expected to be higher than the Gelation Temperature (Venkatesan, Singh, & Fogler, 2002).

4.3. RELAXATION DURING WAX CRYSTALLIZATION

Accurate modeling of waxy-oil gelation is important because of its effect on the restarting conditions of sub-sea oil pipelines after a period of shut-in for maintenance and other reasons (Ekweribe, Civan, Lee, & Singh, 2009). Effective controlling of these pipelines for safe operation and flow assurance requires proper understanding of waxy-oil gelation phenomenon occurring in such pipelines subjected to cooling during shut-in.

Generally, instantaneous (time-independent) crystallization assumption has been widely considered in various studies (Mehrotra & Bhat, 2007); (Edmonds, Moorwood, Szczepanski, & Zhang, 2008); (Bhat & Mehrotra, 2008); (Mehrotra & Bhat, 2010) as a convenient simplified description of the various processes involving waxy-oil gelation such as wax appearance, separation from oil, and deposition processes occurring inside the pipelines exposed to low temperature. By assuming instantaneous crystallization, the fraction of crystallized wax is predicted by models based on thermodynamic equilibrium such as ideal eutectic mixture, multicomponent model or multiple solid states (Bhat & Mehrotra, 2008). Moreover, it was demonstrated (Coutinho J. A., 2000); (Coutinho, Edmonds, Moorwood, Szczepanski, & Zhang, 2006); (Zou & Zhang, 2008); (Mehrotra & Bhat, 2007) that compositional modeling adequately describes the wax solidification at thermodynamic equilibrium. Whereas, the prediction of crystallized wax given by the ideal eutectic and multiple solid states approaches differ greatly compared to the multicomponent approach (Mehrotra & Bhat, 2007).

However, the instantaneous phase transition assumption is not valid for gelation of waxy-oils because wax separation occurs gradually over a period of time similar to freezing of water in wet soil (Civan & Sliepcevich, 1987); (Civan & Sliepcevich, 1985); (Civan & Sliepcevich, 1984). In fact, several studies (Mehrotra & Bhat, 2007); (Chang, Boger, & Nguyen, 2000); (Zougari & Sopkow, 2007); (Lee, Singh, Thomason, & Fogler, 2008) demonstrated the time-dependency of waxy oil properties. Thus, models assuming instantaneous crystallization are not suitable for predicting wax appearance, separation from oil, and deposition processes occurring inside the pipelines because they are not capable of describing the complicated effect of gelation kinetics on waxy-oil rheology.

The time dependency of wax crystallization has been studied extensively. The complexities of describing the kinetics of wax crystallization can be conveniently avoided by relating the time dependency of the crystallization process directly to the deformation due to shear stress (Mehrotra & Bhat, 2010). More elaborate studies (Chang, Boger, & Nguyen, 2000); (Zougari & Sopkow, 2007); (Lee, Singh, Thomason, & Fogler, 2008) investigated the effect of cooling rate on the structure of the crystal growth, crystallinity, and gel strength. However, the considered waxy-oils were not allowed to rest over a sufficiently long time required for attaining equilibrium in some experimental observations of these studies. Thus, their proposed correlations are based on measurements taken from truncated experiments. Evidently, different cooling rates may induce different series of relaxed or metastable states before the waxy oil reaches equilibrium but all of these series are expected to approach the same equilibrium state

regardless of the path followed during crystallization. When the relaxation of wax crystallization is not considered, it indicated that the effect of gelation kinetics on the waxy-oil rheological properties has not been addressed adequately.

4.4. CRYSTALLINE GROWTH IN WAXY OILS

Crystalline Structure. Crystalline growth mechanisms have been extensively studied for materials undergoing solidifying. However, models for polymer crystallization are preferred for describing the solidification of waxy-oil because of its organic nature. For example, some studies (Ekweribe, Civan, Lee, & Singh, 2009); (Zougari & Sopkow, 2007); (Lopez-Da-Silva & Couthino, 2007) employed a characterization model for crystalline nuclei growth which was initially developed for polymers (Ozawa, 1971).

Several studies investigated the crystalline growth in waxy-oils. Importance of cooling rate (Chang, Boger, & Nguyen, 2000); (Lee, Singh, Thomason, & Fogler, 2008) and effect of inhibitors (Tinsley, et al., 2007) on the structure development of waxy crystals were observed. These studies determined that waxy crystals grow as lattices which entrap oil droplets inside their cage-type structure. Entrapped oil droplets can migrate out of this structure by several mechanisms or form crystals inside the lattice, thus making the crystalline structure more complex (Chang, Boger, & Nguyen, 2000). Typically, the structured growth resembles an orthorhombic shape but the growth of layered platelets is also common. Fundamentally, a gelled waxy-oil constitutes an unconsolidated porous media which can readily deform under stress. Consequently, modeling wax crystallization and subsequent deposition can be accomplished similar to

modeling of processes occurring in porous media (Hoteit, Banki, & Firoozabadi, 2008). Furthermore, the viscoelastic behavior of waxy-oils is attributed to entrapment of oil droplets inside the crystalline structure (Hou & Zhang, 2010).

Wax Appearance Temperature. Frequently, onset temperature of wax solidification or crystallization is referred to as the wax appearance temperature (WAT). The first wax crystal appears when this temperature is reached during a solidification process occurring by cooling. The WAT is not affected by the retardation in crystallization because it is a property attributed to the oil behaving still as a viscous fluid. Viscous fluids exhibit no retardation in response to thermal changes. The WAT defines a material boundary between single liquid phase state and waxy-oil mixture state where all properties present a change in behavior.

Gelation Temperature. Similar to concept applied for polymers, the gelation time of waxy-oils is the time required for wax crystals to self-organize into a gel structure by interlocking of wax crystals. The gel state is characterized by the growth of wax crystals in the form of a lattice which is strong enough for waxy-oil to behave like an elastic solid rather than a viscous fluid. Similarly, the gelation temperature can be defined as the temperature at which the wax crystals can conglomerate into a gel state. Consequently, the gelation temperature is affected by the retardation in crystallization because waxy oils are expected to undergo retardation in response to cooling. Thus, a higher cooling rate will imply lower gelation temperature owing to retardation or delay in response to cooling under the same initial condition.

Pour Point Temperature. In this study, the pour point temperature (PPT) is defined as the temperature at which the waxy-oil changes its nature from a Newtonian fluid to a Non-Newtonian fluid (Oh, Gandhi, Magda, & Deo, 2009). The PPT sets the transition boundary at which wax crystals begin to interlock and form solid structures resembling lattices. Below the PPT, the waxy crystals remain similar to a colloidal suspension that induces higher viscosity but still a Newtonian fluid behavior. Above PPT, the structured growth of waxy crystals occurs and it induces the waxy-oil to exhibit a yield stress due to the friction effect. Alternatively, another widely accepted definition of the PPT is the temperature at which the fluid ceases to flow. Under this definition, the standard methods available for measuring the PTT do not involve any shear rate. Nevertheless, the PPT is often reported and used in rheological studies (Ekweribe, Civan, Lee, & Singh, 2009); (Ronningsen, 1992) because it is recognized the importance of this property in the rheological behavior. Regardless the adopted definition for the PPT, this property is also affected by the retardation in crystallization in a fashion similar to the gelation temperature. However, there is no consensus about the relationship between the gelation temperature and the PPT. Nevertheless, this study theorizes that the region between PPT and gelation temperature is characterized by waxy-oils rendering more like a viscous fluid behavior than an elastic solid.

Effect of cooling rate. Cooling rate is not widely accepted to be a prime parameter affecting the crystalline growth inside waxy-oils. Nevertheless, cooling rate is often taken into account as the major parameter in various model developments (Chang, Boger, & Nguyen, 2000); (Zougari & Sopkow, 2007); (Ozawa, 1971). In spite these

studies relate cooling rate directly to wax gelation, this study assumes an indirect relationship between this properties. In this study, the retardation in crystallization is attributed to the relaxed nature of the viscoelastic behavior of waxy-oils. The cooling rate sets the pace at which the system equilibrium state is changing because the equilibrium state is mainly temperature dependent.

Relaxed Growth: Aging or hardening. Although cooling rate affects the crystalline growth process, it does not change the overall crystallization process in terms of the equilibrium fraction of the crystallized wax (Zougari & Sopkow, 2007) Different cooling rates imply different times required for attaining the temperature of the colder ambient, such as sea water surrounding the pipeline. Thus, comparing the crystalline growth at different cooling rates means a comparison of two different types of relaxed processes. A relaxed process is characterized by gradual shifting in time from an initial state to the equilibrium state. Therefore, assumption of instantaneous growth of the crystalline structures of earlier studies (Mehrotra & Bhat, 2007); (Edmonds, Moorwood, Szczepanski, & Zhang, 2008); (Bhat & Mehrotra, 2008); (Mehrotra & Bhat, 2010) (Lindeloff & Kerjbjerg, 2002); (Tiwary & Mehrotra, 2009) is not correct. In fact, actual experimental comparisons (Chang, Boger, & Nguyen, 2000) (Lee, Singh, Thomason, & Fogler, 2008) revealed that wax crystals grow by different characteristic lengths (sizes) associated with each of relaxed growth processes, induced by different cooling rates.

Consequently, wax precipitation is not an instantaneous process but occurs at a characteristic rate. Therefore, a certain amount of time is required for precipitation of all the wax crystals formed at a given temperature. The kinetic rate determines the pace at

which the wax concentration approaches the thermodynamic equilibrium. The wax is considered aged or hardened when the crystal growth attains an equilibrium concentration.

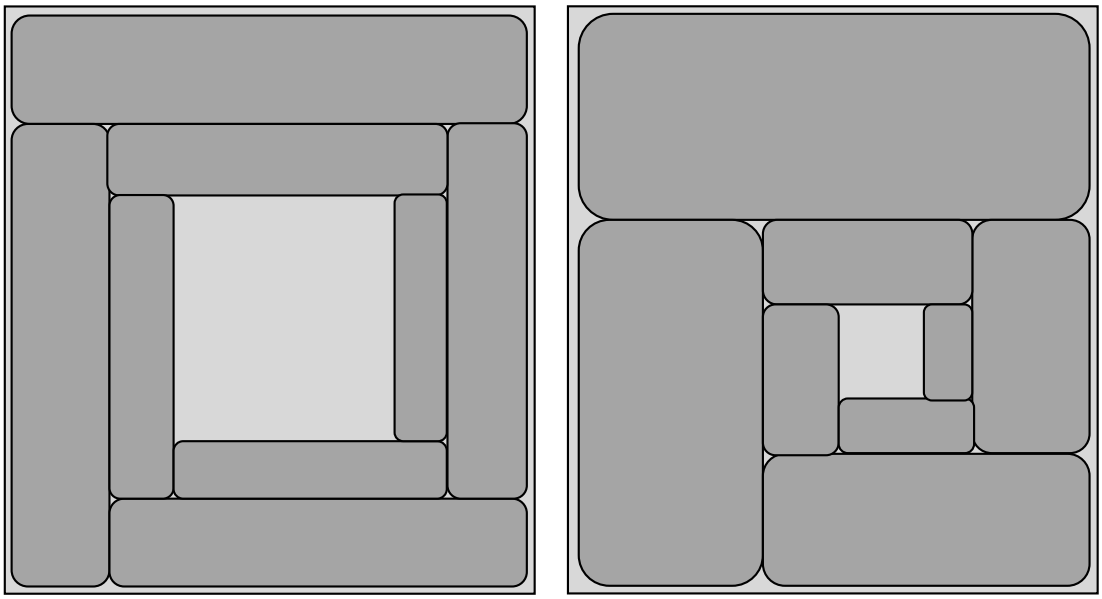

A **B**

Figure 4-1: Fractal growth of partitions with different aspect ratios.
A) Geometric rate of 0.8. B) Geometric rate of 0.9

Fractal Growth. In this study, the crystalline growth is described by a fractal model where the characteristic crystal length (or size) is determined by the nature of growth. The schematic shown in Figure 4-1 describes the fractal growth elapsed from the same initial time of two separate scenarios involving different but constant cooling rates. Both cases are represented as enclosing the same total volume of crystallization to allow comparison on the same basis. Moreover, they are assumed to have the same WAT as the initial temperature but attain different final temperatures. Scenario A is set with a higher final temperature than Scenario B. Thus, the Figure 4-1A represents crystallization occurring at a lower cooling rate than shown in Figure 4-1B.

These growth schemes present different geometric progression rates in series. Although both scenarios contain the same number of partitions, the geometric ratio of each one lead to different volume fraction of crystallization. Therefore, these two different cases are at different transition or metastable states albeit they represent a state after the same time has elapsed from the same initial condition. As discussed later, this study theorizes that the intrinsic nature of wax type dictates the fractal nature of crystalline growth whereas the cooling rate has an indirect effect.

4.5. DYNAMIC BEHAVIOR OF VISCOELASTIC MATERIALS

The dynamic viscoelastic behavior of waxy-oil and its rheology are related in this section. The similarity of the rheological responses under dynamic and static conditions experimentally demonstrated (Chang, Boger, & Nguyen, 2000). Behavior of viscoelastic materials is fundamentally different in that the stress-strain response is partially like an elastic solid and partially like a viscous fluid. This study theorizes that relating viscoelasticity to rheology of viscoelastic materials is a more rigorous approach than the usual basic stress-strain response considered in previous models (Mehrotra & Bhat, 2007); (Bhat & Mehrotra, 2008); (Mehrotra & Bhat, 2010).

A waxy-oil is essentially a viscoelastic material. The gelation temperature at constant pressure (Ekweribe, Civan, Lee, & Singh, 2009); (Venkatesan, Singh, & Fogler, 2002) and the gel strength or yield stress at constant temperature (Chang, Boger, & Nguyen, 2000) can be defined by measuring some viscoelastic properties, such as the storage modulus and the loss modulus. The time elapsed for gelation of a waxy-oil can be

defined as the time required for reaching the gelation temperature. Thus, the overall gelation process can be described in terms of the viscoelastic properties of the waxy-oil (Ekweribe, Civan, Lee, & Singh, 2009); (Lopez-Da-Silva & Couthino, 2007); (Ronningsen, 1992).

Viscoelastic properties can be measured by observing the dynamic behavior of a material (Denn, 2008); (Lakes, 2009). For example, consider a viscoelastic material contained between two parallel platelets. One platelet is fixed and the other is moving back and forward in harmonic oscillation. Therefore, the shear strain applied to the material follows the formulae (Denn, 2008); (Lakes, 2009):

$$\gamma = \gamma_0 \sin \omega t \quad \text{(4-1)}$$

$$\gamma_0 = \frac{L}{H} \quad \text{(4-2)}$$

where γ is the shear strain, γ_0 is the shear strain amplitude, L is the amplitude of oscillation, H is distance between platelets, ω is the frequency and the t stands for time. Under these conditions, a linear viscoelastic material exhibits a shear stress in the form of:

$$\tau = \tau_0 \sin(\omega t + \delta) \quad \text{(4-3)}$$

where τ is the shear stress, τ_0 is the shear stress amplitude and δ is the phase angle.

By rearranging equation 4-3, the shear stress is typically formulated as follows:

$$\tau = G'\gamma_0 \sin\omega t + G''\gamma_0 \cos\omega t \quad \text{(4-4)}$$

$$G' = \frac{\tau_0}{\gamma_0}\cos\delta \quad \text{(4-5)}$$

$$G'' = \frac{\tau_0}{\gamma_0}\sin\delta \quad \text{(4-6)}$$

where *G'* is referred to as storage modulus and *G''* is referred to as loss modulus.

Considering the form of the shear strain stated in equation 4-1 and the resulting derivative with respect to time, the shear stress can be expressed as (Lakes, 2009):

$$\tau = G'\gamma + \eta'\frac{d\gamma}{dt} = G'\gamma + \eta'\dot{\gamma} \quad \text{(4-7)}$$

$$\eta' = \frac{G''}{\omega} \quad \text{(4-8)}$$

where η' is the dynamic viscosity, *v* is the velocity, $\dot{\gamma}$ or $d\gamma/dt$ or dv/dy is the shear rate and *y* stands for the direction normal to both platelets.

This study theorizes that the physical meaning of the equations 4-5 to 4-8 can be understood as the following: a) a material having a phase angle of 0° behaves like a

linear elastic solid, thus the storage modulus stores the energy involved in the deformation; b) a material having a phase angle of 90° behaves like Newtonian fluid, thus the loss modulus dissipates the energy involved in the displacement; c) a phase angle of 45° delimits the boundary between solid-like and fluid-like behavior. Consequently, the gelation temperature is the temperature at which the waxy-oil presents the storage modulus equates the loss modulus leading to having tangent of the phase angle being equal to the unity. Similarly, the PPT is the temperature at which the phase angle deviates from 90° meaning that the value of the storage modulus cannot be longer considered zero.

4.6. KINETICS OF WAXY OIL GELATION

Usually, crystalline growth of waxy-oil gels occurs gradually at a pace that cannot be considered as instantaneous. The rate of crystalline growth has been theoretically modeled as a relaxation phenomenon leading to an equilibrium state. Several studies (Ekweribe, Civan, Lee, & Singh, 2009); (Zougari & Sopkow, 2007); (Lopez-Da-Silva & Couthino, 2007); (Hennessy, Neville, & Roberts, 2004) have defined a parameter for measuring the degree of crystallization of a material in order to describe the crystalline growth. For example, the crystallinity of a waxy-oil can be defined as the power transmittance of the gelled wax (Zougari & Sopkow, 2007); (Hennessy, Neville, & Roberts, 2004). A more useful parameter is the relative crystallization which is obtained by normalizing the measured degree of crystallization using any suitable mean. For example, the normalized storage modulus becomes equivalent to the relative

crystallization when the degree of crystallization is quantified by the storage modulus (Ekweribe, Civan, Lee, & Singh, 2009); (Lopez-Da-Silva & Couthino, 2007);.

Assuming properties remain constant at equilibrium state, i.e. equilibrium temperature, the relaxation of relative crystallization $\overline{X}$ can be described by following a relaxation scheme presented in several studies (Downar-Zapolski, Bilicki, Bolle, & Franco, 1996); (Badur & Banaszkiewicz, 1998); (Civan, 2006); (Michel & Civan, 2008a) for describing the retardation in change of phase:

$$\frac{d\overline{X}}{dt} = -\frac{(\overline{X} - \overline{X}_E)}{\theta} \quad \text{(4-9)}$$

where $\overline{X}_E$ is the equilibrium relative crystallization, t is time elapsed after the initial state, θ is a coefficient referred to as the relaxation time. Thus, this model is suitable for predicting the kinetics of isothermal crystalline growth.

However, in the present study, equation 4-9 is modified for better representation of the fractal nature of crystalline growth as follows:

$$\frac{d\overline{X}}{dN} = -\frac{(\overline{X} - \overline{X}_E)}{\eta} \quad \text{(4-10)}$$

$$N = t^{\beta} \quad \text{(4-11)}$$

$$\eta = \theta^{\beta} \quad \text{(4-12)}$$

where N is the total number of crystallized units, η is the relaxation in crystallization and β is fractal power coefficient (dimension). Here, the quantity of crystallized moles and time are related by a power law. Consequently, the relaxation coefficients are also related by the same power law. The combination of equations 4-10 to 4-12 can be readily integrated in order to yield:

$$\overline{X} = \overline{X}_E - \left(\overline{X}_E - \overline{X}_0\right) e^{-\left(\frac{t}{\theta}\right)^{\beta}} \quad \text{.....(4-13)}$$

where $\overline{X}_0$ is the relative crystallization at the initial state.

Because the relative crystallization is a normalized parameter, the equilibrium relative crystallization is equal to the unity and the initial relative crystallization is equal to zero. Consequently, the final form of the model for describing the relaxation of fractal crystalline growth is given by:

$$\overline{X} = 1 - e^{-\left(\frac{t}{\theta}\right)^{\beta}} \quad \text{.....(4-14)}$$

Since this type of formulation is commonly referred to as the Stretched Exponential or the KWW (Kohlraush-Williams-Watts) model (Lakes, 2009), theoretical basis by means of the fractal growth has been provided by the present study when the KWW model is applied to crystalline growth. For ease understanding of equation 4-14, the schematic given in Figure 4-1 depicts two fractal growths having the same fractal

exponent but for different relaxation times. The fractal exponent dictates the number of partitions occurring according to the time elapsed from the beginning of crystallization. Therefore, both scenarios shown in Figure 4-1 present the same number of partitions.

The Avrami model (Avrami, 1940) is commonly applied as a constitutive equation for modeling the relative crystallinity (Ekweribe, Civan, Lee, & Singh, 2009); (Zougari & Sopkow, 2007); (Lopez-Da-Silva & Couthino, 2007) when the crystallization occurs isothermally. It was concluded the theoretical values of the exponent can assigned to be one of the integers 1, 2, 3 and 4 for describing isothermal growth of crystals (Avrami, 1940). However, the KWW model is selected in this study because the KWW is recommended for relaxation phenomena for viscoelastic materials (Lakes, 2009). Nevertheless, the KWW model can be easily rearranged into the form of the Avrami model.

It was demonstrated (Civan, 2008) that properties having some physical meaning and dependent on temperature can be correlated by models resembling the Arrhenius equation. Previous studies (Ekweribe, Civan, Lee, & Singh, 2009); (Lopez-Da-Silva & Couthino, 2007) applied the Avrami model for describing the relaxation of wax solidification and correlated the corresponding rate coefficient with the Arrhenius equation. Similarly, the relaxation time of wax crystallization is correlated in this study using an exponential model similar to the Arrhenius equation, which is commonly referred to as a VTF-type equation (Civan, 2008); (Fulcher, 1925); (Tammann & Hesse, 1926); (Vogel, 1921):

$$\ln\left(\frac{\theta}{a_1}\right) = \frac{a_2}{T - T_c} \quad \text{(4-15)}$$

where a_1, a_2 and T_c are empirical correlation parameters and T stands for temperature.

4.7. RHEOLOGY OF WAXY OILS

This study have theorized that a waxy-oil is effectively a viscoelastic material after pour point is reached. Several models have been proposed for describing the rheology of waxy-oil. Because the structured crystallization changes the nature of the waxy-oil from Newtonian to Non-Newtonian, developing a suitable rheology model can be a complex process. For Non-Newtonian fluids, apparent viscosity μ_{app} has been widely defined as:

$$\mu_{app} = \frac{\tau}{\dot{\gamma}} \quad \text{(4-16)}$$

Although some rheological models have an acceptable performance (Ronningsen, 1992) (A1-Fariss, Jang, Ozbelge, & Ghasem, 1993), most empirical formulations are totally unrelated to the viscoelastic behavior of waxy-oil. The current study theorizes that it is possible to relate the rheological response of a viscoplastic fluid to its viscoelastic nature as demonstrated in the following.

The equation 4-7 implies a linear viscoelastic material can behave like a Bingham plastic fluid. By analogy, the following expressions can be proposed:

$$\tau = \tau_y + \mu_p \dot{\gamma} \quad \text{(4-17)}$$

$$\tau_y = G'\gamma \quad \text{(4-18)}$$

$$\mu_p = \eta' \quad \text{(4-19)}$$

where τ_y is the gel strength or yield stress and μ_p is the plastic viscosity. Thus, the viscoplasticity of a substance can be modeled by formulation developed for linear viscoelastic materials. Behavior of a Bingham plastic material can be replicated by dynamic modeling provided that the following conditions are satisfied:

$$\delta = 0 \quad , \quad \tau < \tau_y \quad \text{(4-20)}$$

$$\tan\delta = \frac{\mu_p}{\tau_y}\omega \quad , \quad \tau \geq \tau_y \quad \text{(4-21)}$$

However, the rheology behavior of most waxy-oils can be captured by the Herschel–Bulkley model which is a more general model than the Bingham plastic model:

$$\tau = \tau_y + K\dot{\gamma}^n \quad \text{(4-22)}$$

where K is the flow consistency index and n is the flow behavior index. Similar to the Bingham model, the same analogy presented in equation 4-19 can be drawn for the gel strength and this analogy for the dynamic viscosity is given by:

$$\eta' = K\dot{\gamma}^{n-1} \quad \text{(4-23)}$$

The behavior stated by equation 4-22 can be replicated by the linear viscoelastic model if the conditions provided by equation 4-20 and 4-24 are met.

$$\tan\delta = \frac{K}{\tau_y}\omega\dot{\gamma}^{n-1} = \frac{K}{\tau_y}\omega^n\gamma^{n-1}\cot^{n-1}\omega t \quad , \quad \tau \geq \tau_y \qquad \text{(4-24)}$$

The following correlations for the generalized rheological model are developed in the present study for describing the temperature dependence of waxy-oils undergoing crystallization.

$$\tau_y = b_1\left(T_{pp} - T\right)^{b2} \qquad \text{(4-25)}$$

$$K = \mu_{PPT} + b_3(T_{pp} - T)^{b_4} \qquad \text{(4-26)}$$

$$n = e^{b_5\left(T_{pp} - T\right)} \qquad \text{(4-27)}$$

where μ_{PTT} is the viscosity of the fluid at the PPT, T_{pp} is the pour point temperature, and b_1, b_2, b_3 ,b_4 and b_5 are empirically determined correlation coefficients. This model was formulated to yield Newtonian behavior at the Pour Point Temperature for all shear rates. The power-law relationship between the gel strength and temperature as stated by equation 4-25 is supported by an experimental study (Chang, Boger, & Nguyen, 2000).

4.8. VISCO-ELASTIC RELAXATION OF COOLING WAX

New theoretical approaches are developed and investigated for predicting the effect of the relaxation phenomenon on rheological properties such as gel strength and viscosity. Specifically, three models are presented which can accurately describe the wax hardening process, commonly referred to as aging, the proper understanding of which can be instrumental in maintaining flow assurance in sub-sea pipelines. The presented models closely describe the retardation or relaxation in the waxy-oil rheology during cooling until equilibrium (steady-state). However, retardation effect is more evident when heat transfer to colder environment (sea water) surrounding the pipeline is allowed to occur at large cooling rates.

Experimental observations (Denn, 2008); (Lakes, 2009) reveal that rheological response to stress is significantly delayed or relaxed for viscoelastic materials such as waxy-oils. Thus, the magnitude of their properties, such as gel strength, is also relaxed. Consequently, rapid cooling may not allow sufficient time for waxy-oil to reach equilibrium and its properties to attain equilibrium values. For example, gel strength cannot reach its maximum equilibrium value when the oil is cooled rapidly.

Several efforts have been made in predicting the effect of cooling rate and time-dependency on crystallization (Chang, Boger, & Nguyen, 2000); (Zougari & Sopkow, 2007). However, the effect of cooling rate and kinetics on the rheological properties remains unclear. The rheological properties are expected to be dependent on the level of molecular self-organization. The organization involved in crystal growth is described by

the proposed relaxation model for waxy-oil crystallization. Any retardation in solid state organization of the waxy crystals implies entropy generation. Thus, entropy is generated when relative crystallization is relaxed. In the present work, three approaches are introduced for investigating the sensitivity to added entropy by the cooling rate and kinetics effects into the wax crystallization.

First Approach. The storage modulus is a property attributed to the elastic-solid nature of a viscoelastic material. Because crystallization follows a relaxation behavior, the storage modulus is expected to be relaxed as well. Both relative crystallization and storage modulus can be interpreted as measurement of the degree of solidification or crystal organization.

A relaxed storage modulus implies that the gelation time under prescribed operating conditions may be substantially different than the one measured, calculated, or in fact predicted at equilibrium conditions. This means the relaxation phenomena also affects the gelation temperature. It was theorized and demonstrated elsewhere (Ekweribe, Civan, Lee, & Singh, 2009); (Lopez-Da-Silva & Couthino, 2007) that the relative (fractional) crystallization can be related to the relative storage modulus for waxy-oils. The relative crystallization can be expressed as:

$$\overline{X} = \frac{G' - G'_{\min}}{G'_{\max} - G'_{\min}} \qquad (4\text{-}28)$$

where G'_{max} is the storage modulus of the waxy-oil corresponding to complete crystallization of the wax (equilibrium) and G'_{min} is the storage modulus of the waxy-oil corresponding to no crystallization at all.

This study relates the gel strength directly to crystallization growth by the means of viscoelastic properties for a waxy-oil. The relaxation of the gel strength can be formulated by combining equations 4-18 and 4-28. Then, the relative crystallization is relaxed by the fractal model stated in equation 4-14. Assuming the displacement of a viscoelastic fluid is under constant shear strain, the resulting expression for the time dependency of the gel strength is:

$$\overline{X} = \frac{\tau_y - \tau_{y0}}{\tau_{ye} - \tau_{y0}} \qquad \text{(4-29)}$$

where τ_{ye} is the gel strength at equilibrium conditions (complete crystallization) and τ_{y0} is the gel strength corresponding to the initial conditions. In order to couple the presented rheology model for waxy-oils with their gelation kinetics, equation 4-29 can be substituted into equation 4-22 as:

$$\tau = [(\tau_{ye} - \tau_{y0})X + \tau_{y0}] + K\dot{\gamma}^n \qquad \text{(4-30)}$$

Having the initial state as the pour-point temperature, the fluid is still a Newtonian fluid so that its gel strength is zero. Thus, the apparent viscosity under this condition becomes:

$$\mu_{app} = \tau_{ye} X \dot{\gamma}^{-1} + K \dot{\gamma}^{n-1} \quad \text{(4-31)}$$

Second Approach. The previous approach assumes the added entropy due to relaxation is originated by the solid particles only. However, it is possible the liquid fraction of the wax can also contribute to entropy generation, thus leading to a relaxed behavior. This was evidenced in an experimental study (Ronningsen, 1992) where the time dependency of wax viscosity was observed to follow an exponential growth behavior.

This study considers that, according to equations 4-5 and 4-6, the relaxation of the storage modulus implies a relaxation of the loss modulus. Consequently, the loss modulus can also be related to the relative crystallization in the same form as the storage modulus is described in equation 4-28. Accordingly, the relaxation of the loss modulus is determined by:

$$\overline{X} = \frac{G'' - G''_{\min}}{G''_{\max} - G''_{\min}} \quad \text{(4-32)}$$

where G''_{max} is the loss modulus of the waxy-oil corresponding to complete crystallization of the wax (equilibrium) and G''_{min} is the loss modulus of the waxy-oil corresponding to no crystallization at all. Note that the relative crystallization is relaxed by the fractal model presented in equation 4-14. Then, the relaxation of the second term in equation 4-22 can be formulated by combining equations 4-8, 4-23 and 4-32. Assuming a constant frequency for the displacement of the viscoelastic fluid, the resulting expression for this relaxation is given by:

$$\overline{X} = \frac{K\dot{\gamma}^{n-1} - K_0\dot{\gamma}^{n0-1}}{K_e\dot{\gamma}^{ne-1} - K_0\dot{\gamma}^{n0-1}} \quad \text{(4-33)}$$

where K_e and n_e are the flow consistency index and the flow behavior index at equilibrium conditions (complete crystallization), respectively; and K_0 and n_0 are the flow consistency index and the flow behavior index corresponding to the initial conditions, respectively. Equation 4-33 is introduced into equation 4-30 for consideration of the relaxed behavior in the loss modulus:

$$\tau = [(\tau_{ye} - \tau_{y0})X + \tau_{y0}] + [(K_e\dot{\gamma}^{ne-1} - K_0\dot{\gamma}^{n0-1})X + K_0\dot{\gamma}^{n0-1}]\dot{\gamma} \quad \text{(4-34)}$$

Having the initial state as the pour-point temperature, the fluid is still a Newtonian fluid so that the flow consistency index is equal to the viscosity at pour-point temperature and the flow behavior index is equal to the unity. Thus, the apparent viscosity under this condition becomes:

$$\mu_{app} = (\tau_{ye}\dot{\gamma}^{-1} + K_e\dot{\gamma}^{ne-1} - \mu_{PPT})X + \mu_{PPT} \quad \text{(4-35)}$$

This formulation becomes a generalization of a rheological model that was previously theorized (Ronningsen, 1992) where the gel strength exhibits a crystalline growth with unity fractal dimension and the flow behavior index is equal to the unity.

Third Approach. Alternatively, the relaxation phenomena are considered to be caused by the retardation in the molecular self-organization during solidification in this study.

This type of metasatble state is commonly known as an undercooling or supercooling state. Delay in crystalline growth implies some molecules do not participate in the expected solid arrangement at crystallization conditions. Thus, it is possible such metastable states would present the same behavior of a stable or equilibrium state having the same molecular self-organization.

Since temperature is a measure of the degree of molecular organization because it measures the kinetic energy of the molecules, this study considers that if a metastable state presents a similar distribution and organization of molecules than an equilibrium state then all properties at this metastable state should behave as if they were at a temperature corresponding to that of the equilibrium state. As stated before, the relative crystallization is also an indicator of molecular organization. Therefore, the crystal growth relaxation can be used in a linear interpolation for estimating this equivalent or apparent temperature for a metastable state.

$$\overline{X} = \frac{T^* - T_0}{T - T_0} \qquad (4\text{-}36)$$

where T^* is the apparent temperature, T is the actual temperature and T_0 is the initial temperature. Consequently, all parameters and coefficients are affected by the relaxation phenomenon because they are calculated using the relaxed temperature for describing the effect of the kinetics in the waxy-oil rheology. Having the initial state same as the pour-point temperature, the apparent temperature T^* is calculated based on relative crystallization as:

$$\bar{X} = \frac{T^* - T_{pp}}{T - T_{pp}} \quad \text{(4-37)}$$

4.9. MODELING THE EFFECT OF THERMAL HISTORY

By allowing the rheology to be dependent on both temperature and time, a model can describe the effect of thermal history on the flow behavior of a waxy-oil. In this work, this is achieved by combining the introduced correlation model for wax rheology, given by equations 4-22, 4-25, 4-26 and 4-27, and the proposed relaxation model, given by equations 4-14 and 4-15.

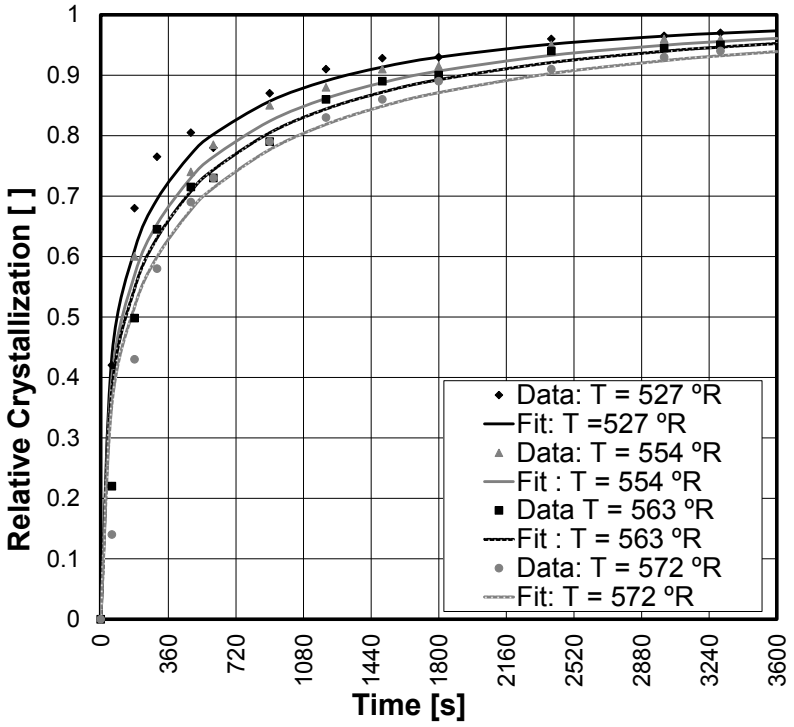

Figure 4-2: Correlation of the experimental data for GOM oil

A crystallinity measurement by experimentation (Zougari & Sopkow, 2007) is correlated by combining the KWW model (equation 4-14) with equation 4-15. All correlation coefficients are adjusted for minimizing the residual sum of squares (RSS).

The KWW model is fitted for each considered type of oils (Zougari & Sopkow, 2007). The optimal regression corresponding to the GOM and SEA type of oils are illustrated in Figures 4-2 and 4-3, respectively.

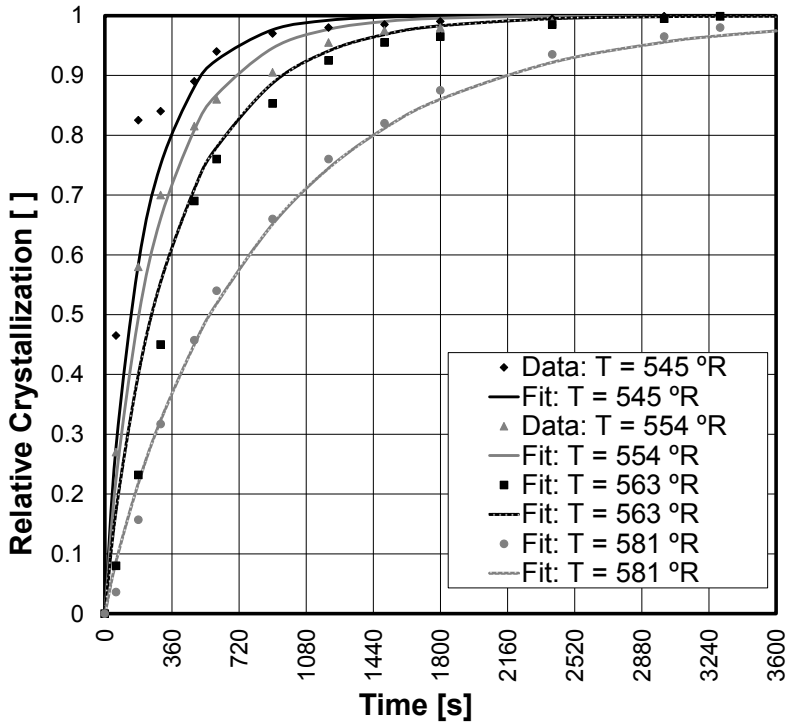

Figure 4-3: Correlation of the experimental data for SEA oil

The values of the resulting best estimate of the various empirical coefficients are presented in Table 4-1. These correlation coefficients yield a temperature dependency of the relaxation time as depicted in Figure 4-4.

Table 4-1: Correlation coefficients for fitting the relative crystallization

GOM Oil			SEA Oil		
a1 =	111.8	sec	a1 =	217.7	sec
a2 =	-56.3	ºR	a2 =	-565.0	ºR
Tc =	620	ºR	Tc =	685	ºR
b =	0.450		b =	0.901	

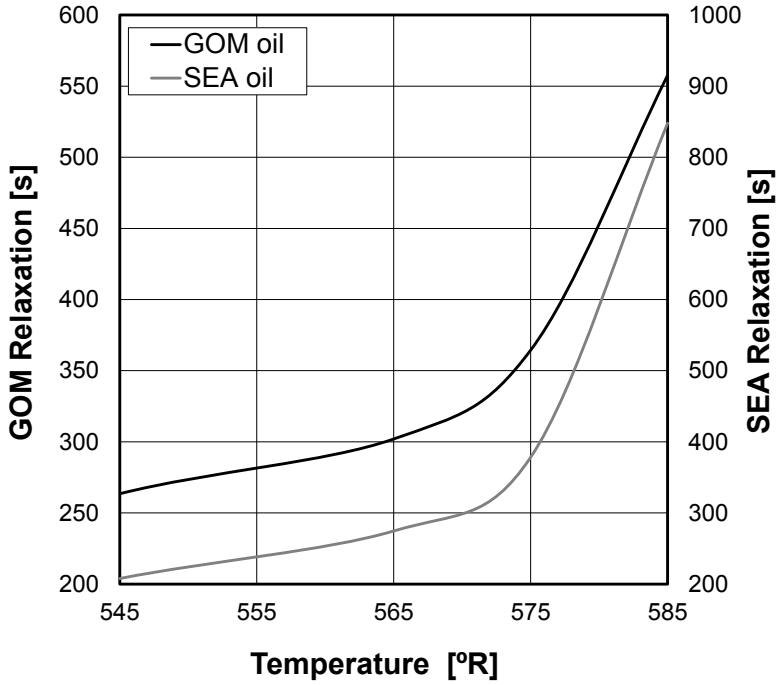

Figure 4-4: Temperature dependency of the Relaxation Time

Figures 4-5 and 4-6 delineate optimal regression using rheological data corresponding to some waxy-oils which was measured experimentally (Ajienka & Ikoku, 1991). The available data corresponds to the rheology of two types of oil. For Oil A, the measured Pour point temperature is 100 °F and pour point viscosity is 17.96 cp For Oil D, the measured Pour point temperature is 100 °F and pour point viscosity is 13.26 cp. Equation 4-22 combined with equations 4-25, 4-26 and 4-27 are employed as the correlating model where the RSS is minimized. The values of the resulting best estimate of the various empirical coefficients are presented in Table 4-2. These correlation coefficients yield a temperature dependency of the gel strength, the flow consistency index and the flow behavior index as illustrated in Figures 4-7, 4-8 and 4-9, respectively.

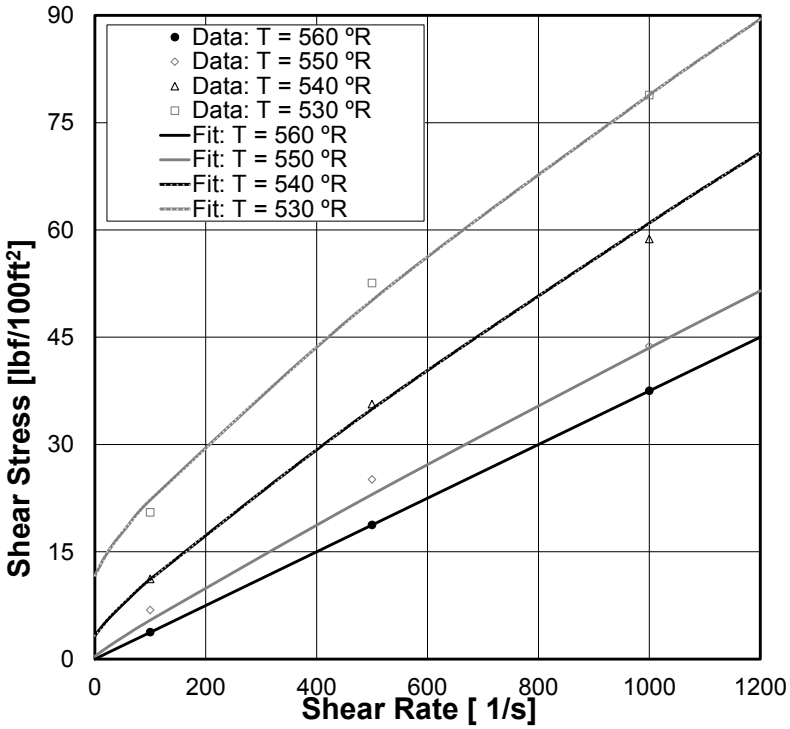

Figure 4-5: Correlation of the experimental data for Oil A

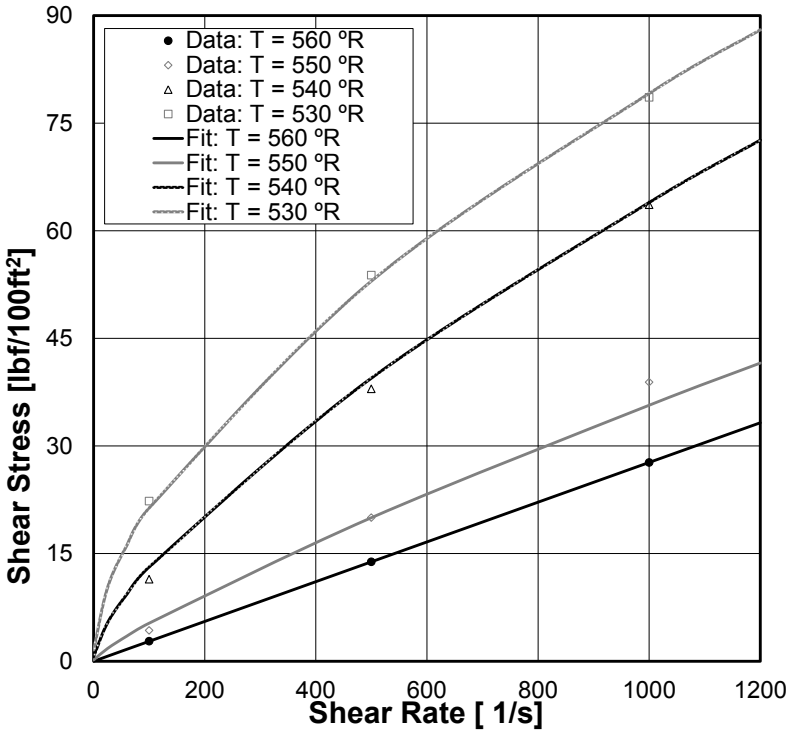

Figure 4-6: Correlation of the experimental data for Oil D

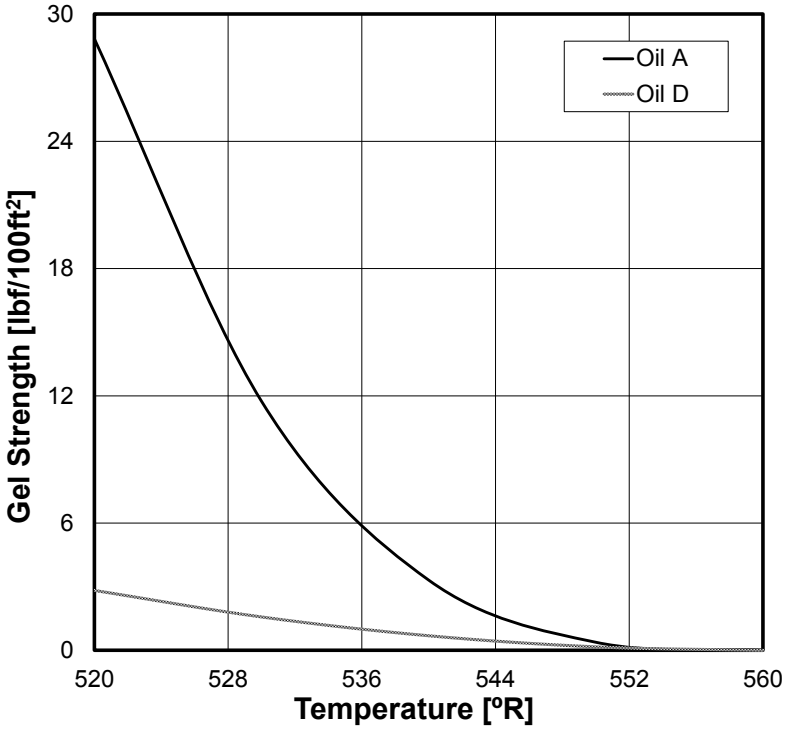

Figure 4-7: Temperature dependency of the Gel Strength

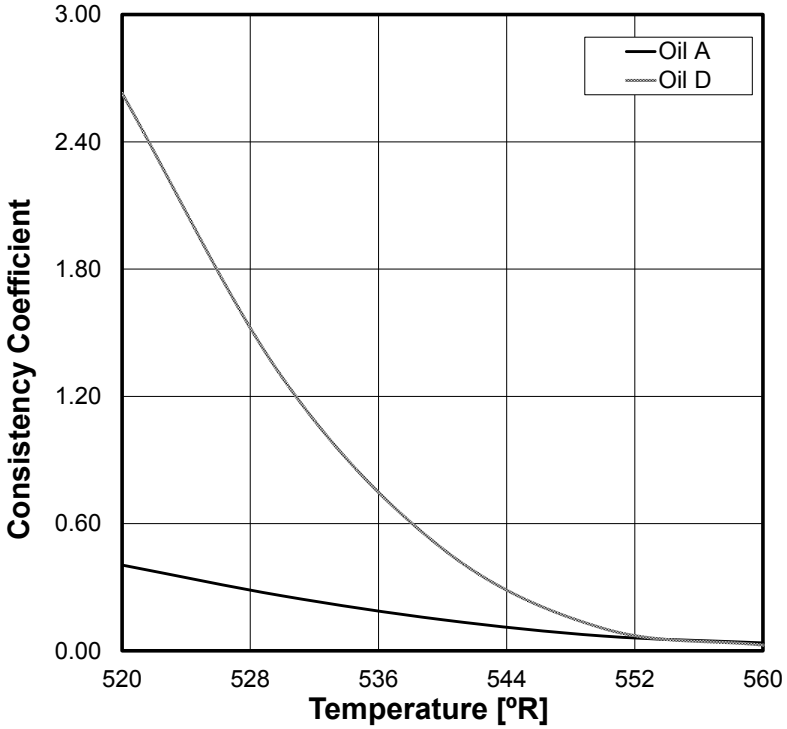

Figure 4-8: Temperature dependency of the Flow Consistency Index

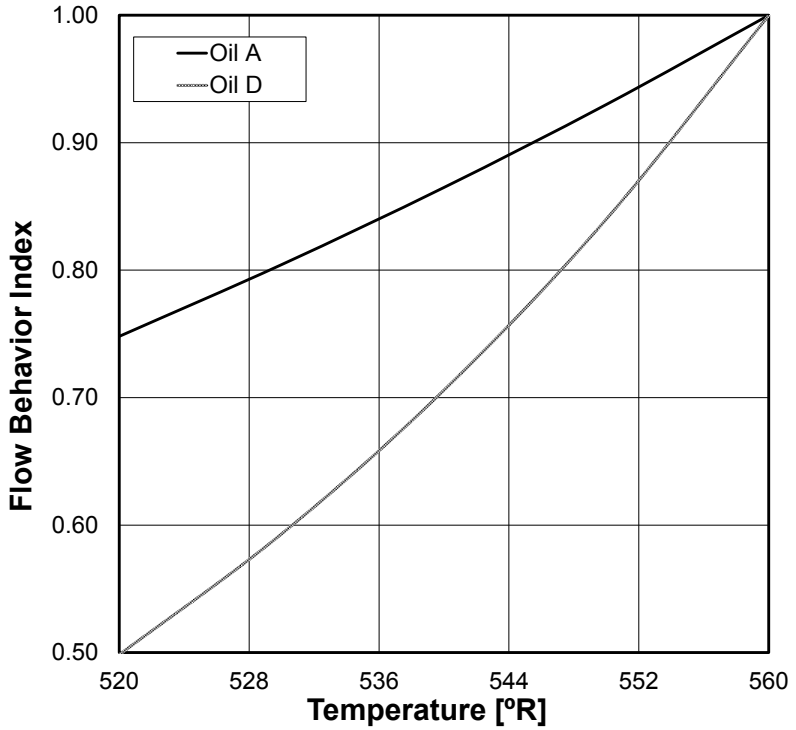

Figure 4-9: Temperature dependency of the Flow Behavior Index

Table 4-2: Correlation coefficients for fitting the wax rheology

Oil A		Oil D	
b_1 =	2.867E-04	b_1 =	1.599E-03
b_2 =	3.122	b_2 =	2.027
b_3 =	5.773E-04	b_3 =	2.412E-04
b_4 =	1.750	b_4 =	2.517
b_5 =	-7.257E-03	b_5 =	-1.741E-02

The relaxed behavior of GOM oil and rheology of Oil D are adopted for illustration of the applicability of the present model. Also, the initial condition is set to be the PPT in spite of having a different initial condition corresponding to the GOM oil, which is the WAT. Moreover, the present modeling approach relates the rheological measurements at dynamic conditions, i.e. oscillatory, with its static counterpart, i.e. controlled stress.

The current study assumes the dynamic and static rheological response of wax exhibit similar trends when normalized. This is corroborated by a previous experimental study (Chang, Boger, & Nguyen, 2000). Furthermore, the wax crystalline growth is set to be induced by an exponential decay of temperature at constant cooling rate. Therefore, the relaxed crystalline growth is estimated by executing the classical second order of the Runge-Kutta methods (Heun's method) for numerical differentiation directly to equation 4-10. The effect of the crystalline growth kinetics on wax rheology is illustrated on Figures 4-10 to 4-15 by combining the properties of GOM oil and Oil D. All cases are calculated using a shear rate of 25 s^{-1}. Each of these figures shows a comparison between the calculations of the equilibrium case and the above-mentioned three alternative approaches for approximating the relaxed case. As mentioned previously, the cooling rate has an indirect effect in the current modeling.

The relaxation over the wax apparent viscosity is depicted in Figures 4-10, 4-11 and 4-12 at constant exponential rates of 0.05, 0.07 and 0.1 min^{-1}, respectively. On each figure, the temperature decreases exponentially with time at the corresponding cooling rate from 560 °R (the pour point temperature) to a minimum of 520 °R. This means the waxy-oil temperature will present an asymptote in 520 °R.

Likewise, the relaxation over the gel strength is delineated in Figures 4-13, 4-14 and 4-15 at the exponential cooling rates of 0.05, 0.07 and 0.1 min^{-1}, respectively. Note that the criteria for gel strength relaxation are the same for the first and second approaches.

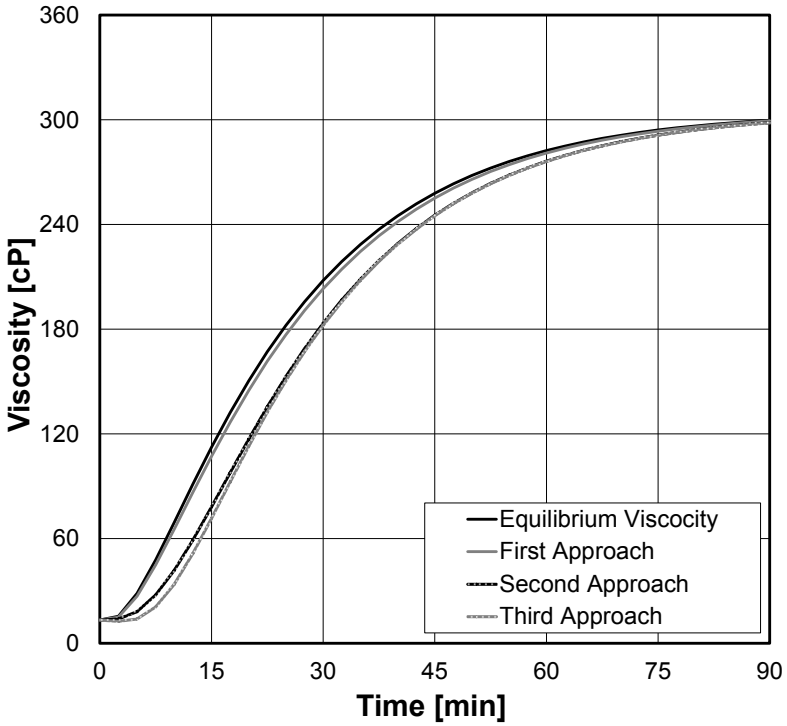

Figure 4-10: Predicted relaxation of wax viscosity at a cooling rate of 0.05 min^{-1}

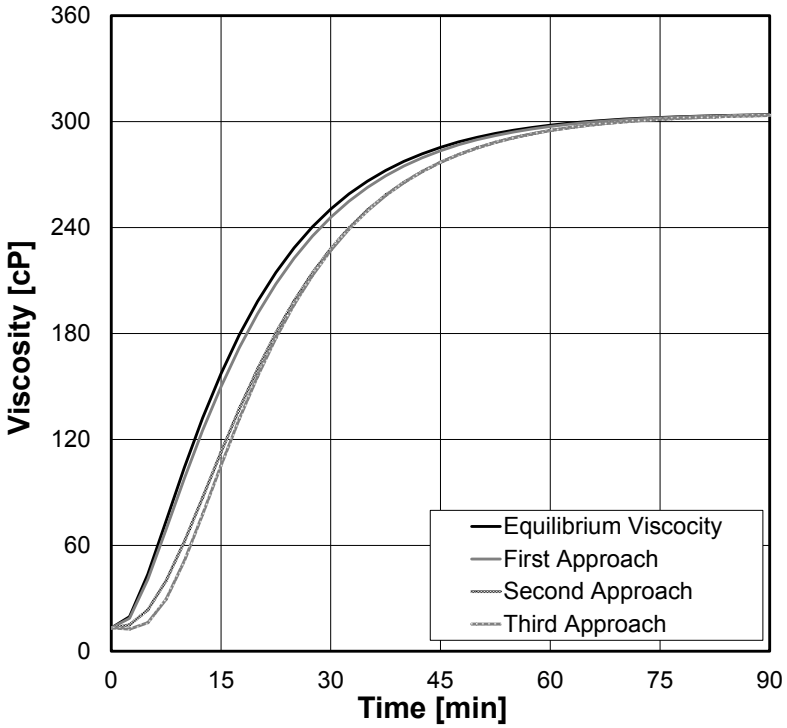

Figure 4-11: Predicted relaxation of wax viscosity at a cooling rate of 0.07 min^{-1}

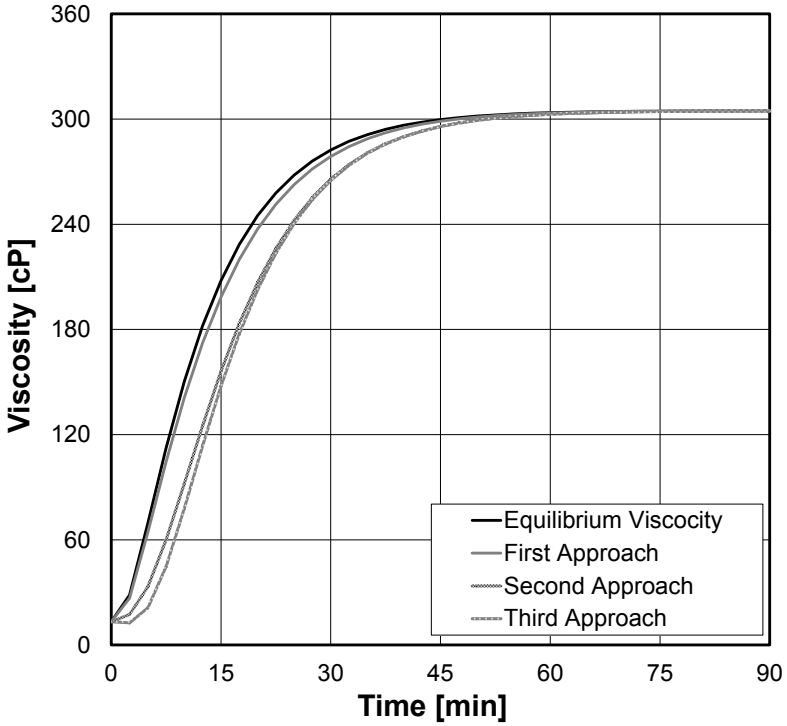

Figure 4-12: Predicted relaxation of wax viscosity at a cooling rate of 0.1 min^{-1}

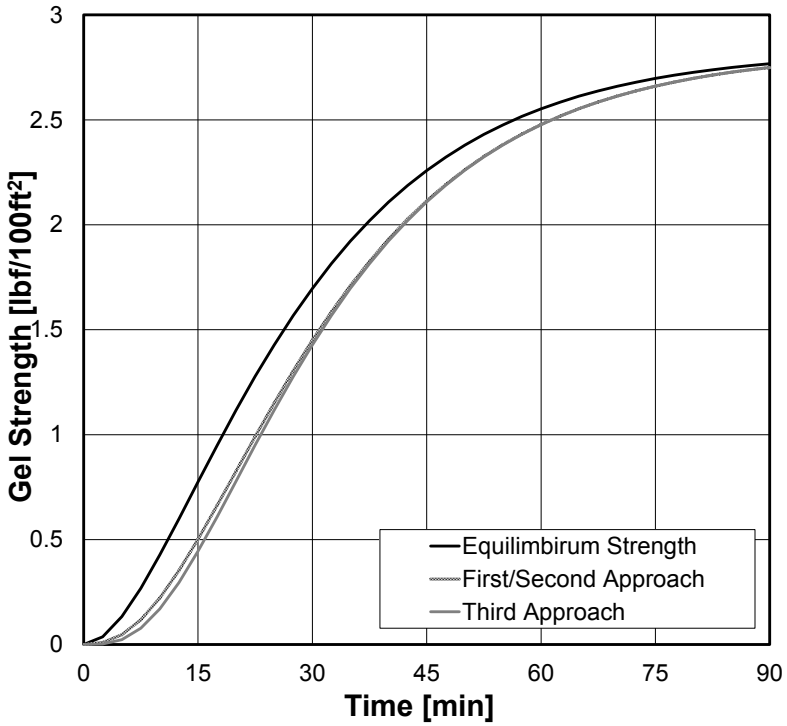

Figure 4-13: Predicted relaxation of gel strength at a cooling rate of 0.05 min^{-1}

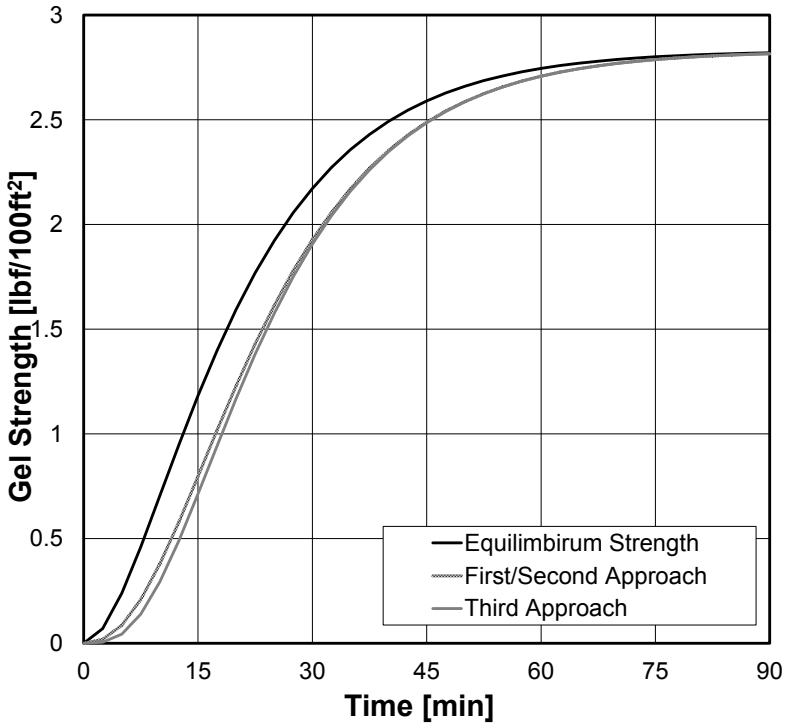

Figure 4-14: Predicted relaxation of gel strength at a cooling rate of 0.07 min^{-1}

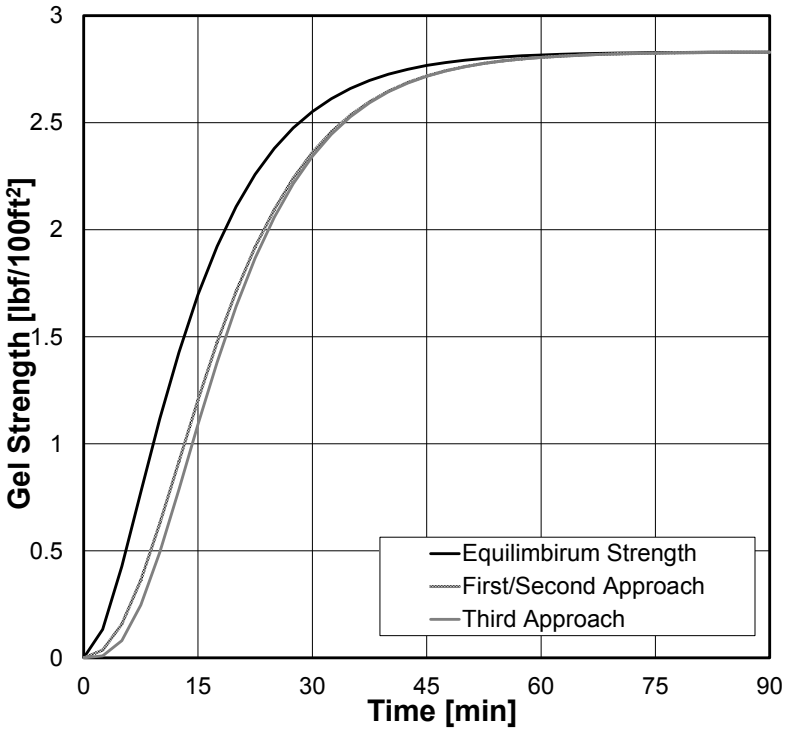

Figure 4-15: Predicted relaxation of gel strength at a cooling rate of 0.1 min^{-1}

An inflection point can be observed on each of Figures 4-10 to 4-15. At this point, the effect of relaxation is predicted to reach its maximum. If the experimental observation is terminated at this point (or any intermediate point) for all considered cooling rates, then it would appear that different cooling rates can lead to different final states. This behavior was observed in experimental studies (Chang, Boger, & Nguyen, 2000); (Zougari & Sopkow, 2007). It is possible that significantly high cooling rates might lead to different solid states for waxy oils as observed in other materials, i.e., water, glass, etc. Nevertheless, it seems highly unlikely that the typical relatively low cooling rates encountered under usual operating conditions would lead to more than one solid state. For this reason, the modeling proposed in this study predicts the same final state (equilibrium) for all cases if the cooling is left to rest over a sufficiently long period of time Thus, the relaxed trend predicted by the present modeling approach is more likely to describe the observed realistic experimental behavior.

Whether one of the three alternative approaches presented here would or would not apply to a certain type of wax depends on its intrinsic nature. The first approach is expected to be more suitable to a wax having a considerable relaxation on the solid crystals only. On the other hand, the second approach would be more appropriate if the relaxation is affecting the solid and the viscous nature of a viscoelastic wax. However, if relaxation is occurring in the inherent nature of molecular self-organization then the third approach is expected to be more representative.

CHAPTER 5

MODELING WAX GELATION AS A HOMOGENEOUS MULTIPHASE SYSTEM IN VERTICAL SUBMARINE PIPES

5.1. OVERVIEW

A modeling of wax deposition in submarine oil pipelines undergoing a cooling process after shut-in is presented based on previous publications (Michel & Civan, 2009b) (Michel & Civan, 2011). The wax/oil mixtures are modeled as a continuously varying multiphase system. A two-phase modeling approach to wax gelation in shut-in submarine pipelines is developed. A correlation applicable to the fraction of wax precipitated is validated using experimental data. Accurate correlation of pressure dependence of the Wax Appearance Temperature is developed. Relevant mechanisms of wax gelation without forced convection are described in detail. Initial temperature profile of oil flowing through a pipeline under steady-state conditions is estimated based

on an analytical solution obtained for turbulent flow of a single-phase system undergoing heat transfer. The natural convection phenomenon is represented by assigning a proper value to thermal conductivity of the liquid phase. Transport models for transient cooling in a circular pipe cross-section and along vertical pipelines are developed. The simulation results indicate that prevailing pressure conditions of vertical submarine pipelines greatly affects the wax precipitation phenomenon. Conversely, the relaxation of wax precipitation has no significant effect with proper insulation.

5.2. LITERATURE REVIEW

Most of wax gelation studies are focused on wax deposition phenomena which occur at flow conditions. Wax gelation inside pipes is characterized by an inward layered growth of waxy crystals starting at the pipe wall is expected when waxy-oil resides inside pipes subject by heat loss to surroundings across the wall surface. At constant flow rate, the shear stress and the convective heat transfer will prevent the radial growth to reach the cross-sectional center. Thus, a maximum layer thickness is attained under given the flow conditions. Some of the efforts in describing the wax deposition phenomena and wax gelation without force convection are presented in the following.

The computation of the radial temperature profile for waxy-oil flowing inside a pipe at wax precipitation and constant flow rate conditions (wax deposition) can be simplified to an exponential equation (Lindeloff & Kerjbjerg, 2002). The mixture properties, such as heat capacity, are calculated by mass-averaging for all paraffinic components. Thus, a compositional thermodynamic model is used. The radial concentration profile is

assumed to be binary, which means either complete or no wax precipitation has occurred at a given a radius.

A much simplified approach is to consider binary radial profiles for both temperature and wax precipitation (Edmonds, Moorwood, Szczepanski, & Zhang, 2008). The energy balance is performed by computing the heat loss between the wax-free oil (bulk) and the composite film between precipitated wax and the pipe wall (wax deposition). Mass balance is achieved by computing mass diffusion for each component. The mass conservation law is coupled with the activity coefficient model known as Universal Quasi-chemical model (UNIQUAC) for predicting the concentration in the bulk and the film for each component.

Higher shear rates in turbulent flow are suspected to deform the gelled film of wax making the deposit layer thinner (Tiwary & Mehrotra, 2009); (Mehrotra & Bhat, 2010). Likewise, higher shear rates in laminar flow are suspected to decrease the mass per unit surface of deposited wax and its thermal conductivity (Bhat & Mehrotra, 2008). This was demonstrated by using the binary profile approach coupled with a shear deformation model applied to the deposited wax (Mehrotra & Bhat, 2007). Also, the heat transfer occurring at the liquid/gel interface is incorporated into this approach. For this reason, models for describing the advancement of the interface and the compositional change due to cooling are required to complete this approach.

However, the wax precipitation does not occur instantaneously as a sudden jump to complete precipitation once the temperature has fallen below WAT. Instead, a gradual

increase is experimentally observed when cooling a waxy-oil below the WAT (Coto, Martos, Espada, Robustillo, Pena, & Gomez, 2009); (Martos, Coto, Espada, Robustillo, Gómez, & Peña, 2008). This implies any continuous temperature profile induces a continuous precipitation profile. The radial temperature profile during wax precipitation has been experimentally measured (Bidmus & Mehrotra, 2008a); (Bidmus & Mehrotra, 2008b). The observed temperature profile is continuous but a sudden change in slope occurs at the WAT. An unusual high temperature drop is observed although no precipitation has occurred and natural convection is suspected to cause this effect. Natural convection would effectively increase the liquid thermal conductivity which would be inducing internal heat exchange through mobilization of the liquids. This is observed during gelation at both the force convection and the shearing stress conditions.

5.3. WAX GELATION INSIDE COOLED SUBMARINE PIPES

Wax appearance inside pipelines is an important phenomenon for transportation of hydrocarbon fluids where the temperature of the surroundings is below the phase-transition temperature. Although such pipelines are usually properly insulated for preventing wax appearance and related problems, prolonged exposure to cooler environments may cause sufficient drop in temperature favorable for inducing wax separation from the liquid oil phase. Hence, a proper model for describing the waxy-oil gelation can be instrumental for effective management of the shut-in submarine pipelines because wax gelation can affect the restarting conditions significantly (Ekweribe, Civan, Lee, & Singh, 2009).

Shut-in pipelines are often scheduled for maintenance or emergency reasons. After shut-in of a submerged pipeline, potential of complete wax separation is created by the cooler submarine environment. Wax and liquid oil usually form a highly viscous gel characterized by a solid-like structure. Thus, wax precipitation may reduce the cross-sectional area of pipeline available for flow (choking) when the production operations are resumed. Even worse, prolonged exposure to cold surroundings may result in complete plugged the pipe and loss of production facility (Gluyas & Underhill, 2003).

Therefore, appropriate modeling of wax precipitation and gelation is essential for ensuring flow assurance in submarine pipelines subject to cold sea-water temperatures. Several experimental studies have demonstrated that wax separation is mainly driven by thermodynamic interactions in systems containing hydrocarbons and the surrounding sea-water environment. Cooling due to heat loss in the liquid oil causes the separation of heaviest components (wax) in the form of a crystalline structure saturated with oil.

Pressure drop at dynamic and static conditions has almost no effect on wax precipitation. Change in pressure induces little wax appearance because waxy crystals can be considered incompressible and liquid hydrocarbons can be considered slightly compressible. A large pressure differential is required to alter the specific volume, and thus change the mass fractions in both waxy crystals and the liquid hydrocarbon.

However, the shear stress induced by flowing conditions plays a significant role in wax deposition. Shear stress causes erosion on the waxy layers deposited around the pipe

wall. Therefore, the thickness of layered deposition reaches a plateau owing to equilibrium between growth and erosion under flowing conditions.

Conversely, a submarine pipeline that has been shut-in is susceptible to complete gelation because the sea-water temperature is generally below the phase-transition temperature. Even though proper insulation may deter wax precipitation and gelation for some time, extended exposure to the low sea-water temperature conditions without such heating source may eventually induce complete wax precipitation and subsequent gelation problems. Wax appearance causes a significant change in the nature of hydrocarbons. For instance, the fluid behavior varies from Newtonian to non-Newtonian. After wax precipitation, wax crystals may aggregate and interlock, and thus the wax/oil mixture behaves as a highly viscous gel. A solid-like state is attained when the waxy-oil is allowed to cool down over prolonged periods of time by heat loss towards the sea-water environment.

5.4. PRIMARY MECHANISMS OF QUIESCENT WAX GELATION

The wax concentration and temperature gradients are not dependent only upon the heat transfer towards the surroundings. Other mechanisms can also affect the behavior of the crystalline growth, including natural convection, pressurization, wax aging or hardening, and wax sedimentation, as described in the following.

5.4.1 HEAT TRANSFER TOWARDS SURROUNDINGS

The colder sea-water-water temperature induces a heat transfer through the pipe-wall surface. The heat loss towards the surroundings is determined by the difference in temperature between the sea-water and the pipe wall. This outward heat flow occurring at the pipe wall sets the wall temperature to be lowest in the radial direction over the cross-sectional area of the pipe. Accordingly, the region that cools down first to the WAT is the wall surface. Furthermore, the first wax crystals precipitate at the pipe-wall interface around its perimeter over any given cross-sectional area. This induces a layered aggregation of wax crystals and an inward laminar growth of the gelled wax region where some droplets of the liquid phase are trapped inside the crystalline structure. This means, the crystal growth in a shut-in submarine pipeline takes place from the wall to the center. Thus, the temperature and wax concentration gradients occur in the radial direction after the wax appearance because of the presence of the two phases.

The local heat capacity and thermal conductivity vary as more wax separates from the liquid oil near the wall. The wax crystals form a resistance to heat transfer once the local temperature drops to below the WAT. Consequently, the greater resistance near the pipe-wall acts as insulation for the liquid in the pipe center which is relatively warmer. Moreover, the heat loss outward to the surroundings induces more separation of wax that provides greater insulation to the center region and the crystalline growth starts to build up. Therefore, the difference in physical properties between the various phases keeps the center warmer than the wall (outer perimeter) and waxy crystals more

abundant in the wall. This leads to a higher concentration of wax observed near the pipe-wall.

5.4.2 NATURAL CONVECTION

It was observed that the temperature profile in the radial direction remained approximately constant until the temperature dropped to below the WAT in experimental studies where the temperature change in time was measured during wax gelation, (Bidmus & Mehrotra, 2008a) (Bidmus & Mehrotra, 2008b). A temperature gradient over the cross-section is expected to prevail if the heat transfer is driven by conduction alone. This proves that heat transfer towards the surroundings is greater than the heat transfer induced by conduction alone while the fluid (oil) is still in a liquid state. It was concluded that heat transfer due to natural convection occurring inside the liquid fluid was responsible for the apparent enhancement in the heat loss. Thus, the role of natural convection is important in wax gelation during shut-in because of the absence of forced convection.

Moreover, the same heat loss enhancement is expected for the liquid phase of waxy-oils. Furthermore, permeation process of oil droplets through crystalline structures occurring inside of gelled waxes induces another type of natural convection. The trapped droplets present inside the crystalline layers may migrate towards the liquid phase by molecular diffusion (Hoteit, Banki, & Firoozabadi, 2008). The trapped droplets permeate through the crystalline layers which act as a semi-permeable membrane.

It was demonstrated that the overall effect of natural convection can be taken into account simply by adopting an apparent thermal conductivity concept for the liquid phase which is greater than the actual value (Michel & Civan, 2009b).

5.4.3. PRESSURIZATION

A Wax Precipitation Curve (WPC) depicts the dependence of mass fraction of precipitated wax on temperature at atmospheric pressure. However, the effect of pressurization on wax precipitation is not yet completely understood.

It was observed experimentally that pressure alters the WAT non-monotonically (Daridon, Xans, & Montel, 1996). There is no data on the effect of pressure on the mass fraction of wax precipitated from waxy-oil. Without any experimental evidence, we assume that the pressurization only affects the WAT (Michel & Civan, 2011). This means that the Wax Precipitation Curve would shift without distorting its shape by changes in pressure.

Pressurization of waxy oil under shut-in conditions at a given depth is governed by stress imposed by the combination of the hydrostatic pressure and the wax column above the local cross-section. Pressure effect due to inertia, shear stress, and shear removal do not exist because there is no forced convection.

5.4.4. WAX AGING AND HARDENING

Wax growth is a gradually relaxed process involving retardation until attaining equilibrium concentration. Consequently, wax precipitation is not an instantaneous

process but occurs at a characteristic rate. Therefore, a certain amount of time is required for precipitation of all the wax crystals formed at a given temperature. The kinetic rate determines the pace at which the wax concentration approaches the thermodynamic equilibrium. The wax is considered aged or hardened when the crystal growth attains an equilibrium concentration.

Experimental studies on the kinetics of wax precipitation indicated that the relaxation of wax precipitation may last several hours depending on the cooling rate and local temperature (Lopez-Da-Silva & Couthino, 2007); (Zougari & Sopkow, 2007). Hence, wax aging or hardening depends on the conditions of the cooling.

The kinetics of crystalline precipitation has been accurately described for processes occurring isothermally (Avrami, 1940) or having a constant cooling rate (Ozawa, 1971). However, the cooling experienced by shut-in submarine pipes is certainly not isothermal nor is characterized by cooling at a constant rate. Nevertheless, these models can be adapted for approximating the effect of wax aging or hardening (Michel & Civan, 2011).

5.4.5. SEDIMENTATION OF WAX CRYSTALS

The wax crystals formed after appearance of wax are suspended in the liquid phase. The density difference between the crystals and the liquid phase causes the crystals to fall at a terminal velocity. Therefore, wax crystal sedimentation can change the total wax concentration mechanically in a pipe section. Higher concentration of wax crystals results in higher viscosity and even changing the Newtonian nature of fluid to Non-

Newtonian (Ajienka & Ikoku, 1991). Also, higher concentration accelerates the complete wax gelation of a cooled pipe. Upon sufficient cooling, the waxy crystals can conglomerate and interlock into a gelled state. No settling is expected, hence, after gelation.

Because the sea-water temperature is much below the gelation temperature for most waxy oils, the sedimentation of wax crystals occurs over a certain period of time for shut-in submarine pipes. This time period is set by the temperature range on which waxy-oils behave as a Newtonian fluid. It begins with wax appearance and ends when wax crystals attain a critical concentration. This critical concentration sets the boundary between the Newtonian and Bingham-plastic behavior. Bingham-plastic fluids may deter but most likely prevent the settling of particles depending on the operating conditions (Reynolds & Jones, 1989) since Bingham-plastic fluids would require the buoyancy of waxy crystal to exceed the yield stress in order to allow motion. This renders the settling of waxy crystals negligible when the liquid phase behaves as a Bingham-plastic fluid. Hence, the settling during wax gelation is expected to be important only when the fluid behaves as a Newtonian fluid.

The magnitude of the settling velocity is directly related to the shape and size of the crystals and inversely related to the viscosity of the liquid. The hydraulic diameter of the waxy crystals was experimentally observed to vary typically between 2μm and 10 μm (Marie, Chevalier, Brunel, Eydoux, Germanaud, & Flores, 2004). The estimated settling velocity ranges between 0.1 mm/min to 1.2 mm/min. Consequently, a wax crystal would fall a distance of approximately 1.73 meters after one day of settling if the

fluid behaves as Newtonian during that time. However, the time required for complete wax gelation is usually less than a day when a submarine pipe is shut-in. This means that the crystals would fall less than 1.73 m distance once complete gelation has occured, which is a significantly small for alteration of the total wax concentration appreciably for any section of the pipe. Consequently, change in total wax concentration due to wax sedimentation is not significant for shut-in submarine pipes. The sedimentation becomes important when a shut-in pipe is subjected to prolonged exposure to the surrounding temperature below the WAT but high enough for allowing the wax crystals to remain suspended.

5.5. MODELING WAX PRECIPITATION

Accurate prediction of the wax fraction is very important in modeling wax precipitation inside pipelines. Comprehensive models considering thermodynamic interactions between the solid and liquid phases during wax deposition are still in development. Some compositional models have shown adequate prediction of wax appearance and the phase mass fractions (Zou & Zhang, 2008); (Coutinho J. A., 2000). However, application of these models for simulation purposes requires an extensive computational effort. In this study, a more convenient approach developed by the means of an empirical correlation model suitable for capturing the behavior of the wax mass fraction against temperature and pressure predicted by a compositional analysis or measured directly in experimental tests.

Wax precipitation envelope. The present study theorizes that the phase equilibrium of wax precipitation at standard pressure, referred to as Wax Precipitation Curve (WPC), can be described by the empirical model (Michel & Civan, 2009b):

$$\ln\left(\frac{X^E}{X_T - X^E}\right) = c_0 + \frac{c_1}{T - T^0_{wax}} + c_2\left(T - T^0_{wax}\right)^2 \quad \text{.....(5-1)}$$

Here, the variable X^E is the equilibrium fraction of wax precipitated. The parameters c_0, c_1 and c_2 are correlation coefficients. The parameters x_T and T^0_{wax} are the total wax content and the wax appearance temperature measured at the standard reference pressure, and, respectively, which are known values. Equation 5-1 represents an extension of the VTF equation (Vogel, 1921); (Tammann & Hesse, 1926);(Fulcher, 1925)which generalizes the Arrhenius equation.

The experimental data measured in two previous studies (Martos, Coto, Espada, Robustillo, Gómez, & Peña, 2008); (Coto, Martos, Espada, Robustillo, Pena, & Gomez, 2009) are considered to validate the correlation model presented above. The WPC obtained experimentally in these studies offer a representative sample. Two of the studied waxes are naphtenic and three of them are paraffinic. One of the paraffinic waxes was reported to be highly paraffinic. Also, two WPC are presented for each examined wax: one measuring the gel obtained and the other subtracting the oil trapped inside the gel (waxy crystals only). Figures 5-1 through 5-5 show the actual measurements as dotted lines and the correlated curve as solid lines. Also, the corresponding mean error is reported for each WPC. Note that, lower error is obtained

for the WPC considering only the mass fraction of the waxy crystals (no trapped oil). These results provide a definitive prove for validity of the proposed model for wax precipitation as a satisfactory correlating model. The values of the correlation coefficients for WPC without trapped oil of each wax are presented in Table 5-1.

Table 5-1: Empirical coefficients for correlating wax precipitation

OIL TYPE	c_0 [fraction]	c_1 [°F]	c_2 [1/°F^2]
Naphthenic 1	-2.484	5.264	8.811E-04
Naphthenic 2	-1.902	10.06	1.101E-03
Paraffinic 1	-0.424	5.416	6.514E-03
Paraffinic 2	-2.125	3.806	1.996E-03
Paraffinic 3	-4.128	4.156	9.594E-04

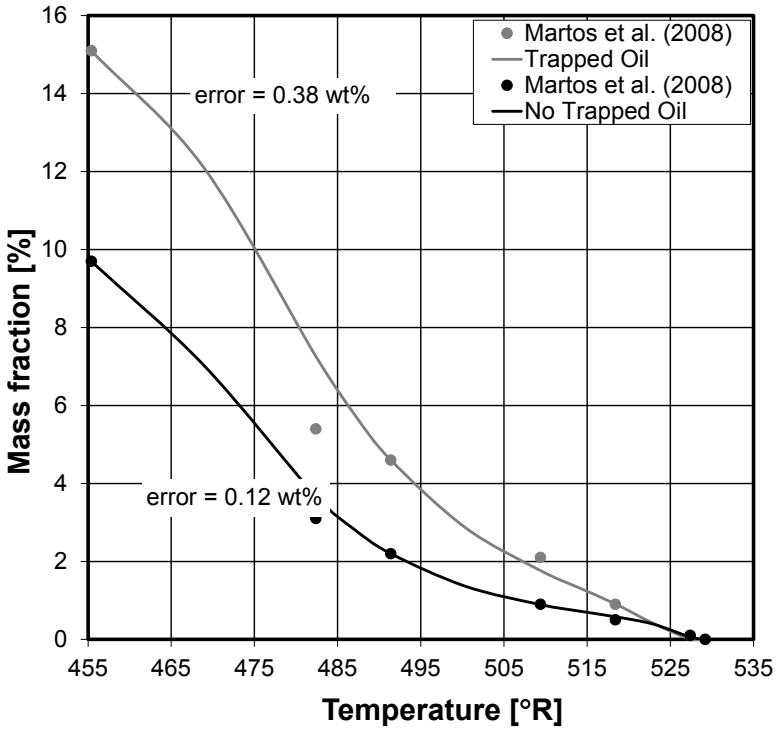

Figure 5-1: Precipitated fraction of Naphtenic wax 1.
Dots: Experimental. Lines: Correlation

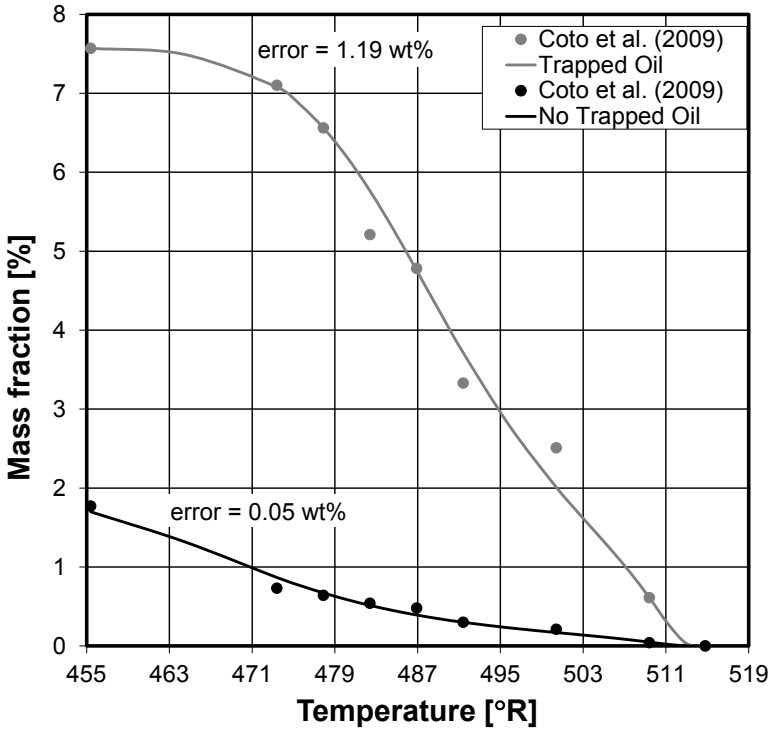

Figure 5-2: Precipitated fraction of Naphtenic wax 2.
Dots: Experimental. Lines: Correlation

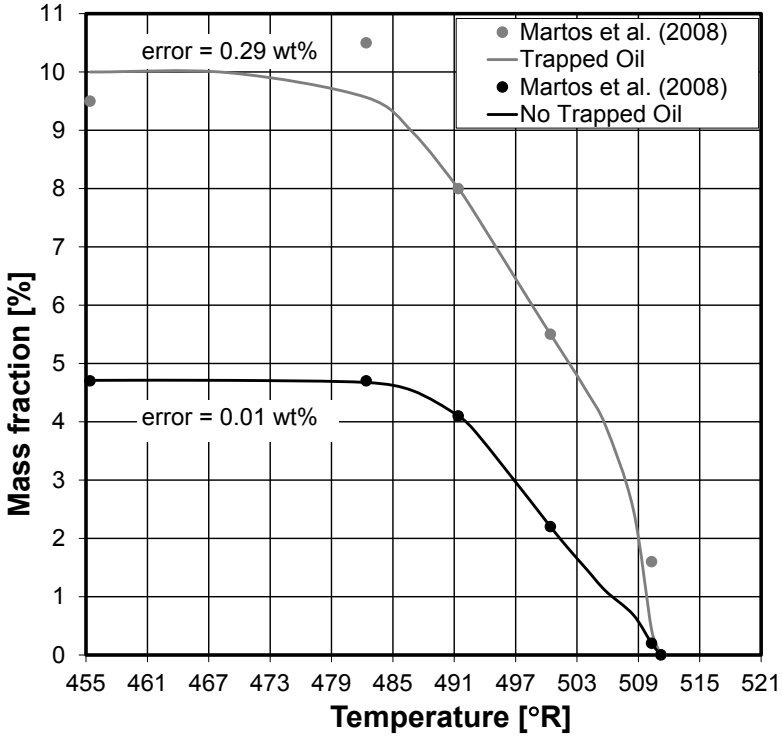

Figure 5-3: Precipitated fraction of Paraffinic wax 1.
Dots: Experimental. Lines: Correlation

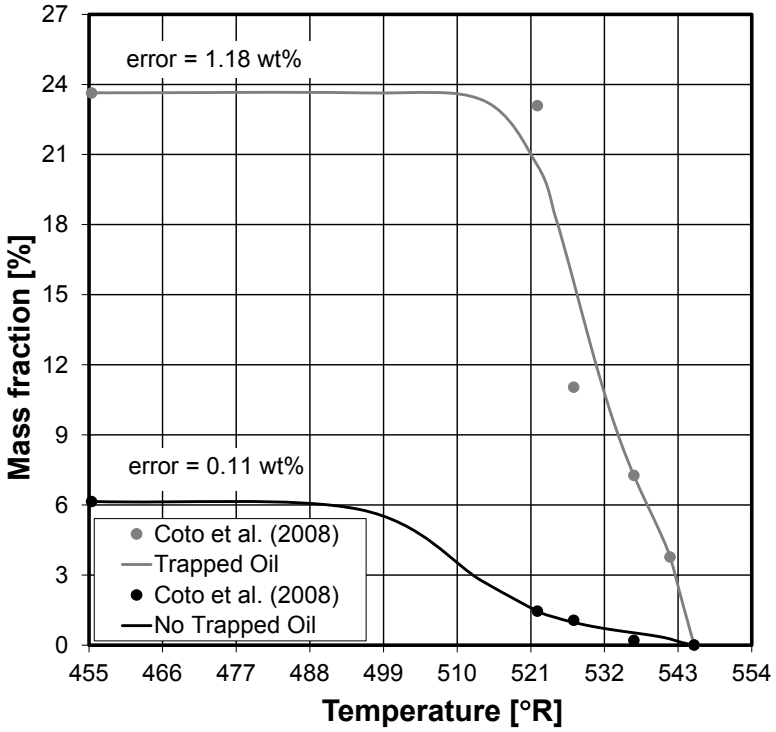

Figure 5-4: Precipitated fraction of Paraffinic wax 2.
Dots: Experimental. Lines: Correlation

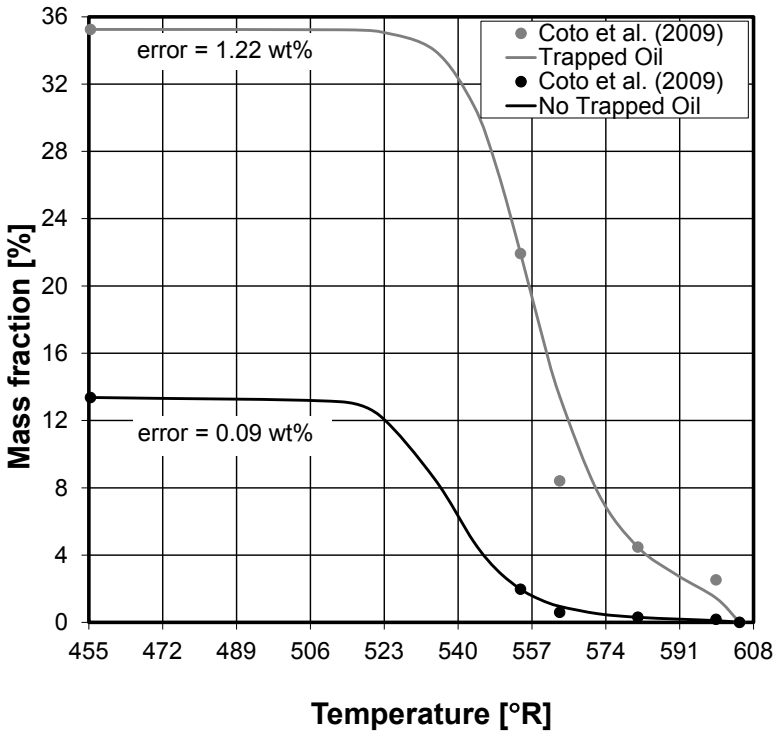

Figure 5-5: Precipitated fraction of Paraffinic wax 3.
Dots: Experimental. Lines: Correlation

The WAT and pressure are related non-monotonically. A minimum is expected where the wax appearance curve intersects with the bubble-point curve. The present study theorizes that the pressure dependence of the WAT (T_{wax}) for a given waxy-oil can be modeled by (Michel & Civan, 2011):

$$T_{wax} = T_{wax}^{0} + d_0 \frac{P - P_0}{(P - P_0) + d_1} + d_2 (P - P_0) \quad \text{.....(5-2)}$$

Here, d_0, d_1, and d_2 are some correlation parameters, and P_0 (14.7 psia) is the standard pressure. This pressure dependence model is validated by correlating experimental data (Daridon, Xans, & Montel, 1996). The observed WAT at various pressures correspond to different blends of paraffin wax mixed with a methane/decane system. The paraffin wax was designed to be constituted by different compositions while preserving molecular weight of the wax constant. Figure 5-6 shows the actual experimental measurements as hollow markers and the correlated curves as solid lines. The best-estimate values of the correlation coefficients obtained by the least-squares regression method for each wax/oil mixture are presented in Table 5-2.

Table 5-2: Best-estimate values of the coefficients used for correlating WAT against Pressure

	Wax A	**Wax B**	**Wax C**	**Wax D**	
d0 =	-13.88	-17.37	-22.41	-26.77	[°F]
d1 =	1005	1436	2155	3124	[psia]
d2 =	2.644E-03	3.080E-03	3.373E-03	3.983E-03	[°F/psia]
WAT0 =	68.45	78.17	74.75	104.27	[°F]

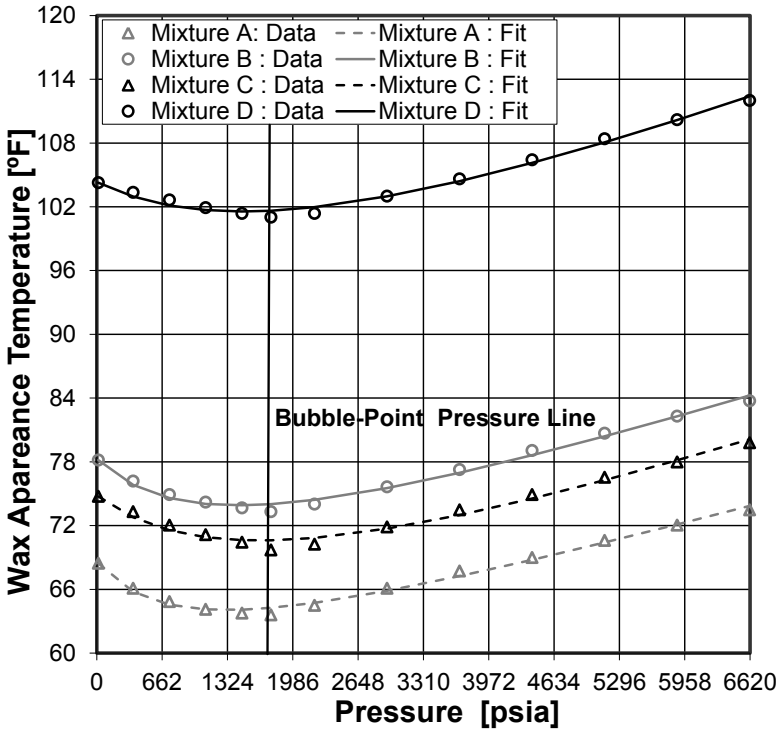

Figure 5-6 : Wax Appearance Temperature dependence on pressure for different wax/oil blends (Daridon, Xans, & Montel, 1996)

Consequently, the wax precipitation envelope is approximated in this study by generalizing equation 5-1 into the form:

$$\ln\left(\frac{X^E}{X_T - X^E}\right) = c_0 + \frac{c_1}{T - T_{wax}} + c_2\left(T - T_{wax}\right)^2 \quad \text{.....(5-3)}$$

where the WAT is computed using equation 5-2.

Relaxation of wax precipitation. The model and correlations presented in section 4.6 are adopted for describing the kinetics of wax gelation. The relaxation of wax precipitation occurring in submerged pipes during shut-in is non-isothermal cooling with variable

cooling rate. Consequently, the isothermal model stated in equation 4-13 cannot be used but the differential form of the model, stated in equation 4-10, is adopted. Then, the relaxed precipitation of wax is described by:

$$\frac{dX}{dt} = -\beta \frac{(X - X_E)}{t} \left(\frac{t}{\theta} \right)^{\beta} \quad \text{.....(5-4)}$$

The relaxed fractal growth is approximated by executing the classical second order of the Runge-Kutta methods (Heun's method) for numerical differentiation. This is an improvement to an approach presented elsewhere (Michel & Civan, 2011) which computes the relaxed precipitation with an isothermal relaxation model applying an stepwise temperature profile in time.

5.6. MODELING WAXY GELATION AS A WAX/OIL SYSTEM

Previous studies assume the solidification process advances as an instantaneously-forming moving front with piston-like separation of phases (Mehrotra & Bhat, 2007); (Edmonds, Moorwood, Szczepanski, & Zhang, 2008); (Bhat & Mehrotra, 2008) (Mehrotra & Bhat, 2010); (Lindeloff & Kerjbjerg, 2002); (Tiwary & Mehrotra, 2009). Most models proposed for analytical or numerical solutions of wax deposition divide the hydrocarbon system into two different regions. One region represents a waxy fluid (slurry) and the other a wax-free liquid phase (oil). These regions are separated by a moving boundary defined by the Wax Appearance Temperature (WAT), which is a property similar to the cloud point. The region above WAT is considered free of waxy crystals whereas the region below WAT is expected to have a uniform wax

concentration. Nevertheless, an accurate prediction of the moving boundary has proven to be a complicated issue.

The consideration of a moving boundary between waxy gel and liquid oil is unnecessary (Michel & Civan, 2009b). Instead, the wax precipitation can be modeled as a two-phase system. This approach facilitates a continuum modeling of the thermal and wax concentration gradients and the incorporation of the relevant mechanisms affecting wax precipitation and gelation without forced convection.

The two-phase fluid properties are estimated by volume-averaging. The pertinent phases are the liquid phase, which is the wax-free oil; and, the gelled phase, which is the fluid with wax precipitated crystals. Therefore, the density of the two-phase system is set to equal to gelled phase when all wax crystals have been precipitated. The density of this two-phase system is formulated as:

$$\frac{1}{\rho} = \frac{1}{\rho_{gel}}\left(\frac{X}{X_T}\right) + \frac{1}{\rho_{oil}}\left(1 - \frac{X}{X_T}\right) \quad \text{(5-5)}$$

where X is the local fraction of wax precipitated, ρ_{gel} is the density of gelled waxy-oil and ρ_{oil} is the density of wax-free oil. This density formulation is similar to equation 2-11. Note that, the weighing factor considered for calculating the various properties is the actual mass fraction of precipitated wax and not the mass fraction of precipitated wax at phase equilibrium Likewise, system heat capacity c_p and the volumetric fraction occupied by the gelled waxy-oil H_{gel} are expressed as:

$$H_{gel} = \frac{\rho}{\rho_{gel}}\left(\frac{X}{X_T}\right) \quad (5\text{-}6)$$

$$c_p = c_{p,gel}\left(\frac{X}{X_T}\right) + c_{p,oil}\left(1 - \frac{X}{X_T}\right) \quad (5\text{-}7)$$

where is $c_{p,gel}$ heat capacity of the gelled waxy-oil and $c_{p,oil}$ is the heat capacity of the wax-free oil. The system thermal conductivity is calculated as described by equation 2-16:

$$k = k_{gel}H_{gel} + k_{oil}\left(1 - H_{gel}\right) \quad (5\text{-}8)$$

where is k_{gel} thermal conductivity of the gelled waxy-oil and k_{oil} is the thermal conductivity of the wax-free oil.

5.7. MODELING WAX GELATION FOR A CIRCULAR CROSS-SECTION

In this section, a transient-state model for circular cross-sections subject to heat transfer is applied and validated with experimental data corresponding to wax precipitation where the cooling is applied from the wall surface and close to equilibrium state. The temperature profile is generated with a two-phase model and compared against the experimental data. For this purpose, the present study simplifies equation 2-39 for a two-phase system with constant pressure and converted from volume-averaged to area-averaged model.

$$\rho \frac{\partial h}{\partial t} = \frac{1}{r} \frac{\partial}{\partial r} \left(r\, k \frac{\partial T}{\partial r} \right) \quad \text{(5-9)}$$

Then, the final form of the model is obtained by introducing equation 2-17 and rearranging into:

$$\frac{\partial T}{\partial t} = \frac{k}{\rho c_p r} \frac{\partial T}{\partial r} + \frac{k}{\rho c_p} \frac{\partial^2 T}{\partial r^2} \quad \text{(5-10)}$$

subject to:

$$\frac{\partial T}{\partial r} = 0 \qquad r = 0 \quad \text{(5-11)}$$

$$\frac{\partial T}{\partial r} = -\frac{U}{k}\left(T - T_s\right) \qquad r = R \quad \text{(5-12)}$$

$$T = T_0 \qquad t = 0 \quad \text{(5-13)}$$

where R is the pipe inner radius and T_0 is the initial temperature.

This two-phase model presented facilitates the characterization of the temperature profile during wax precipitation and gelation across a circular cross-section. The area-averaging is executed by assuming all the properties of the wax-free oil and the gelled waxy-oil remain constant, and the temperature profile is axisymmetric in the radial direction. Figure 5-7 demonstrates the validity of the two-phase modeling of wax precipitation and gelation by comparing against experimental data (Bidmus &

Mehrotra, 2008a). The hollow markers represent the experimentally measured temperature at different distances from the center. The solid lines are the simulation predictions using incomplete data.

All the values of the various parameters employed for performing the numerical simulation of transient cooling are shown in Table 5-3. The parameters in the experimental study are assigned some representative values. The numerical simulation is accomplished by finite differences as elaborated in Appendix B. The WPC was not provided; thus suitable values for the WAT are assumed and the correlation parameters c0, c1 and c2 required in equation 5-1. Also, a high (effective) thermal conductivity for the wax-free phase is used to account for natural convection as recommended elsewhere (Michel and Civan 2009).

Table 5-3: Input parameters used for simulating transient cooling of a circular cross-section

Physical Property	Value	Units	Correlation Parameter	Value	Units
Oil gravity =	0.86		c0 =	4	[fraction]
Gel gravity =	0.92		c1 =	3.6	[°R]
Oil Heat capacity =	0.5017	[BTU/lbm°R]	c2 =	0.1543	[1/°R^2]
Gel Heat capacity =	0.6211	[BTU/lbm°R]			
Effective Oil Conductivity =	3.1786	[BTU/hr ft°R]			
Gel Conductivity =	0.0809	[BTU/hr ft°R]			
Heat Transfer Coefficient =	15.8537	[BTU/hr ft^2°R]			
Ambient Temperature =	534.6	[°R]			
Initial Temperature =	590.4	[°R]			
WAT =	557.1	[°R]			
Internal Radius =	2	[in]			

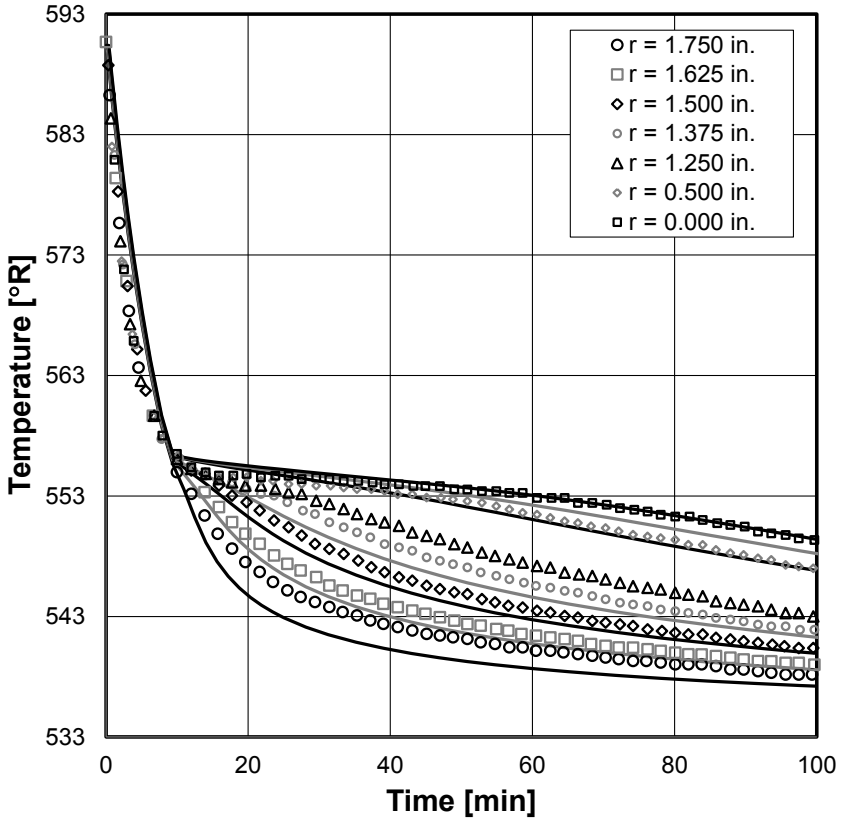

Figure 5-7: Transient temperature profiles of cooling waxy oil from the wall surface

5.8. MODELING WAX GELATION INSIDE COOLED SUBMARINE PIPES

In this section, the transient model developed for wax gelation in a circular cross-section is extended to vertical pipes subject to heat transfer. An analytical model is introduced for estimating the initial temperature profile required for simulating the transient wax precipitation after shut-in. Three simulation scenarios of transient wax precipitation occurring inside a shut-in submarine pipeline are conducted involving constant WAT without the pressure effect assuming instantaneous wax precipitation, pressure dependent WAT assuming instantaneous wax precipitation, and pressure dependent WAT considering a gradual wax precipitation process.

5.8.1. TRANSIENT WAX COOLING WITHOUT FORCED CONVECTION

The circular cross-section model presented previously in this study is extended into a two-dimensional model in space. The resulting transient modeling facilitates the description of the temperature profile for shut-in submarine pipelines subject to heat loss towards the sea-water environment. It is also necessary to determine the pressure profile because the WAT is pressure dependent. The following assumptions are made in this transient-state modeling:

- All the properties of the liquid and solid phases remain constant.
- The temperature profile is axisymmetric in the radial direction.
- The pressure varies only in the longitudinal direction.
- There is no longitudinal heat flow at the inlet and outlet surfaces.

The wax precipitation and gelation occurring inside a vertical submarine pipe at shut-in conditions can be characterized by simplifying equations 2-38 and 2-39. This system of equations can be reformulated as:

$$\frac{\partial T}{\partial t} = \frac{k}{\rho c_p r}\frac{\partial T}{\partial r} + \frac{k}{\rho c_p}\frac{\partial^2 T}{\partial r^2} + \frac{k}{\rho c_p}\frac{\partial^2 T}{\partial l^2} \quad \text{(5-14)}$$

$$\frac{\partial P}{\partial l} = -\bar{\rho} g \quad \text{(5-15)}$$

The following conditions are considered:

$$\frac{\partial T}{\partial r} = 0 \qquad r = 0 \qquad (5\text{-}16)$$

$$\frac{\partial T}{\partial r} = -\frac{U}{k}\left(T - T_s\right) \qquad r = R \qquad (5\text{-}17)$$

$$\frac{\partial T}{\partial l} = 0 \qquad l = 0, \quad l = L \qquad (5\text{-}18)$$

$$T = T_0(l, r) \qquad t = 0 \qquad (5\text{-}19)$$

$$P = P_0 - \int_0^l \bar{\rho} g \, dl \qquad t = 0 \qquad (5\text{-}20)$$

where $\bar{\rho}$ is the average density and $T_0(l.r)$ is a function representing the initial temperature. The cross-sectional average fluid density is given by:

$$\bar{\rho} = \frac{\int_0^R 2\pi\rho r \, dr}{\pi R^2} \qquad (5\text{-}21)$$

The initial temperature profile is known and has different values along the pipe. The inlet is the deepest location along the pipe. Since shut-in conditions are assumed, the effective value corresponding to the oil thermal conductivity must be used. This effective value is necessary in order to account for natural convection. A procedure for approximating the initial condition is elaborated in the next section.

5.8.2. INITIAL TEMPERATURE PROFILE AFTER SHUT-IN

Solving the transient modeling for shut-in submarine pipelines subject to heat loss towards requires a proper estimation of the temperature profile of the subsea-water pipeline prior to shut-in. This temperature profile represents the initial condition of the transient cooling model. This study theorizes the following assumptions are reasonable in order to approximate the initial conditions by an analytical model:

- The flow is at steady-state and turbulent, thus considering constant fluid velocity at all locations.
- Sufficient insulation is assumed for avoiding wax appearance so that the temperature is above the WAT at all locations initially.
- All the properties of the fluid remain constant while pressure and temperature vary.
- The sea-water temperature is constant at all depths.
- The temperature profile is axisymmetric in the radial direction.
- The conduction heat transfer can be neglected in the longitudinal direction so that the convective heat transfer is dominant and accounts for the overall heat transfer.

In view of these assumptions, the temperature profile before shut-in can be approximated by solving the following partial differential equation:

$$\rho c_p u \frac{\partial T}{\partial l} = \frac{k}{r} \frac{\partial}{\partial r}\left(r \frac{\partial T}{\partial r} \right) \quad \text{(5-22)}$$

subject to:

$$T \in \Re \qquad r = 0 \tag{5-23}$$

$$T = T_{0,0} \qquad r = 0, \quad l = 0 \tag{5-24}$$

$$-\int_0^L 2\pi RU\left(T\big|_{r=R} - T_s\right)dl = \int_0^L \int_0^{2\pi} \int_0^R \rho c_p u \frac{\partial T}{\partial l} r\, dr\, d\varphi\, dl \tag{5-25}$$

where $T_{0,0}$ is the temperature at the center of the inlet, which is required to be a known value. Equation 5-25 ensures that an overall heat balance of the system making all heat loos passing through the wall surface plus all heat transfer over the entire pipe volume to be equal to zero. Equation 5-22 can be rearranged in dimensionless form as:

$$Gz \frac{\partial \Theta}{\partial \zeta} = \frac{1}{\varsigma} \frac{\partial}{\partial \varsigma r}\left(\varsigma \frac{\partial T}{\partial \varsigma}\right) \tag{5-26}$$

subject to:

$$\Theta \in \Re \qquad \varsigma = 0 \tag{5-27}$$

$$\Theta = 1 \qquad \varsigma = 0, \quad \zeta = 0 \tag{5-28}$$

$$-Bi\int_0^1 \Theta\big|_{\varsigma=1}\, d\zeta = Gz\int_0^1 \int_0^1 \frac{\partial \Theta}{\partial \zeta} \varsigma\, d\varsigma\, d\zeta \tag{5-29}$$

where Θ is the dimensionless temperature, ζ is the dimensionless length, ς is the dimensionless radius, Gz is the Graetz number and Bi is the Biot number. These dimensionless variables and numbers are defined as:

$$\Theta = \frac{T - T_s}{T_{0,0} - T_s} \quad \text{(5-30)}$$

$$\zeta = \frac{l}{L} \quad \text{(5-31)}$$

$$\varsigma = \frac{r}{R} \quad \text{(5-32)}$$

$$Gz = \frac{\rho c_p u R^2}{kL} \quad \text{(5-33)}$$

$$Bi = \frac{UR}{k} \quad \text{(5-34)}$$

In the calculation of the Graetz and Biot numbers the actual value of oil thermal conductivity must be used. The effective value is necessary at shut-in conditions where no force convection occurs and natural convection has a key role. At flowing conditions, natural convection is neglected. A solution technique for approximating the initial temperature profile for submarine pipes after shut-in is presented in Appendix C.

5.8.3. SIMULATING WAX GELATION INSIDE COOLED SUBMARINE PIPES AT SHUT-IN CONDITIONS

In the present study, representative numerical simulations according to the finite difference method presented in Appendix D are performed applied to shut-in vertical pipes subject to heat transfer. Three case scenarios are considered:

- Base case: the WAT is considered constant (no pressure dependence) and the wax precipitation is instantaneous.
- Case 1: the WAT is considered pressure dependent and the wax precipitation is instantaneous.
- Case 2: the WAT is considered pressure dependent and the wax precipitation is gradually increased until equilibrium is attained.

Table 5-4: Input parameters used for simulating transient cooling of a vertical pipe

Physical Property	Value	Units	Correlation Parameter	Value	Units
Oil gravity =	0.86		c0 =	-2.3	[fraction]
Gel gravity =	0.94		c1 =	4.32	[°F]
Oil Heat capacity =	0.5256	[BTU/lbm°R]	c2 =	0.0278	[1/°F^2]
Gel Heat capacity =	0.9078	[BTU/lbm°R]	WAT0 =	73.52	[°F]
Effective Oil Conductivity =	2.8896	[BTU/hr ft°R]	d0 =	-22.32	[°F]
Oil Conductivity =	0.0982	[BTU/hr ft°R]	d1 =	2160.9	[psia]
Gel Conductivity =	0.1445	[BTU/hr ft°R]	d2 =	3.24E-03	[°F/psia]
Heat Transfer Coefficient =	0.3171	[BTU/hr ft^2°R]	Tc =	152	[°F]
Inlet Temperature =	101.6	[°F]	a1 =	1280	[sec]
Inlet Pressure =	2940	[°psia]	a2 =	-43.2	[°F]
WAT@Inlet Pressure =	70.18	[°F]	Beta =	0.9	[dimension]
Pipe Length =	3346	[ft]			
Internal Radius =	7	[in]			

The values of the various parameters employed for performing the numerical simulation of these case scenarios are shown in Table 5-4. The simulations are executed by finite differences as elaborated in Appendix D. Additionally, the required temperature profile of the sea-water is depicted in figure 5-8. The initial temperature profile is illustrated in figure 5-9 for a flow rate of 50 Mstb/D. This temperature profile is estimated by the procedure described in the previous section.

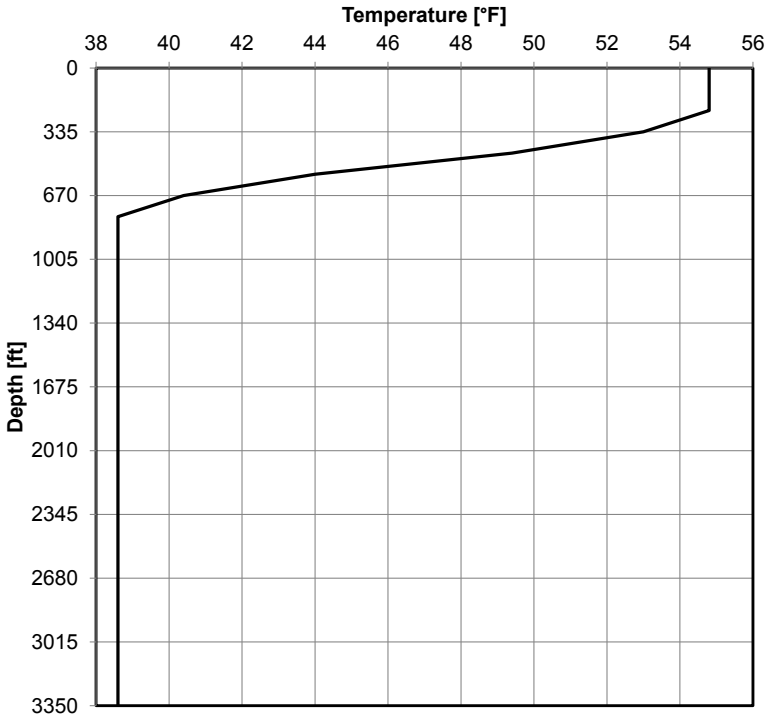

Figure 5-8: Sea-water temperature profile estimated for numerical simulation

The estimated mass fraction of wax precipitated relative to the total wax concentration after 24 hours of cooling is depicted in figures 5-10 to 5-12. The difference in the profiles for the base case and scenario 1 is evident. Not only is the change of phase boundary closer to the pipe center line but also more precipitation occurs as a location

gets closer to the inlet (bottom). Conversely, a slight difference can be seen between scenario 1 and 2. The same trend is observed after 28 and 32 hours of cooling, as shown in figures 5-13 to 5-15 and 5-16 to 5-18, respectively.

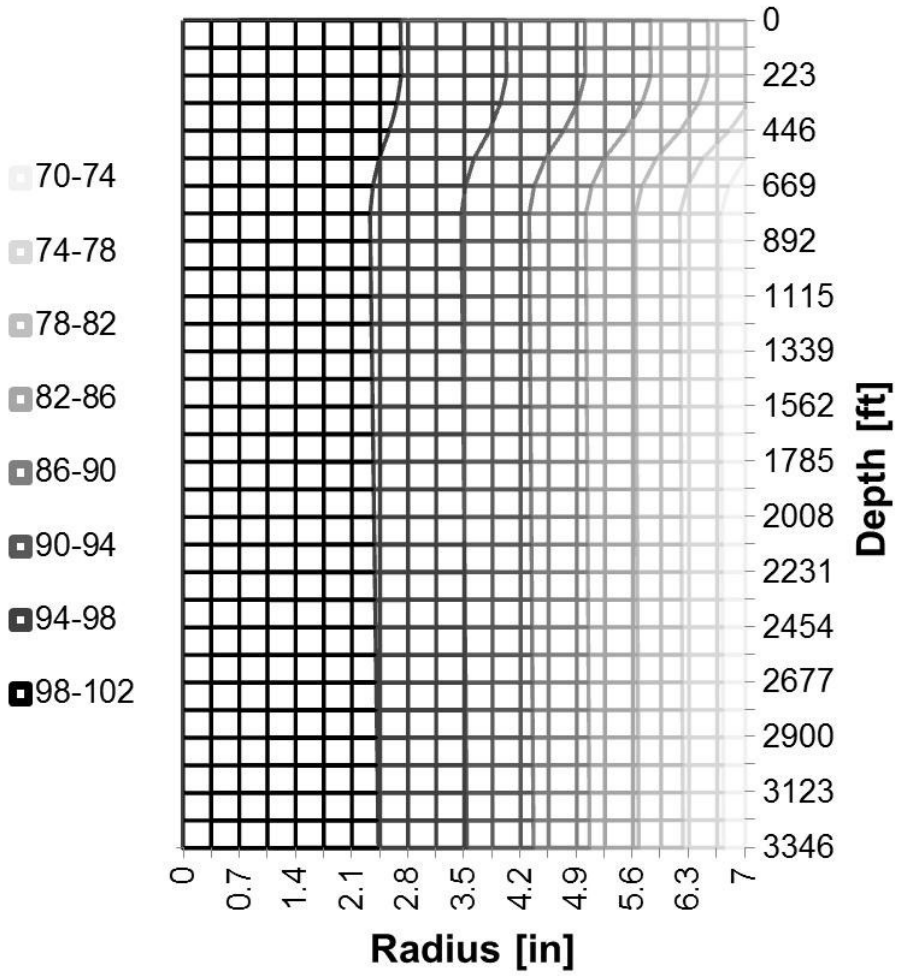

Figure 5-9: Estimated temperature profile for a flow rate of 50 Mstb/d

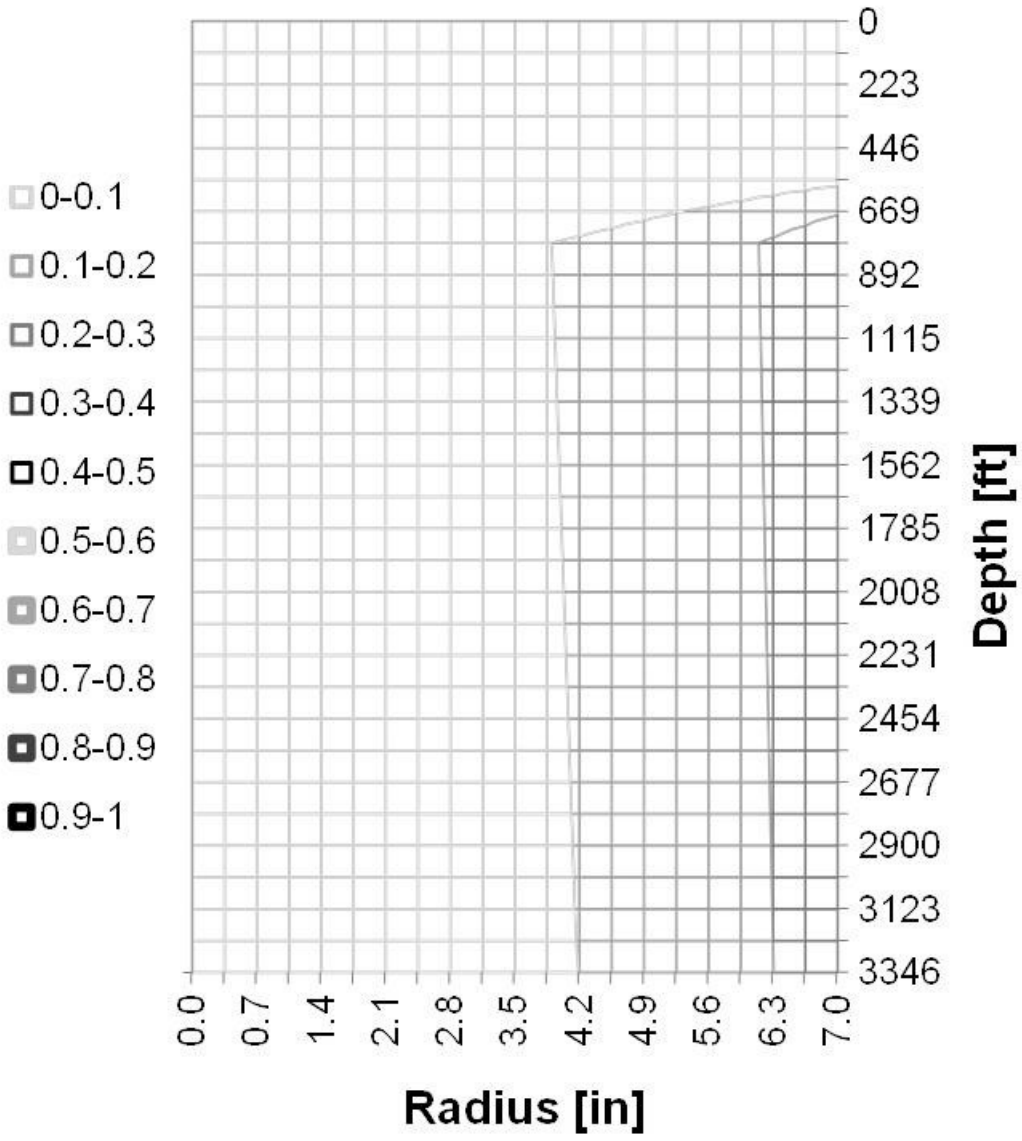

Figure 5-10: Wax precipitation profiles after 24 hours of cooling for the base case

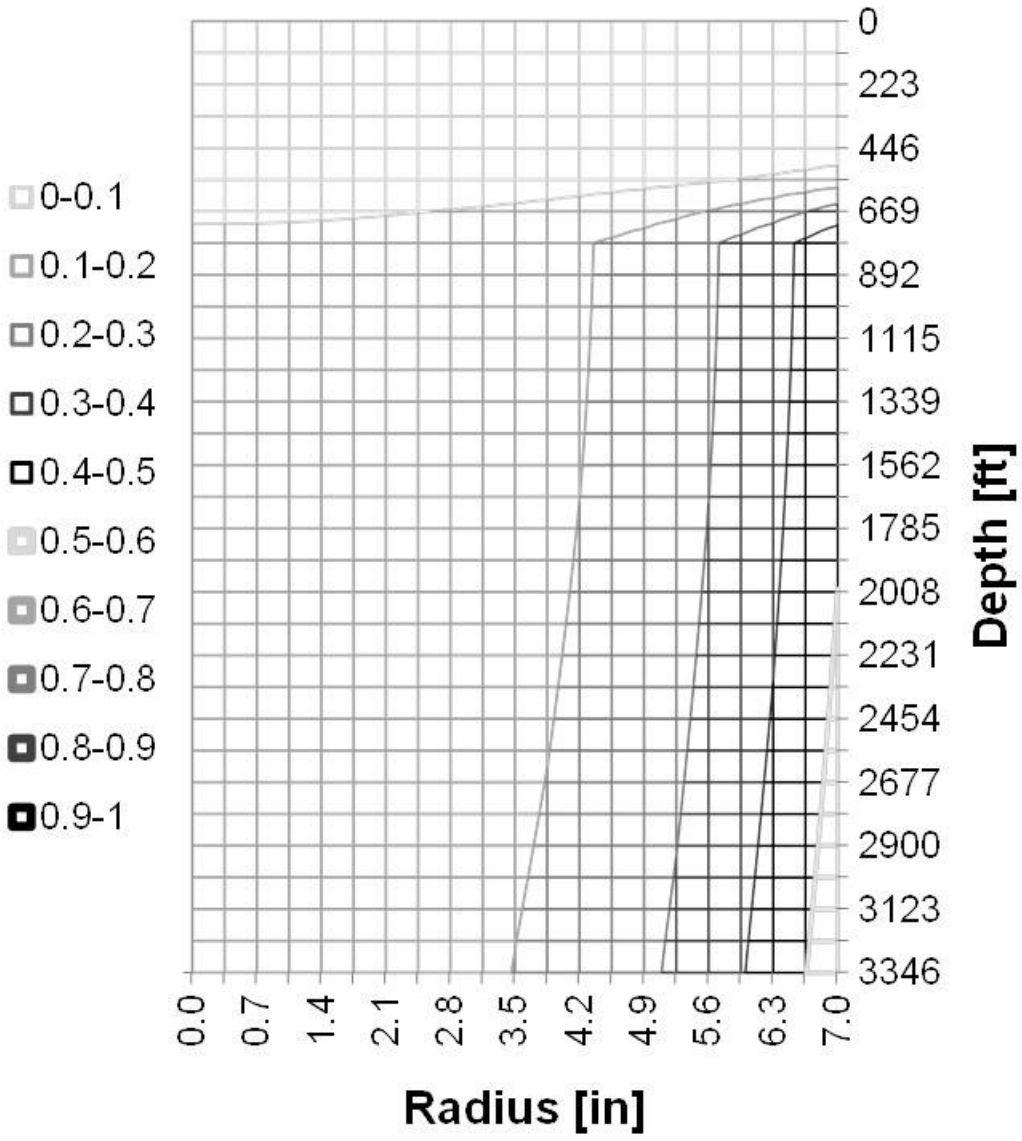

Figure 5-11: Wax precipitation profiles after 24 hours of cooling for scenario 1

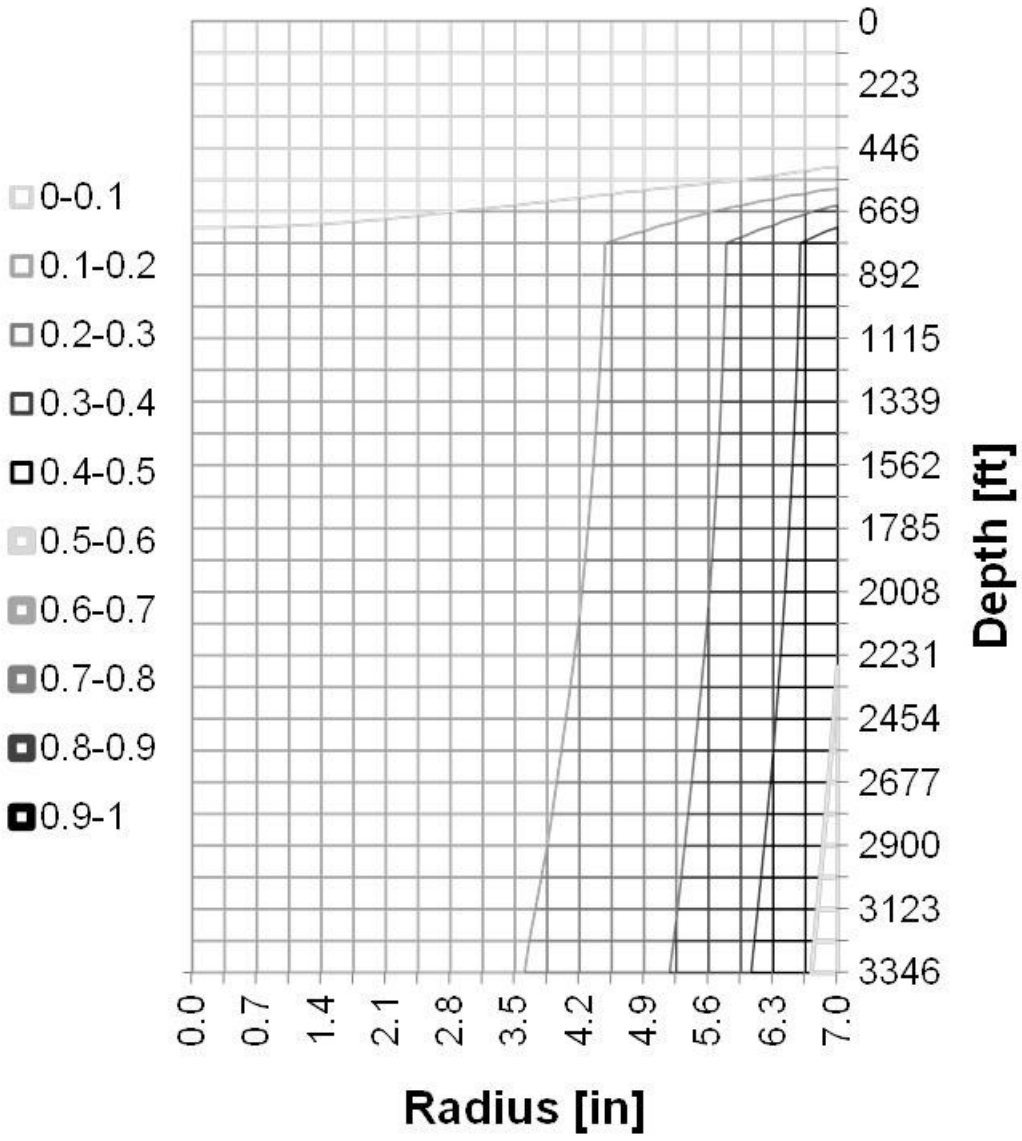

Figure 5-12: Wax precipitation profiles after 24 hours of cooling for scenario 2

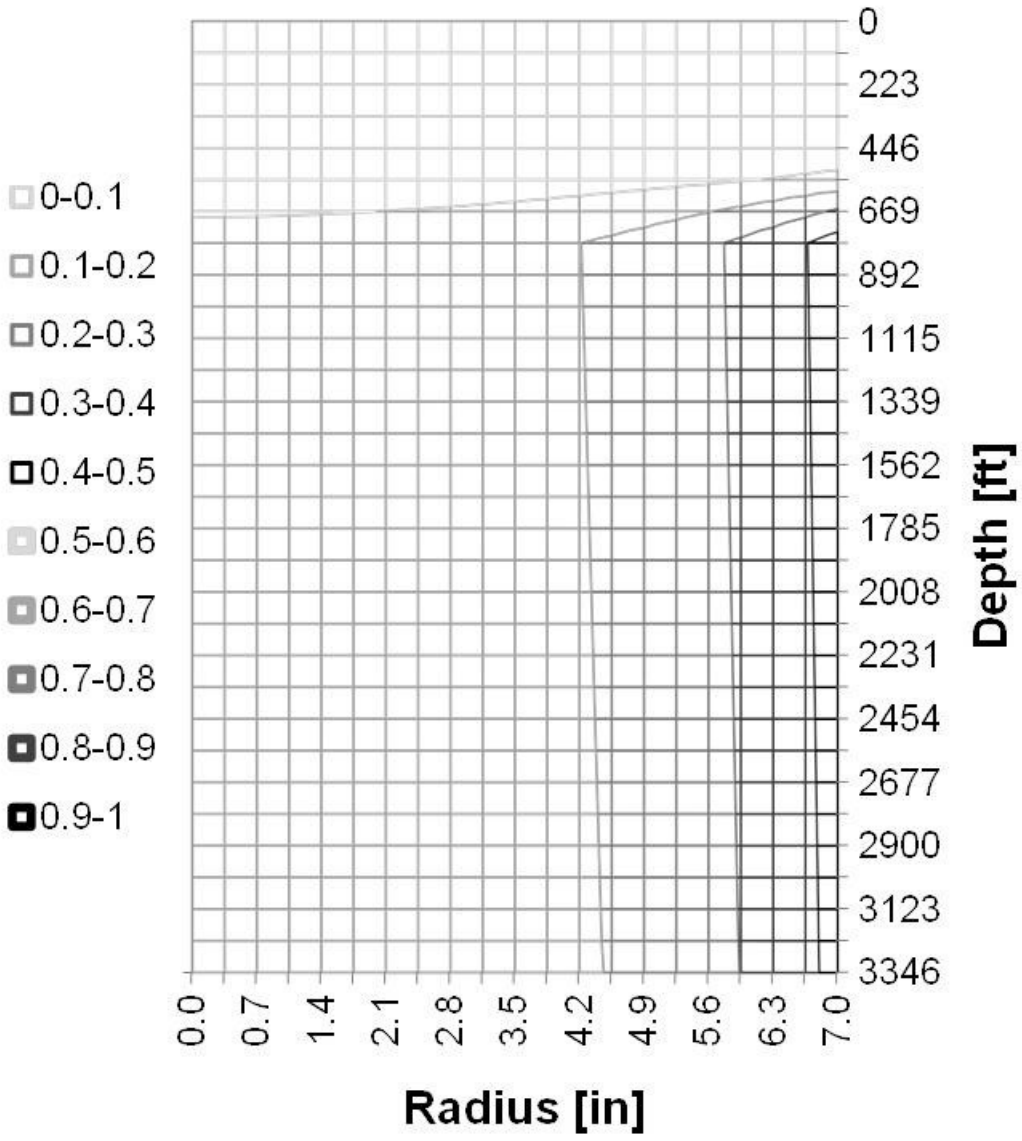

Figure 5-13: Wax precipitation profiles after 28 hours of cooling for the base case

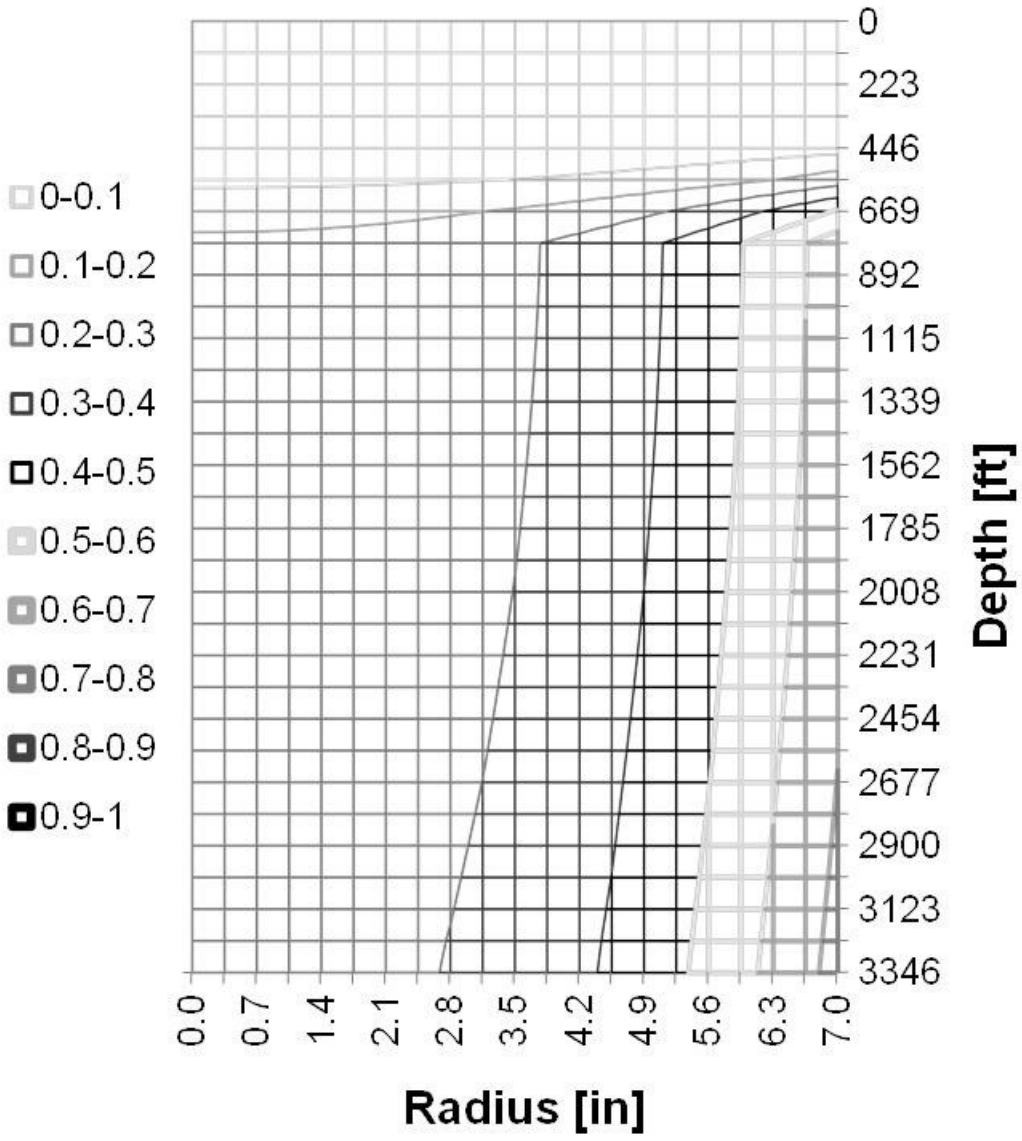

Figure 5-14: Wax precipitation profiles after 28 hours of cooling for scenario 1

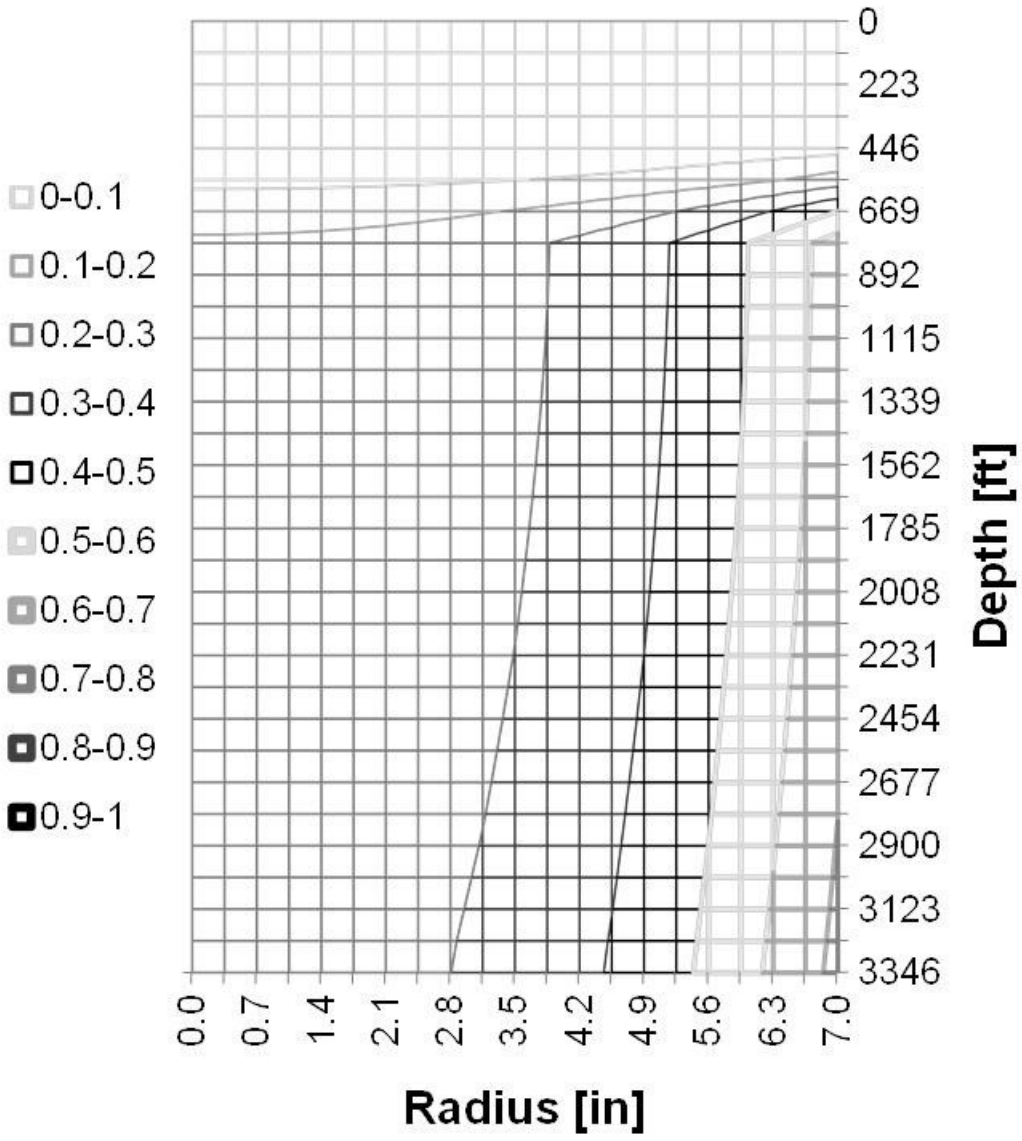

Figure 5-15: Wax precipitation profiles after 28 hours of cooling for scenario 2

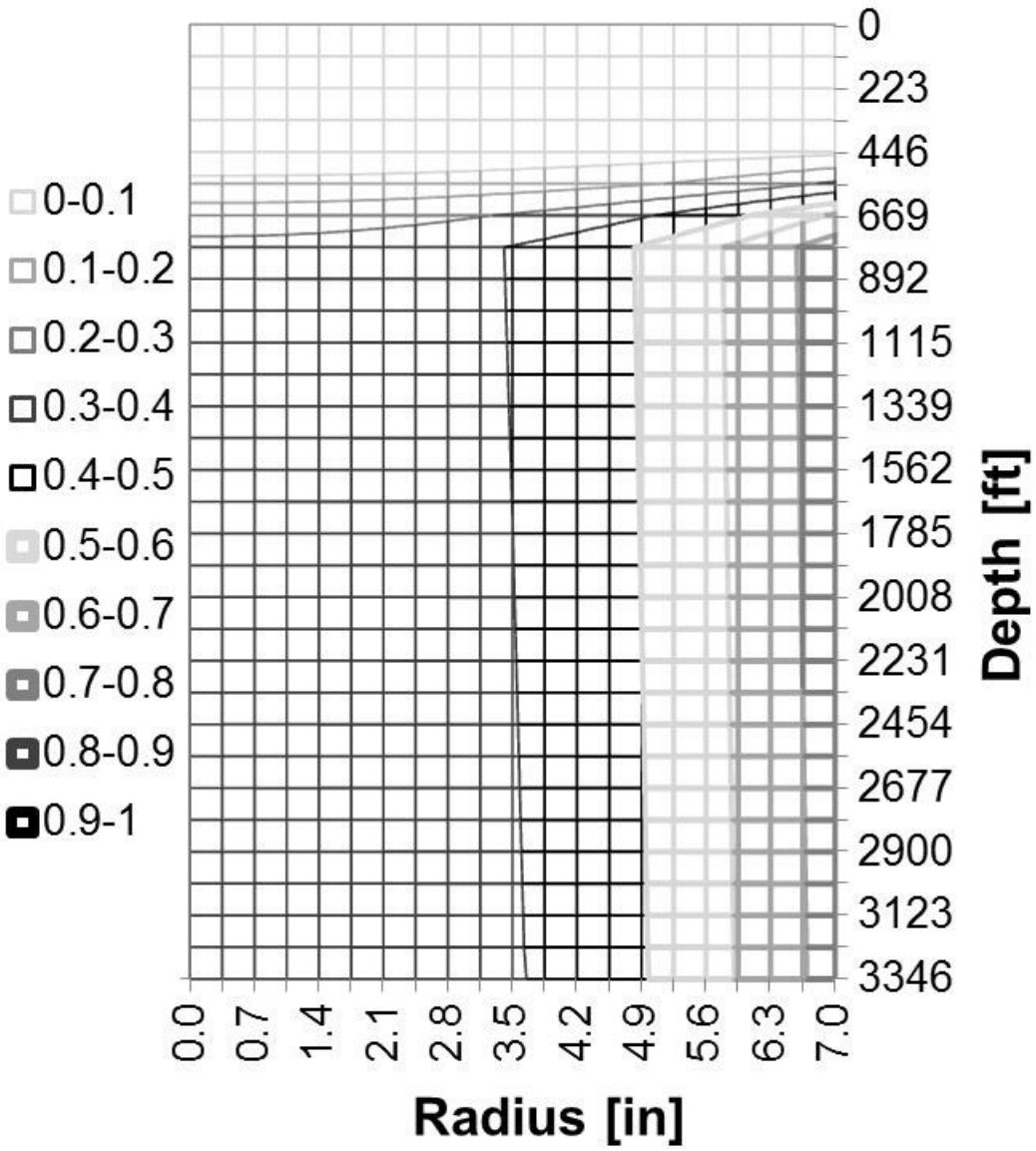

Figure 5-16: Wax precipitation profiles after 32 hours of cooling for the base case

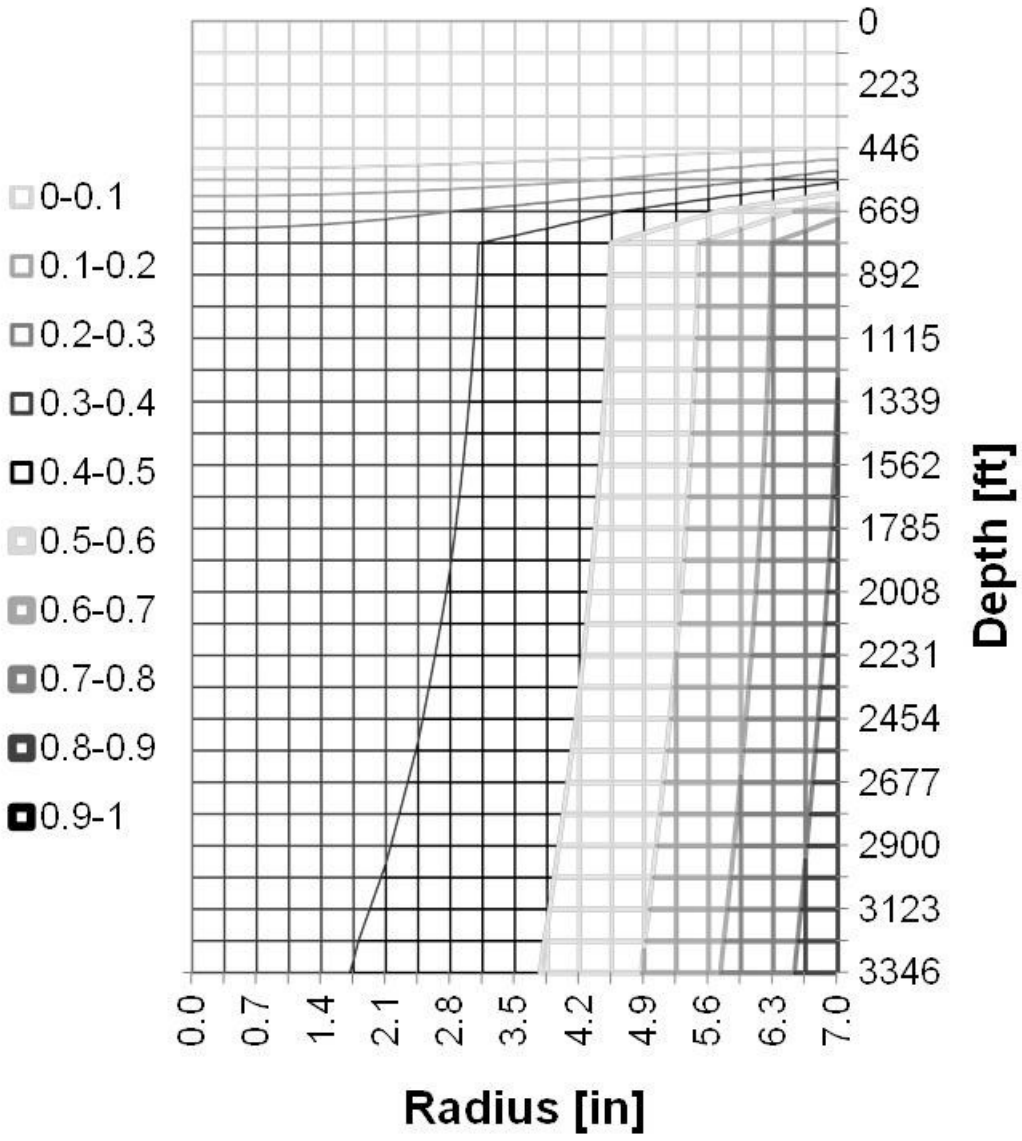

Figure 5-17: Wax precipitation profiles after 32 hours of cooling for scenario 1

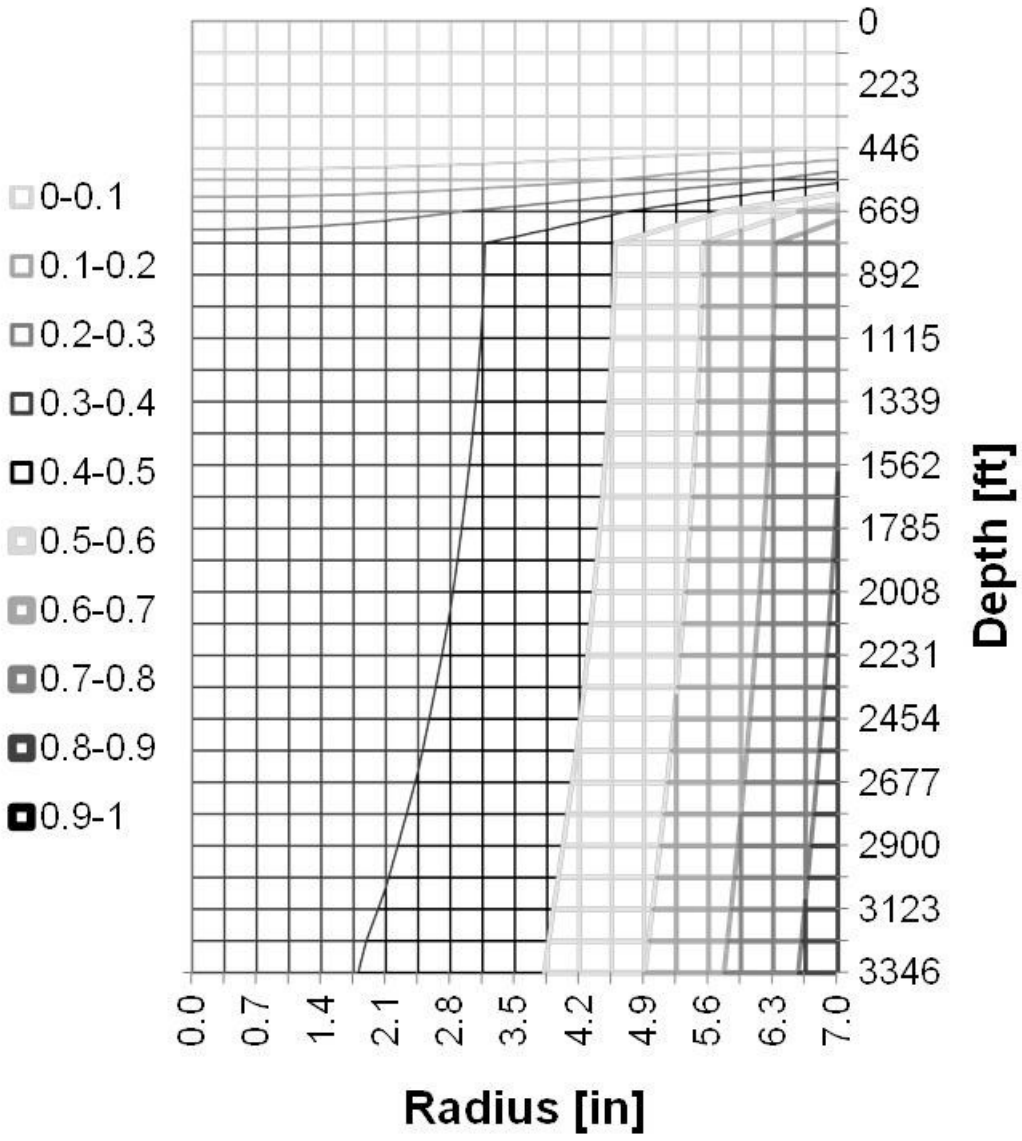

Figure 5-18: Wax precipitation profiles after 32 hours of cooling for scenario 2

Clearly, pressurization is an important mechanism that should be considered when estimating the wax precipitation. The simulations carried out above indicate about a 1 °F difference between the inlet WAT and the outlet WAT due to pressurization. Although small, this makes a substantial difference in the prediction of wax precipitation. This demonstrates the sensitivity of wax precipitation to the value of the WAT.

The role of relaxation in wax precipitation resulted in a minor effect because the high degree of insulation considered here induced only very low cooling rates. Thus, the wax precipitation attained the phase equilibrium rapidly. The adopted level of insulation falls within the operational range (Tillinghast, 1982) (Guo, Duan, & Ghalambor, 2006). Hence, the waxy-oil has not reached a complete state of a gelled system after 32 hours of cooling under this level of insulation conditions. However, the relaxation of wax precipitation may become important for low-degree of insulation because of high cooling rates to be experienced.

CHAPTER 6

DISCUSSION AND CONCLUSIONS

6.1. DISCUSSION

In this study, the relaxation effect on phase transition has been applied to gas separation and crystal precipitation from liquids. Specifically, the gas separation from oil and water has been relaxed in order to explain liquid holdup; and, the relaxed precipitation of wax from oil has been both related to wax rheology in order to explain aging and applied to wax gelation simulation.

The liquid holdup modeling is conventionally addressed by estimating the liquid volumetric fraction during multiphase flow based on the different flow regimes. The prediction of flow regime is accomplished according the flow rates of each phase by

assigning an empirical correlation for each flow regime. The accepted understanding of liquid holdup is that liquids tend to flow slower than the gas. Consequently, the liquids slip past the gas and an accumulation in the lower section of the pipe takes place which induces a higher concentration of liquid. In this study, one single constitutive equation is applied based on the relaxation of gas separation from liquids instead of applying a correlation for each flow regime in the prediction of liquid holdup. The higher liquid concentration observed along the pipe is explained by this apparent relaxation of gas separation. Then, the proposed constitutive equation is applied separately to the brine and oil phase for predicting liquid holdup in gas/oil/brine systems. It is demonstrated that lumping the liquids into on phase does not describe adequately the mass transfer from the liquids to gas.

Conventionally, the effect of liquid holdup on the overall flow is incorporated by calculating an effective mixture density using an estimated liquid fraction. Then, this effective density is employed in the calculation of the pressure drop. Thus, several assumptions and simplifications are incurred in the conventional approach by applying this artificial fixing of the density mixture. However, most of these remained unspecified in the revised bibliography. In section 2.5.3, the most relevant assumptions and simplifications are presented. There, the fluid flow experiencing liquid holdup is modeled as a homogenous multiphase system where the phases are allowed to flow at different velocities and mixture properties are calculated by area-averaging.

Aging or hardening of wax is the process on which gradual precipitation of wax crystal is undergoing until all waxy crystal has been precipitated. In other words, aging is the

relaxed crystallization of a waxy-oil. Naturally, the response to shear stress of an aging wax is time dependent since a changing solid concentration increases the resistance to flow. The relaxed response to shear stress has been extensively documented in the revised bibliography. In oscillatory tests, the relaxed viscoelastic response is evident when waxy-oil is subject to cooling. For constant shear rate tests, the relaxed nature of the apparent viscosity is also evident. The relaxation in wax crystallization has been proven to describe the relaxation in viscoelastic response. In this study, the relaxed crystallization is related to plastic response in order to incorporate the effect of aging in the gel strength and apparent viscosity. In this effort, a theoretical equivalence has been mathematically proven between the viscoelastic and plastic response of a material. Moreover, the wax crystallization is modeled with a relaxed fractal growth.

The definition of Wax Appearance Temperature has been widely standardized as the onset of wax crystallization. However, no clear definition is given to both the Pour Point Temperature (PPT) and the Gelation Temperature (GT) in the revised bibliography. In this study, clear definitions of these properties have been adopted and related to waxy-oil rheology. The adopted definition of GT, proposed in some of the revised bibliography, sets this temperature as the boundary between predominant elastic and predominant viscous behavior of a waxy-oil. The adopted definition of PPT, proposed in some of the revised bibliography, sets this temperature as the boundary between Newtonian and Non-Newtonian viscous nature. Alternative definition of PPT is the temperature at which a fluid ceases to flow. However, this alternative definition is adopted since it is ambiguous. The cause of cessation of flow may be different among

gelation processes. In example, the cessation of flow in a pipeline undergoing wax gelation is caused by lack of pressurization which cannot induce more breaking (ultimate failure) of gelled wax. On the other hand, the cessation of flow in a standard ASTM 5853 test is caused by lack of gravitational pull which cannot overcome weak gel strength. In the definition of GT, there is no consensus in the revised bibliography but some authors imply an equivalent definition to PPT.

In the modeling of transient wax gelation inside pipes, the area-averaged homogenous model it is not recommended. The layered inward growth of wax prevents the modeling of an even phase distribution over an elemental cross-section. This advancing wax precipitation from the perimeter to the center is induced by heat loss towards the sea environment for the case of submarine pipes at shut-in conditions. For this reason, the common approach of modeling wax solidification is to separate the material into a wax-free and a gelled regions. Here, the gelation is described as a piston-like advancing front having a binary solid concentration. However, the temperature is modeled having a gradual change in the radial direction. Experimental observations prove wax precipitates continuously depending on temperature. Thus, a thermal gradient over a cross-section implies a wax concentration gradient. In this study, wax gelation is modeled as the cooling of a homogenous two-phase system constituted by a wax-free phase and a gelled phase. This facilitates the description of wax gelation as continuous not binary precipitation of waxy crystals.

A continuous modeling of wax precipitation requires the development of solid-liquid phase diagram for waxy-oils. The mass fraction of precipitated wax dependent on

temperature is referred to as Wax Precipitation Curve, which is implied to be at atmospheric pressure. The dependency of wax precipitation on pressure is yet to be determined. However, the pressure dependence of the WAT has been already experimentally observed. In this study, empirical correlations are provided for estimating the fraction of wax precipitated given a temperature and the WAT given a pressure. Since the WPC depends on the WAT, a simple phase diagram is obtained by combining both correlations. The proposed phase diagram model is applied to a homogenous two-phase model in order to simulate wax gelation for a cross-section. A finite difference scheme is expressly developed in order to facilitate this type of simulations. The simulation results are in good agreement with experimental measurements of wax gelation. During simulations, the wax-free phase is assigned with apparent heat conductivity in order to account the effect of natural convection. Then, the proposed diagram is applied to a homogenous two-phase model for simulation of wax gelation inside vertical submarine pipes at shut-in conditions. A finite difference scheme is expressly developed in order to facilitate this type of simulations. The effect of pressurization and relaxation in wax crystallization are investigated. The simulation results show that the effect of pressurization is greater than the effect of relaxation.

6.2. CONCLUSIONS

The following conclusions concerned with the present stud have been reached:

1. Modeling the transport of reservoir fluids for steady multiphase flow and transient solidification can be eased by applying homogenous models.
2. The developed finite difference models for calculating the thermal changes

during transient wax gelation proved to perform adequately.

3. Liquid holdup occurring in steady-state multiphase flow inside productions pipes can be modeled as a relaxed gas separation from liquids. And, lumping the liquid phases as one liquid phase proved to be inadequate.
4. The effect of aging on wax rheology can be incorporated by applying a relaxation model to the rheological properties based on the relaxed fractal growth of waxy crystals.
5. Wax gelation inside submarine vertical pipes at shut-in conditions can be modeled as a homogenous multiphase system. And, the effect of pressurization is greater than the effect of relaxed wax crystallization.

BIBLIOGRAPHY

A1-Fariss, T., Jang, L., Ozbelge, H., & Ghasem, N. (1993). A new correlation for the viscosity of waxy oils. *J. Petr. Sci.&Eng., 9*, 139-144.

Ajienka, J., & Ikoku, C. (1991). The Effect of Temperature on the Rheology of Waxy Crude oils. *SPE 23605*.

Ansari, A., Sylvester, N., Sarica, C., Shoham, O., & Brill, J. (1994, May). A Comprehensive Mechanistic Model for Upward Two-Phase Flow in Wellbores. *SPE Production & Facilities*, 143-152.

Asheim, H. (1986, May). MONA, An Accurate Two-Phase Well Flow Model Based on Phase Slippage. *SPE Production Engineering*, 221-230.

Avrami, M. (1940). Kinetics of Phase Change II Transformation-Time Relations for Random Distribution of Nuclei. *J. Chem. Phys.*, 212–224.

Ayala, L. F., & Adewumi, M. A. (2003). Low-Liquid Loading Multiphase Flow in Natural Gas Pipelines. *J. of the Energy Res. Tech., 125*, 284-293.

Aziz, K., Govier, G. W., & Fogarasi, M. (1972, July/September). Pressure Drop in Wells Producing Oil and Gas. *J. of Can. Petr. Tech.*, 38-48.

Badur, J., & Banaszkiewicz, M. A. (1998, January). Model of two-phase flow with relaxation-gradient microstructure, Third International Conference on Multiphase Flow, . *Third International Conference on Multiphase Flow*.

Beggs, H. D., & Brill, J. (1973, May). A Study of Two-Phase Flow in Inclined Pipes. *JPT 829, Trans. AIME, 255*.

Bhat, N. V., & Mehrotra, A. K. (2008). Modeling the Effect of Shear Stress on the Composition and Growth of the Deposit Layer from "Waxy" Mixtures under Laminar Flow in a Pipeline. *Energy&Fuels, 22*, 3237-3248.

Bidmus, H., & Mehrotra, A. (2008a). Measurement of the Liquid/Deposit Interface Temperature during Solids Deposition from Wax/Solvent Mixtures under Static Cooling Conditions. *Energy&Fuels, 22*(2), 1174-1182.

Bidmus, H., & Mehrotra, A. (2008b). Measurement of the Liquid/Deposit Interface Temperature during Solids Deposition from Wax/Solvent Mixtures under Sheared Cooling. *Energy&Fuels, 22*(6), 4039-4048.

Bilicki, Z., & Kestin, J. (1990, April 9). Physical Aspects of the Relaxation Model in Two-Phase Flow. *Proceedings of the Royal Society of London, Series A, Mathematical and Physical Sciences, 428*(1875), 379-397.

Bird, B., Stewart, W., & Lightfoot, E. (1965). *Transport Phenomena* (5th ed.). New York: Wiley & Sons Inc.

Brill, J. P., & Mukherjee, H. (1999). *Multiphase Flow in Wells.* Richardson, TX, USA: SPE Monograph.

Cazaraez-Candia, O., & Vásquez-Cruz, M. (2005). Prediction of Pressure, Temperature and Velocity Distribution of Two-Phase Flow in Oil Wells. *J. of Petr. Sci.&Eng., 46*, 195-208.

Chang, C., Boger, D., & Nguyen, Q. (2000). Influence of Thermal History on the Waxy Structure of Statically Cooled Waxy Crude Oil. *SPE 57959. SPE Journal, 5*(2), 148-157.

Chapra, S., & Canale, R. (1998). *Numerical Methods for Engineers: with Programming and Software Applications* (3rd ed.). McGraw-Hill.

Chierici, G., Ciucci, G., & Sclocchi, G. (1974, August). Two-Phase Vertical Flow in Oil Wells – Prediction of Pressure Drop. *SPE Journal of Petroleum Technology*, 927-938.

Civan, F. (2006). Including Non-equilibrium Relaxation in Models for Rapid Multiphase Flow in Wells. *SPE Production&Operations, 21*(1), 98-106.

Civan, F. (2008). Use Exponential Functions to Correlate Temperature Dependence. *Chem. Eng. Progress, 104*(7), 46-52.

Civan, F., & Sliepcevich, C. (1984). Efficient Numerical Solution for Enthalpy Formulation of Conduction Heat Transfer with Phase Change. *Int. J. Heat Mass Transfer, 27*(8), 1428-1430.

Civan, F., & Sliepcevich, C. (1985). Comparison of the Thermal Regimes for Freezing & Thawing of Moist Soils. *Water Resources Research, 21*(3), 407-410.

Civan, F., & Sliepcevich, C. (1987). Limitation in the Apparent Heat Capacity Formulation for Heat Transfer with Phase Change. *Proceedings of the Oklahoma Academy of Science, 67*, 83-88.

Coto, B., Martos, C., Espada, J. J., Robustillo, M. D., Pena, J. L., & Gomez, S. (2009). Assessment of a Thermodynamic Model To Describe Wax Precipitation in Flow Assurance Problems. *Energy&Fuels, 23*, 1294-1298.

Coutinho, J. A. (2000). A Thermodynamic Model for Predicting Wax Formation in Jet and Diesel Fuels. *Energy&Fuels, 14*, 625-631.

Coutinho, J. A., Edmonds, B., Moorwood, T., Szczepanski, R., & Zhang, X. (2006). Reliable Wax Predictions for Flow Assurance. *Energy&Fuels, 20*, 1081-1088.

Daridon, J., Xans, P., & Montel, F. (1996). Phase Boundary Measurement On A Methane + Decane + Multiparaffins System. *Fluid Phase Equilibria, 117*, 241-248.

Denn, M. (2008). *Polymer Melt Processing.* New York: Cambridge University Press.

Downar-Zapolski, P., Bilicki, Z., Bolle, L., & Franco, J. (1996). The Non-equilibrium Relaxation Model for One-Dimensional Flashings Liquid Flow. *Int. J. Multiphase Flow, 22*(3), 473-483.

Edmonds, B., Moorwood, T., Szczepanski, R., & Zhang, X. (2008). Simulating Wax Deposition in Pipelines for Flow Assurance. *Energy&Fuels, 22*, 729-741.

Ekweribe, C., Civan, F., Lee, H. S., & Singh, P. (2009, September). Pressure Effect onwaxy-Crude Pipeline-Restart Conditions Investigated by a Model System. *SPE Projects, Facilities&Construction*, 61-74.

Faghri, A., & Zhang, Y. (2006). *Transport Phenomena in Multiphase Systems.* Elsevier Academic Press.

Feburie, V., Goit, M., Granger, S., & Seyhaeve, J. M. (1993). A Model for Chocked Flow through Cracks with Inlet Subcooling. *Int. J. Multiphase Flow, 19*(4), 541-562.

Fulcher, G. (1925). Analysis of Recent Measurements of the Viscosity of Glasses. *J. Am. Ceram. Soc., 8*, 339–355.

Gluyas, J., & Underhill, J. (2003). The Staffa Field, Block 3/8b, UK North Sea-water. *Geological Society, Memoirs, 20*, 327-333.

Gray. (1978). SSCSV Sizing Computer Program. *User's Manual for API 14B, Appendix B, Second*, 38-41. API.

Guo, B., Duan, S., & Ghalambor, A. (2006, February). A Simple Model for Predicting Heat Loss and Temperature Profiles in Insulated Pipelines. *SPE 86983. SPE Production&Operations*.

Hagedorn, A. R., & Brown, K. E. (1965, April). Experimental Study of Pressure Gradients Occurring During Continuous Two-Phase Flow in Small-Diameter Vertical Conduits. *J. of Petr. Tech.*, 475-484.

Hennessy, A., Neville, A., & Roberts, K. (2004). In-Situ SAXS/WAXS and Turbidity Studies of the Structure and Composition of Multihomologous n-Alkane Waxes Crystallized in the Absence and Presence of Flow Improving Additive Species. *Crystal Growth&Design, 4*(5), 1069-1078.

Hoteit, H., Banki, R., & Firoozabadi, A. (2008). Wax Deposition and Aging in Flowlines from Irreversible Thermodynamics. *Energy&Fuels, 22*, 2693–2706.

Hou, L., & Zhang, J. A. (2010). Study on Creep Behavior of Gelled Daqing Crude Oil. *J. Petr. Sci.&Eng., 28*, 690–699.

Jawed, R. (2006). Experimental Determination of the Diffusion Coefficient of Carbon Dioxide in Crude Oil. *MS thesis*. Norman, OK, USA: The University of Oklahoma.

Lakes, R. (2009). *Viscoelastic Materials.* New York: Cambridge University Press.

Lee, H., Singh, P., Thomason, W., & Fogler, H. (2008). Waxy Oil Gel Breaking Mechanisms: Adhesive versus Cohesive Failure. *Energy&Fuels, 22*, 480–487.

Lee, J., & Wattenbarger, R. (2004). *Gas Reservoir Engineering.* Richardson, TX, USA: SPE Texbook Series.

Lindeloff, N., & Kerjbjerg, K. (2002). A Compositional Model Simulating Wax Deposition in Pipeline Systems. *Energy&Fuels, 16*, 887-891.

Lopez-Da-Silva, J., & Couthino, J. (2007). Analysis of the Isothermal Structure Development in Waxy Crude Oils under Quiescent Conditions. *Energy&Fuels, 21*, 3612–3617.

Marie, E., Chevalier, Y., Brunel, S., Eydoux, F., Germanaud, L., & Flores, P. (2004). Settling of paraffin crystals in cooled middle distillate fuels. *J. Colloid and Interface Sci., 269*, 117–125.

Martos, C., Coto, B., Espada, J., Robustillo, M., Gómez, S., & Peña, J. (2008). Experimental Determination and Characterization of Wax Fractions Precipitated as a Function of Temperature. *Energy&Fuels, 22*(2), 708-714.

Mehrotra, A. K., & Bhat, N. V. (2007). Modeling the Effect of Shear Stress on Deposition from "Waxy" Mixtures under Laminar Flow with Heat Transfer. *Energy&Fuels, 21*, 1277-1286.

Mehrotra, A. K., & Bhat, N. V. (2010). Deposition from "Waxy" Mixtures under Turbulent Flow in Pipelines: Inclusion of a Viscoplastic Deformation Model for Deposit Aging. *Energy&Fuels, 24*, 2240-2248.

Michel, G. (2007). Modeling of Multiphase Flow in Wells under Nonisothermal and Nonequilibrium Conditions. *MS thesis*. Norman, OK, USA: The University of Oklahoma.

Michel, G., & Civan, F. (2008a). Modeling Nonisothermal Rapid Multiphase Flow in Wells under Nonequilibrium Conditions. *SPE 102231. SPE Production&Operations, 23*(2), 125-134.

Michel, G., & Civan, F. (2008b, September 21–24). Accurate Modeling of Relaxation Time and Liquid Holdup for Multiphase Flow in Production Wells. *SPE 115738*. Denver, Colorado, USA: SPE Annual Technical Conference and Exhibition.

Michel, G., & Civan, F. (2008c, June 9-20). Simulation of Nonisothermal and Nonequilibrium Multiphase Wellbore Hydraulics. Istanbul, Turkey: 18th ITU Petroleum and Natural Gas Engineering Seminar and Exhibition.

Michel, G., & Civan, F. (2009a, May 31 - June 5). Accurate Well-Bore Hydraulics Simulation Considering Non-Isothermal and Liquid-Slippage Phenomena for Multiphase Flow in Oil and Gas Wells. *OMAE2009-80068*. Honolulu, Hawaii, USA: ASME 28th International Conference on Ocean, Offshore and Arctic Engineering.

Michel, G., & Civan, F. (2009b, 4–7 October). Modeling Multiphase Wax Deposition in Submarine Pipelines after Shut-In. *SPE 124725*. New Orleans, Louisiana, USA: SPE Annual Technical Conference and Exhibition.

Michel, G., & Civan, F. (2011, 2-5 May). Robust Phenomenological Model for Simulation of Transient Wax Gelation in Submarine Pipelines. *OTC 21248*. Houston, Texas, USA: Offshore Technology Conference.

Ogundare, T. (2004). Experimental Investigation of Gas Diffusion in Oil-Field Fluids. *MS thesis*. Norman, OK, USA: The University of Oklahoma.

Oh, K., Gandhi, K., Magda, J., & Deo, M. D. (2009). Yield Stress of Wax Gel using Vane Method. *Pet. Sci. & Tech., 27*(17), 2063 — 2073.

Ozawa, T. (1971). Kinetics of non-isothermal crystallization. *Polymer, 12*(3), 150-158.

Rasmussen, M., & Civan, F. (2009, January). Parameters of Gas Dissolution in Liquids Obtained by Isothermal Pressure Decay. *AICHE J., 55*(1), 9-23.

Reynolds, P., & Jones, T. (1989). An Experimental Study of the Settling Velocities of Single Particles in Non-Newtonian Fluids. *Int. J. Mineral Processing, 25*, 47-77.

Ronningsen, H. (1992). Rheological behaviour of gelled, waxy North Sea crude oils. *J. Petr. Sci.&Eng., 7*, 177-213.

Ros, N. C. (1961, October). Simultaneous Flow of Gas and Liquid as Encountered in Well Tubing. *J. of Petr.Tech.*, 1037-1049.

Tammann, G., & Hesse, W. (1926). Die abhängigkeit der viskosität von der temperature bei unterkühlten flüssigkeiten. *Z. Anorg. Allg. Chem., 156*, 245–257.

Tannehill, J. C., Anderson, D. A., & Pletcher, R. H. (1997). *Computational Fluid Mechanics and Heat Transfer* (2nd ed.). Philadelphia, PA, USA: Taylor&Francis.

Tillinghast, W. (1982, 9-12 February). Udang "B" Insulated Subsea-water Pipelines – Design and Installation. *SPE 10447*. Singapore, Singapore: Offshore Shout East Conference.

Tinsley, J., Prud'homme, R., Guo, X., Adamsom, D., Shao, S., Amin, D., et al. (2007). Effects of Polymers on the Structure and Deposition Behavior of Waxy Oils. *SPE 106204. SPE Interntional Symposium on Oilfield Chemistry*.

Tiwary, R., & Mehrotra, A. K. (2009). Deposition from Wax-Solvent Mixtures under Turbulent Flow: Effects of Shear Rate and Time on Deposit Properties. *Energy&Fuels, 23*, 1299-1310.

Venkatesan, R., Singh, P., & Fogler, H. (2002, December). Delineating the Pour Point and Gelation Temperature of Waxy Crude Oils. *SPE 72237. SPE Journal*, 349-352.

Vogel, H. (1921). Das temperature-abhängigketsgesetz der viskosität von flüssigkeiten. *Phys. Zeit., 22*, 645–646.

Walas, S. M. (1991). *Modeling with Differential Equations in Chemical Engineering.* Boston: Butterworth-Heinemann Series in Chemical Engineering.

Zou, J. Y., & Zhang, D. (2008). Wax Formation from Synthetic Oil Systems and Reservoir Fluids. *Energy&Fuels, 22*(4), 2390-2395.

Zougari, M., & Sopkow, T. (2007). Introduction to Crude Oil Wax Crystallization Kinetics: Process Modeling. *Ind. Eng. Chem. Res., 46*, 1360-1368.

NOMENCLATURE

Symbols

A = cross-sectional area of the producing pipe, L^2

B = formation value factor, dimensionless

C_D = dimensionless concentration, dimensionless

c_p = specific heat, $L^2\theta^{-2}T^{-1}$

D = pipe diameter, L

f = friction factor, dimensionless

g = gravitational acceleration, $L\theta^{-2}$

G' = storage modulus, $ML^{-1}\theta^{-2}$

G'' = loss modulus,

h = specific enthalpy, $L^2\theta^{-2}$

H = volumetric fraction, dimensionless

k = thermal conductivity, $ML\theta^{-3}T^{-1}$

K = flow consistency index

l = distance measured from the surface, L

L = length of the producing pipe, L

$\dot{m}$ = mass rate, $M\theta^{-1}$

Mw = molecular weight, dimensionless

n = flow behavior index

P = pressure, $ML^{-1}\theta^{-2}$

Q = heat-flux rate, $ML^{-1}\theta^{-3}$

r = radius, L

R = solubility ratio, dimensionless

Re = Reynolds number, dimensionless

f = volumetric rate ratio, dimensionless

t = time, θ

T = Temperature, T

T_{wax} = Wax Appareance Temperature, T

T_{pp} = Pour Point Temperature, T

u = volumetric flux, $L\theta^{-1}$

U = overall heat transfer coefficient, $M\theta^{-3}T^{-1}$

v = velocity, $L\theta^{-1}$

$\dot{V}$ = volume rate, $L^3\theta^{-1}$

X = mass fraction, dimensionless

$\overline{X}$ = relative mass fraction, dimensionless

α_G = thermal gradient, $L^{-1}T$

β = fractal dimension, dimensionless

χ = mass fraction, dimensionless

δ = phase angle, degrees

γ = specific gravity, dimensionless

γ = shear strain, dimensionless

$\dot{\gamma}$ = shear rate, θ^{-1}

Γ = interface mass-transfer rate, $ML^{-3}\theta^{-1}$

ε = roughness, L

η = Joule-Thompson coefficient, $M^{-1}L\theta^2T$

η = relaxation in crystallization

η' = dynamic viscosity, $ML^{-1}\theta^{-1}$

N = units of crystallization

φ = pipe angle from the azimuth, degrees

κ = non-equilibrium coefficient, θ^{-1}

λ = slip ratio, dimensionless

μ = viscosity, $ML^{-1}\theta^{-1}$

π = trigonometric constant, dimensionless

Π = degree of entropy

ρ = density, ML^{-3}

θ = relaxation time, θ

τ_y = gel strength, $ML^{-1}\theta^{-2}$

τ_w = wall shear stress, $ML^{-1}\theta^{-2}$

ω = frequency, θ^{-1}

Ω = interface energy-transfer rate, $ML^{-1}\theta^{-3}$

ξ = salinity, ML^{-3}

Ψ = interface momentum-transfer rate, $ML^{-2}\theta^{-2}$

Subscripts

0 = initial

a = air

app = apparent

b = bubble-point

c = critical

D = dimensionless

e = equilibrium

g = gas phase

gel = gelled phase

G = gas pseudo-component

i = ith phase

L = liquid phases

M = Moody

min = minimum

max = maximum

o = oil phase

oil =oil phase

O = oil pseudo-component

od =dead-oil

PPT = Pour-Point Temperature

pc = Pseudo-critical

pr = Pseudo-reduced

R = reservoir

s = surrounding or external

w = water phase

W = water pseudo-component

wh = well-head

Superscripts

0 = initial

E = equilibrium

l = longitudinal direction

r = radial direction

s =standard

APPENDIX A: SUPPORTING EQUATIONS AND CORRELATIONS

The correlations used in this study have been obtained from Lee and Wattenbarger (2004), and Brill and Mukherjee (1999). These correlations are summarized in the following, involving the units, given below.

B_g : [ft^3/scf]	B_o : [bbl/stb]	B_w : [bbl/stb]
c : [$psia^{-1}$]	C_p : [BTU/lbm-ºR]	D : [ft]
Mw : [lbm/lbmol]	P : [psia]	T : [ºR]
R: [scf/stb]	U : [BTU/s-ft^2-ºR]	ρ : [lbm/ft^3]
μ : [cp]	ε : [ft]	ξ : [wt%]

Pseudo-critical Temperature and Pressure. The gas phase is assumed to be free of contaminants. Therefore, the Sutton correlations can be applied.

$$T_{pc} = 169.2 + 349.5\gamma_g - 74.0\gamma_g^2 \quad \text{(A-1)}$$

$$P_{pc} = 756.8 - 131.0\gamma_g - 3.6\gamma_g^2 \quad \text{(A-2)}$$

Pseudo-reduced Temperature and Pressure. These properties are defined as follows:

$$T_{pr} = \frac{T}{T_{pc}} \quad \text{(A-3)}$$

$$P_{pr} = \frac{P}{P_{pc}} \quad \text{(A-4)}$$

Gas compressibility factor. The Dranchuk and Abu-Kassem correlation is used to compute an approximation of the Standing and Katz chart for gas compressibility factor.

$$z = \left(A_1 + \frac{A_2}{T_{pr}} + \frac{A_3}{T_{pr}^3} + \frac{A_4}{T_{pr}^4} + \frac{A_5}{T_{pr}^5} \right) \rho_{pr} + \left(A_6 + \frac{A_7}{T_{pr}} + \frac{A_8}{T_{pr}^2} \right) \rho_{pr}^2$$

$$- A_9 \left(\frac{A_7}{T_{pr}} + \frac{A_8}{T_{pr}^2} \right) \rho_{pr}^5 + A_{10} \left(1 + A_{11} \rho_{pr}^2 \right) \frac{\rho_{pr}^2}{T_{pr}^3} e^{-A_{11} \rho_{pr}^2} + 1 \quad \text{(A-5)}$$

The pseudo-reduced density is given by:

$$\rho_{pr} = 0.27 \frac{P_{pr}}{z T_{pr}} \quad \text{(A-6)}$$

The eleven constants (A_1 to A_{11}) for equation B-5 are defined as follows:

$A_1 = 0.3265$ $A_2 = -1.0700$ $A_3 = -0.5339$ $A_4 = 0.01569$

$A_5 = -0.05165$ $A_6 = 0.5475$ $A_7 = -0.7361$ $A_8 = 0.1844$

$$A_9 = 0.1056 \qquad A_{10} = 0.6134 \qquad A_{11} = 0.7210$$

Note that equation A-5 formulates the gas compressibility factor as an implicit equation. The evaluation of this factor has been done by the Newton-Raphson iteration technique.

Gas formation-volume-factor. The gas formation-volume factor is known as:

$$B_g = 0.0283 \frac{zT}{P} \qquad \text{(A-7)}$$

Gas density. Equation B-8 states the density of a gaseous hydrocarbon:

$$\rho_g = 10.736 \frac{Mw\,P}{zT} \qquad \text{(A-8)}$$

$$Mw = 28.9625 \gamma_g \qquad \text{(A-9)}$$

Gas viscosity. The Lee et al. correlation is used for estimating the gas viscosity.

$$\mu_g = 10^{-4} K_1 e^{X_1 \left(\frac{\rho_g}{62.36} \right)^{Y_1}} \qquad \text{(A-10)}$$

$$K_1 = \frac{(9.379 + 0.01607 Mw) T^{1.5}}{(209.2 + 19.26 Mw + T)} \qquad \text{(A-11)}$$

$$X_1 = 3.448 + \frac{986.4}{T} + 0.01009 Mw \qquad \text{(A-12)}$$

$$Y_1 = 2.447 - 0.2224Mw \quad \text{(A-13)}$$

Gas solubility of saturated oil. The gas solubility (R_b) is estimated at bubble-point conditions using:

$$R_b = \frac{\dot{V}_G^s}{\dot{V}_O^s} \quad \text{(A-14)}$$

API gravity. The API gravity is defined as:

$$\gamma_{API} = \frac{141.5}{\gamma_o} - 131.5 \quad \text{(A-15)}$$

Oil compressibility. The oil compressibility at pressures above the saturation pressure is estimated using the Vasquez-Beggs correlation.

$$c_o = \frac{5R_b + 17.2(T - 460) + 12.61\gamma_{API} - 1433}{10^5 P} \quad \text{(A-16)}$$

Gas solubility in oil. The Standing correlation states that:

$$R_{g/o} = \gamma_g \left[\left(\frac{P}{18.2} + 1.4 \right) 10^{X_2} \right]^{1.2048} \quad \text{(A-17)}$$

$$X_2 = 0.0125\gamma_{API} - 0.00091(T - 460) \quad \text{(A-18)}$$

Saturation Pressure. The bubble-point pressure (P_b) is obtained by solving for pressure in the Standing correlation.

$$P_b = 18.2\left[\left(\frac{R_b}{\gamma_g}\right)^{0.83} 10^{X_2} - 1.4\right] \quad \text{(A-19)}$$

Oil formation-volume-factor. The Standing correlation for saturated oils is used:

$$B_o = 0.0012\left[R_{g/o}\left(\frac{\gamma_o}{\gamma_g}\right)^{0.5} + 1.25(T-460)\right]^{1.2} + 0.9759 \quad \text{(A-20)}$$

The oil formation-volume-factor at above-bubble-point pressures is computed as follows:

$$B_o = B_{o,b} e^{-c_o(P-P_b)} \quad \text{(A-21)}$$

The oil formation-volume-factor at the bubble-point pressure ($B_{o,b}$) is estimated by replacing the gas solubility at bubble-point conditions in Eq. B-20.

Oil Viscosity. The Beggs-Robinson correlation for saturated oils is used:

$$\mu_o = X_3 \mu_{od}^{\ Y_3} \quad \text{(A-22)}$$

$$\log(\log(\mu_{od} + 1)) = 3.0324 - 0.02023\gamma_{API} - 1.163\log(T-460) \quad \text{(A-23)}$$

$$X_3 = 10.715(R_{g/o} + 100)^{-0.515} \quad \text{(A-24)}$$

$$Y_3 = 5.44(R_{g/o} + 150)^{-0.338} \quad \text{(A-25)}$$

The Vasquez-Beggs correlation for under-saturated oils is used:

$$\mu_o = \mu_{o,b}\left(\frac{P}{P_b}\right)^{X_4} \quad \text{(A-26)}$$

$$X_4 = 2.6P^{1.187}e^{-11.513-0.000089P} \quad \text{(A-27)}$$

The oil viscosity at the bubble-point pressure ($\mu_{o,b}$) is estimated by replacing the gas solubility at bubble-point conditions in Eq. B-22.

Gas solubility in water. The Ahmed correlation is used for the gas/water solubility

$$R_{w/o} = \left(K_5 + X_5 P + Y_5 P^2\right) Z_5 \quad \text{(A-28)}$$

$$K_5 = 2.12 + 3.45\times10^{-3}(T-460) + 3.59\times10^{-5}(T-460)^2 \quad \text{(A-29)}$$

$$X_5 = 0.0107 - 5.26\times10^{-5}(T-460) + 1.48\times10^{-7}(T-460)^2 \quad \text{(A-30)}$$

$$Y_5 = -8.75\times10^{-7} + 3.9\times10^{-9}(T-460) + 1.02\times10^{-11}(T-460)^2 \quad \text{(A-31)}$$

$$Z_5 = 1 - \left[0.0753 - 0.000173(T-460)\right]\xi \quad \text{(A-32)}$$

Water viscosity. The water phase is considered to have some level of salinity. Therefore, the McCain correlation is applied.

$$\mu_w = X_6 (T - 460)^{Y_6} K_6 \quad \text{(A-33)}$$

$$X_6 = 109.574 - 8.40564\xi + 0.313314\xi^2 + 8.72213 \times 10^{-3} \xi^3 \quad \text{(A-34)}$$

$$Y_6 = -1.12166 + 2.63951 \times 10^{-2} \xi - 6.79461 \times 10^{-4} \zeta^2 - 5.47119 \times 10^{-5} \xi^3 + 1.55586 \times 10^{-6} \xi^4 \quad \text{(A-35)}$$

$$K_6 = 0.9994 + 4.0295 \times 10^{-5} P + 3.1062 \times 10^{-9} P^2 \quad \text{(A-36)}$$

Water formation-volume-factor. The water formation-volume-factor is computed using the McCain correlation.

$$B_w = (1 + X_7)(1 + Y_7) \quad \text{(A-37)}$$

$$X_7 = -1.00010 \times 10^{-2} + 1.33391 \times 10^{-4} (T - 460) + 5.50654 \times 10^{-7} (T - 460)^2 \quad \text{(A-38)}$$

$$Y_7 = -1.95301 \times 10^{-9} P(T - 460) - 1.72834 \times 10^{-13} P^2 (T - 460) - 3.58922 \times 10^{-7} P - 2.25341 \times 10^{-10} P^2 \quad \text{(A-39)}$$

Specific heat. The Gambill correlation is used for an estimation of the specific heat for hydrocarbon mixtures.

$$C_p = \frac{0.338 + 0.00045(T - 460)}{\sqrt{\gamma_o}} \quad \text{(A-40)}$$

Overall heat transfer. The Shiu and Beggs correlation is used for computing the overall heat transfer for producing pipes.

$$\frac{C_p \dot{m}}{U \pi D} = 0.0149 \dot{m}^{0.5253} (12D)^{-0.2904} \gamma_{API}^{\ 0.2608} \gamma_g^{\ 4.4146} \rho^{2..9303} \quad \text{(A-41)}$$

Friction factor. The explicit approximation for the Colebrook equation developed by Zigrang and Sylvester is used.

$$\frac{1}{\sqrt{f_M}} = -2 \log\left[\frac{2\varepsilon}{3.7D} - \frac{5.02}{\text{Re}} \log\left(\frac{2\varepsilon}{3.7D} + \frac{13}{\text{Re}}\right)\right] \quad \text{(A-42)}$$

After presenting the necessary correlations for calculating the necessary phase and system properties, the following auxiliary definitions required in the computation of gas/oil/brine flow in wells are given. The Reynolds number of the mixture is obtained as follows:

$$\text{Re} = \frac{\rho v D}{\mu} \quad \text{(A-43)}$$

Mixture Viscosity. The mixture viscosity is estimate by simple area-averaging:

$$\mu = H_g \mu_g + H_o \mu_o + H_w \mu_w \quad \text{(A-44)}$$

Volumetric flow rates. The volumetric flow rates are obtained by using the various correlations presented previously and the known flow rates at the surface:

$$\dot{V}_g = (\dot{V}_G^s - R_{g/o}\dot{V}_O^s - R_{g/w}\dot{V}_W^s)B_g \quad \text{(A-45)}$$

$$\dot{V}_o = \dot{V}_O^s B_o \quad \text{(A-46)}$$

$$\dot{V}_w = \dot{V}_W^s B_w \quad \text{(A-47)}$$

APPENDIX B: WAX GELATION IN A CROSS-SECTION

The equation describing the transient gelation occurring over a cross-section without force convection is stated in equation 5-10. This partial differential equation can ben solved numerically by the finite difference method. Several well-known schemes have been developed in order to solve a partial derivative equation involving first and second order derivatives in space (Tannehill, Anderson, & Pletcher, 1997). Some of these schemes are forward in time and central in space, backward in time and central in space, Crank-Nicholson and Modified Gauss-Seidel.

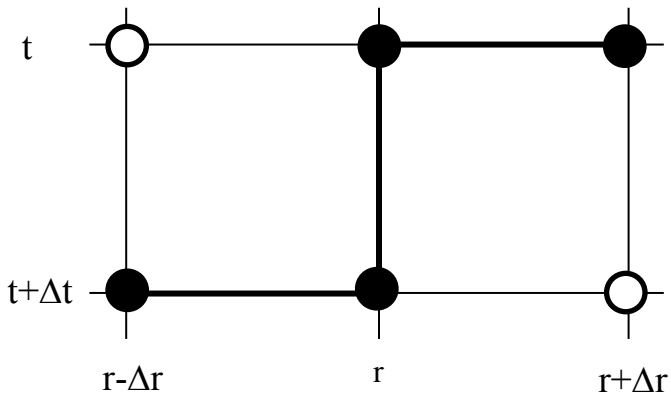

Figure B-1: Stencil of a one-dimensional finite difference

The following finite difference scheme, which is first-order accurate in time and second-order accurate in space, is introduced in this study for numerically computing the transient gelation:

$$\frac{T_r^{t+\Delta t} - T_r^t}{\Delta t} = \frac{k}{\rho c_p} \frac{\left(T_{r+\Delta r}^t - T_{r-\Delta r}^{t+\Delta t}\right)}{2\Delta r} + \frac{k}{\rho c_p} \frac{\left(T_{r+\Delta r}^t - 2T_r^t + T_{r-\Delta r}^{t+\Delta t}\right)}{(\Delta r)^2} \quad \text{(B-1)}$$

where Δt is the time incremental and Δr is radial incremental. The stencil representing this scheme is depicted in figure B-1.

By applying the von Neumann analysis, the error inherent (ψ) in finite difference scheme of equation B-1 can be expressed as:

$$\psi_r^{t+\Delta t} - \psi_r^t = F_1\left(\psi_{r+\Delta r}^t - \psi_{r-\Delta r}^{t+\Delta t}\right) + F_2\left(\psi_{r+\Delta r}^t - 2\psi_r^t + \psi_{r-\Delta r}^{t+\Delta t}\right) \quad \text{(B-2)}$$

$$F_1 = \frac{k\Delta t}{2\rho c_p r \Delta r} \quad \text{(B-3)}$$

$$F_2 = \frac{k\Delta t}{\rho c_p (\Delta r)^2} \quad \text{(B-4)}$$

where F_1 and F_2 are factors in the error propagation. Then, the error propagation is defined as the complex number:

$$\psi_r^t = e^{\alpha \Delta t} e^{\beta r i} \quad \text{(B-5)}$$

where α is a complex parameter and β_r is angle corresponding to the error propagation after using Fourier analysis (Tannehill, Anderson, & Pletcher, 1997). By combining equations B-2 and B-5 with Euler's identity, it can be readily shown that the amplification factor is:

$$e^{\alpha \Delta t} = \frac{\left[1 - 2F_2 + (F_2 + F_1)\cos\beta_r\right] + \left[(F_2 + F_1)\sin\beta_r\right] i}{\left[1 - (F_2 - F_1)\cos\beta_r\right] + \left[(F_2 - F_1)\sin\beta_r\right] i} \quad \text{(B-6)}$$

Consequently, the stability criterion according to the von Neumann analysis is given by:

$$\left\| \frac{\left[1 - 2F_2 + (F_2 + F_1)\cos\beta_r\right] + \left[(F_2 + F_1)\sin\beta_r\right]i}{\left[1 - (F_2 - F_1)\cos\beta_r\right] + \left[(F_2 - F_1)\sin\beta_r\right]i} \right\| \leq 1 \quad \text{(B-7)}$$

Since the amplification factor is a ratio of complex numbers, no direct solution has been found. However, the sufficient stability conditions can be often inferred from numerical calculations (Tannehill, Anderson, & Pletcher, 1997). The amplification factor yields a constant value of equal to the unity for all F_1 and F_2 when β_r takes a zero value. Other values of β_r present the same stability conditions. Some examples of computing the amplification factor dependent on the values of F_1 and F_2 are shown in figures B-2 to B-5.

It is inferred by inspection of several numerical calculations that there is a sufficient stability condition in the form of:

$$(F_1 + F_2 - 1)F_2 \leq 0 \quad \text{(B-8)}$$

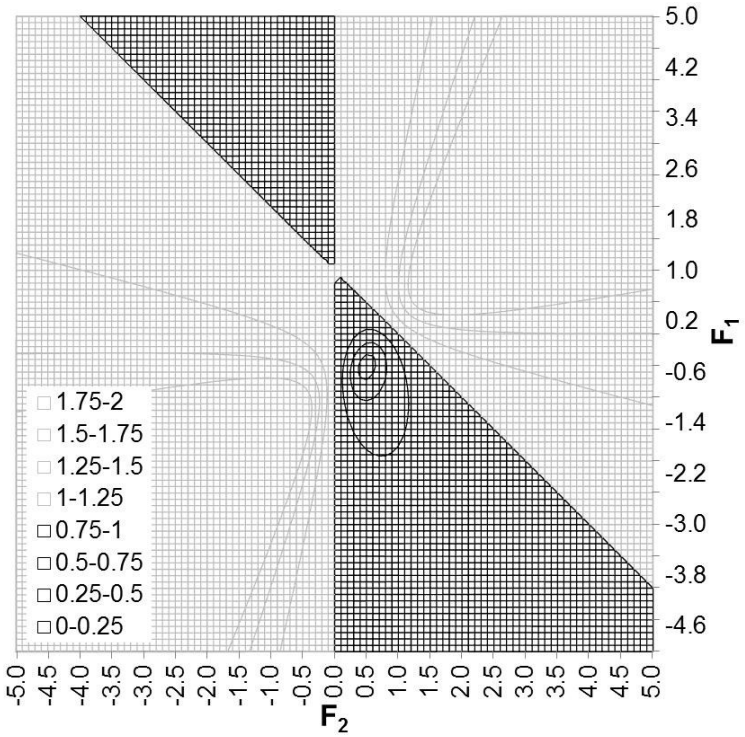

Figure B-2: Amplification factor for $\beta_r = \pi/4$ and $\beta_r = -\pi/4$

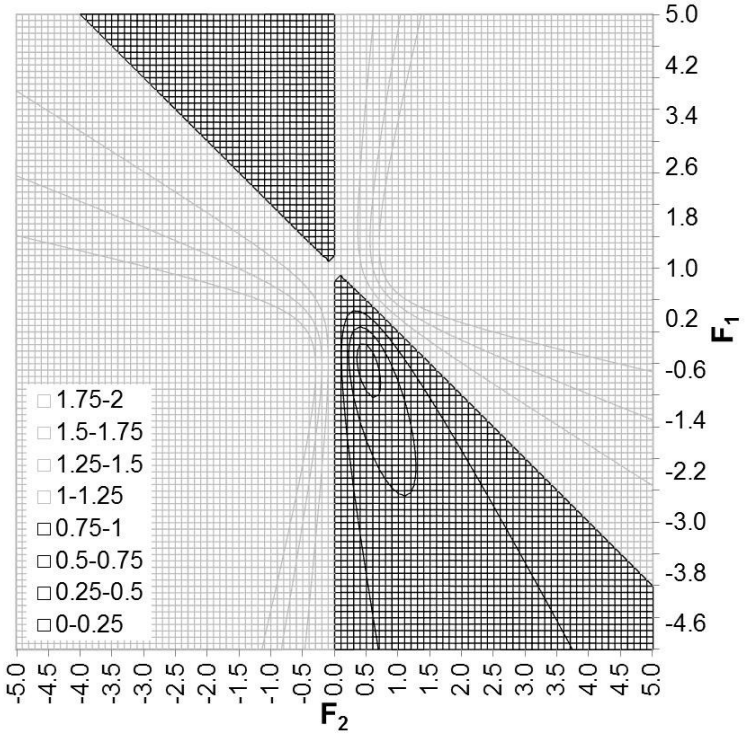

Figure B-3: Amplification factor for $\beta_r = \pi/2$ and $\beta_r = -\pi/2$

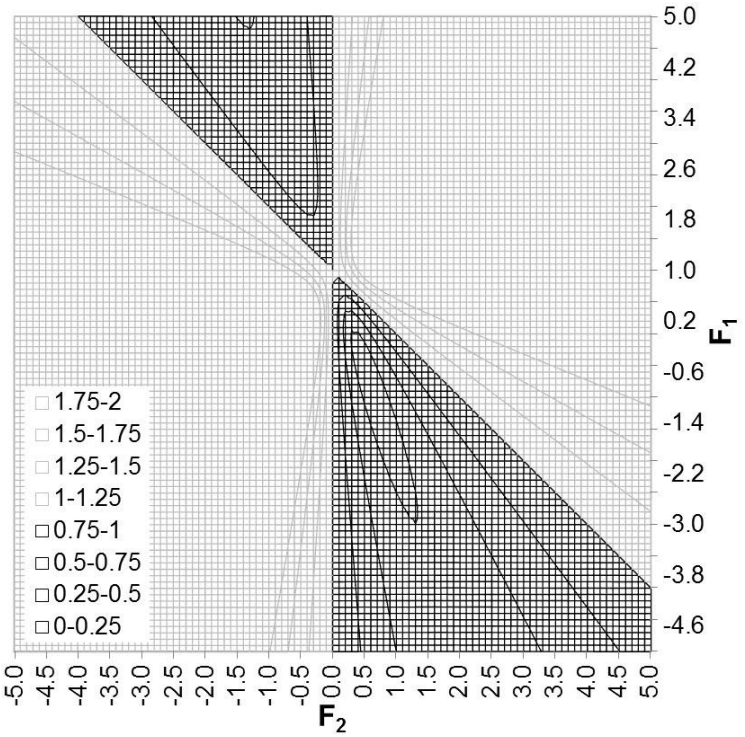

Figure B-4: Amplification factor for $\beta_r = 3\pi/4$ and $\beta_r = -3\pi/4$

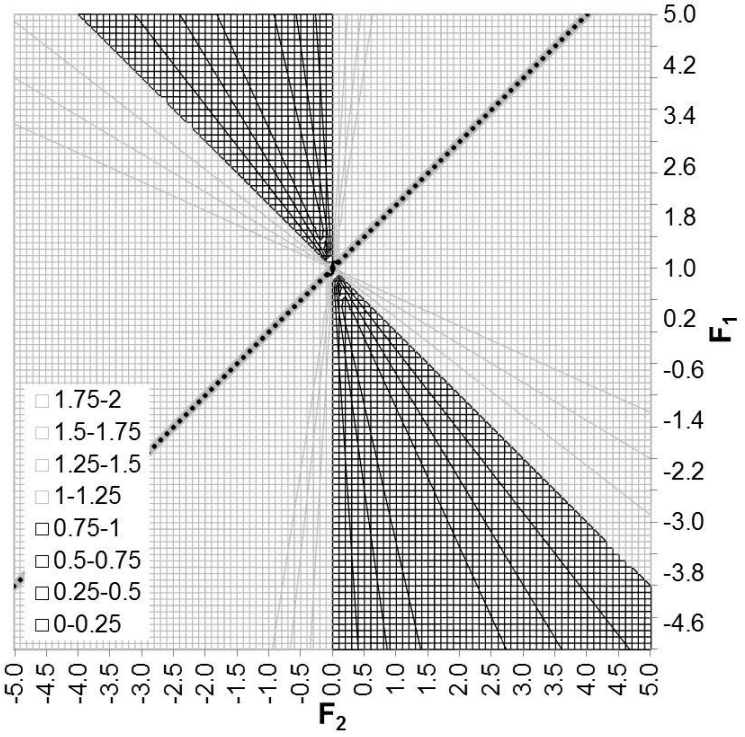

Figure B-5: Amplification factor for $\beta_r = \pi$ and $\beta_r = -\pi$

During the finite difference calculations of equation B-1 the factor F_1 attains its maximum value when r is equal to Δr. Therefore, this case is taken in account since it is needed to insure no instance of the factor F_1 violates the stability criterion during calculations. For this purpose, the factors F_1 and F_2 are related as follows:

$$F_1 = \tfrac{1}{2} F_2 \qquad \text{(B-9)}$$

Combining equations B-4, B-8 and B-9, the stability condition in terms of time incremental, radial incremental and relevant fluid properties is obtained:

$$\frac{\Delta t}{(\Delta r)^2} \leq \frac{2}{3} \frac{\rho c_p}{k} \qquad \text{(B-10)}$$

Since the fluid properties of equation B-10 are always positive, the stability criterion applies for all positive time incremental, radial incremental and radius.

APPENDIX C: INITIAL TEMPERATURE PROFILE AFTER SHUT-IN

The following general solution (Bird, Stewart, & Lightfoot, 1965) for equation 5-26 can be used a substitute for the proper Bessel function:

$$\Theta = c_0\zeta + \Phi(\varsigma) \quad \text{(C-1)}$$

Here, Φ is an auxiliary function and c_0 is a constant. Now, an analytical solution is formulated by applying equation C-1 into equation 5-26 and then integrating twice subject to the conditions specified in equations 5-27 to 5-29:

$$\Theta = c_0\zeta + \frac{Gz}{4}c_0\varsigma^2 + 1 \quad \text{(C-2)}$$

$$c_0 = -\frac{Bi}{\frac{Bi}{2} + \frac{Gz}{2} + \frac{BiGz}{4}} \quad \text{(C-3)}$$

Note that, the value of c_0 has been solved in equation C-3 for constant sea-water temperature. However, in reality, the sea-water temperature is not constant for all depths. Thus, the solution technoque is facilitated for submarine pipelines as described in the following. First, a dimensionless temperature is defined as:

$$\Theta = \frac{T - T_s}{T_{0,0} - \overline{T_s}} \quad \text{(C-4)}$$

where $\overline{T_s}$ is the average sea-water temperature. Then, the constant c_0 is redefining as:

$$c_0 = -\frac{2}{L}\frac{Bi}{Gz}\int_0^L \frac{T\big|_{r=R} - T_s}{T_{0,0} - \overline{T_s}}\,dl \qquad \text{(C-5)}$$

Now, the following iterative procedure is applied to generate a numerical solution for variable sea water temperature:

1. Calculate the average of the known sea-water temperature profile.

2. Calculate an initial guess for c_0 by using equation C-3.

3. Generate a temperature profile of the wall temperature by applying equation C-2 along with equations 5-31 and C-4. Use the proper sea-water temperature introduced at each depth. Use the guessed for c_0 and a value of $\varsigma = 1$.

4. Calculate an updated value of c_0 by performing the integration stated in equation C-5 numerically.

5. Calculate the new approximation of c_0 by averaging the guessed value and the value obtained in step 4.

6. If the difference between the guessed value and the new approximation calculated in steps 5 is greater than an acceptable error then repeat steps 3-5 using the new approximation as the guess for c_0. Else, accept the value calculated in step 5 as the solution for c_0.

7. Generate a temperature profile over the depth of interest by using equation C-2 together with equations 5-31, 5-32, and C-4. Use the chosen approximation for c_0 and the proper sea-water temperature at each depth.

This technique ensures that all the heat lost due to cooling of the fluid inside the pipe is equal to the heat transfer towards the sea environment across the pipe wall.

APPENDIX D: WAX GELATION IN A SUBMARINE VERTICAL PIPE

Since the finite difference method presented for a cross-section successfully represented the transient gelation behavior of experimental data, this scheme is extended to two dimensions in space. The equation describing the transient gelation occurring over a shut-in vertical pipe is stated in equation 5-14. Following the scheme of Appendix B, equation 5-14 is numerically computed as:

$$\frac{T_{r,l}^{t+\Delta t}-T_{r,l}^{t}}{\Delta t}=\frac{k}{\rho c_p}\frac{\left(T_{r+\Delta r,l}^{t}-T_{r-\Delta r,l}^{t+\Delta t}\right)}{2\Delta r}+\frac{k}{\rho c_p}\frac{\left(T_{r+\Delta r,l}^{t}-2T_{r,l}^{t}+T_{r-\Delta r,l}^{t+\Delta t}\right)}{(\Delta r)^2}+\frac{k}{\rho c_p}\frac{\left(T_{r,l+\Delta l}^{t}-2T_{r,l}^{t}+T_{r,l-\Delta l}^{t+\Delta t}\right)}{(\Delta l)^2} \quad \text{(D-1)}$$

where Δl is the length incremental. The stencil representing this scheme is depicted in figure D-1.

The error inherent in the current finite difference scheme can be expressed as:

$$\psi_{r,l}^{t+\Delta t}-\psi_{r,l}^{t}=F_1\left(\psi_{r+\Delta r,l}^{t}-\psi_{r-\Delta r,l}^{t+\Delta t}\right)+F_2\left(\psi_{r+\Delta r,l}^{t}-2\psi_{r,l}^{t}+\psi_{r-\Delta r,l}^{t+\Delta t}\right)+F_3\left(\psi_{r,l+\Delta L}^{t}-2\psi_{r,l}^{t}+\psi_{r,l-\Delta l}^{t+\Delta t}\right) \quad \text{(D-2)}$$

$$F_3=\frac{k\Delta t}{\rho c_p(\Delta l)^2} \quad \text{(D-3)}$$

where F_3 is another factors in the error propagation. Here, the error propagation is defined as the complex number:

$$\psi_{r,l}^{t} = e^{\alpha \Delta t} e^{\beta r\, i} e^{\beta l\, i} \quad \text{(D-4)}$$

Similar to the procedure described in the previous section, the stability criterion is derived as:

$$\left\| \frac{\left[1 - 2(F_2 + F_3) + (F_2 + F_1)\cos\beta_r + F_3 \cos\beta_l\right] + \left[(F_2 + F_1)\sin\beta_r + F_3 \sin\beta_l\right] i}{\left[1 - (F_2 - F_1)\cos\beta_r - F_3 \cos\beta_l\right] + \left[(F_2 - F_1)\sin\beta_r + F_3 \sin\beta_l\right] i} \right\| \leq 1 \quad \text{(D-5)}$$

For the special case when F_1 attains its maximum value, equation B-9 can be introduced in order to simplify the stability criterion.

$$\left\| \frac{\left[1 - 2(F_2 + F_3) + \frac{3}{2} F_2 \cos\beta_r + F_3 \cos\beta_l\right] + \left[\frac{3}{2} F_2 \sin\beta_r + F_3 \sin\beta_l\right] i}{\left[1 - \frac{1}{2} F_2 \cos\beta_r - F_3 \cos\beta_l\right] + \left[\frac{1}{2} F_2 \sin\beta_r + F_3 \sin\beta_l\right] i} \right\| \leq 1 \quad \text{(D-6)}$$

Now, the amplification factor can be computed dependent on the values of F_2 and F_3 for several values of β_r and β_l. When β_r and β_l take a zero value, the amplification factor yields a constant value of equal to the unity for all F_1, F_2 and F_3. Other values of β_r and β_l present different stability conditions but share a common region of stability. Some examples of computing the amplification factor dependent on the values of F_2 and F_3 are shown in figures D-2 to D-6 where the common region of stability has been emphasized.

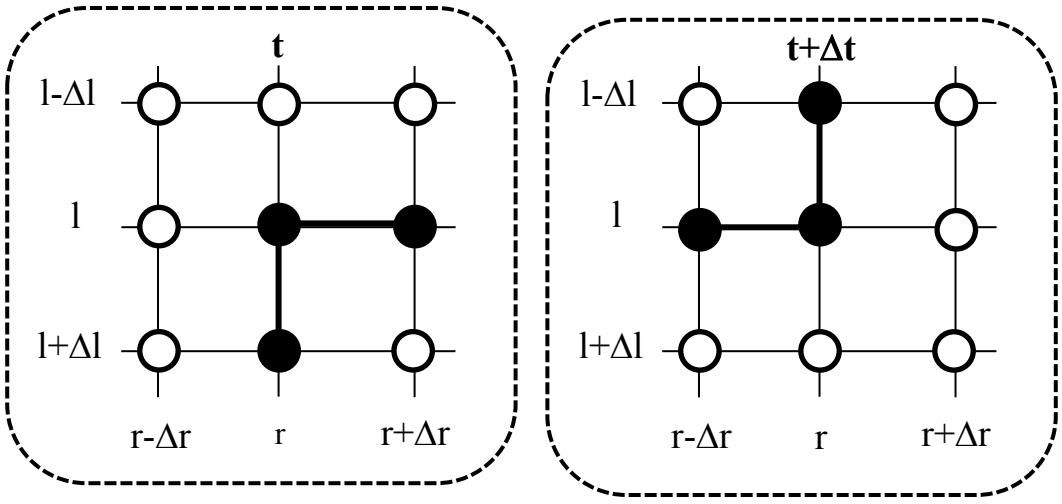

Figure D-1: Stencil of a two-dimensional finite difference

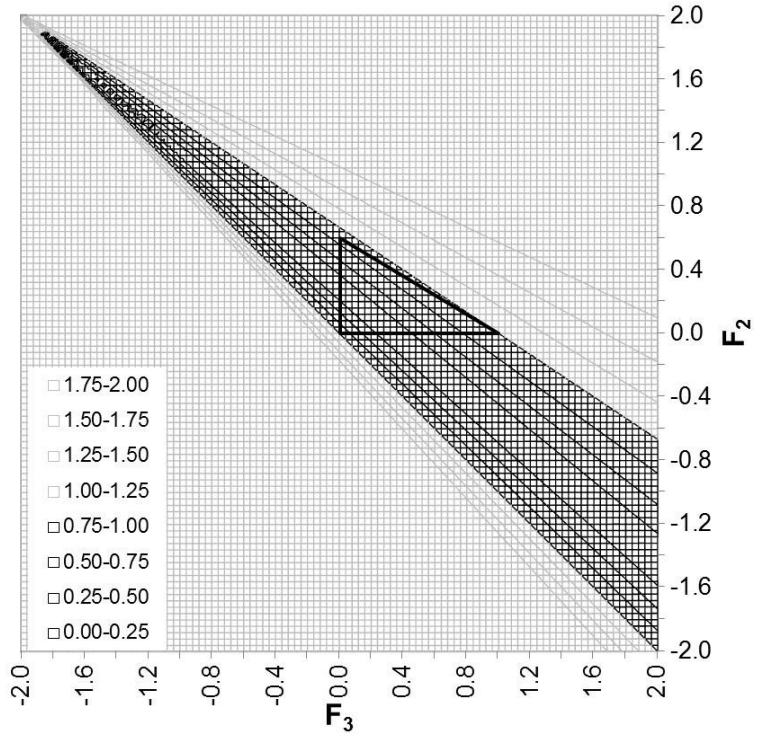

Figure D-2: Amplification factor for the pairs (β_r, β_l) = [(π, π), (π, -π), (-π, π), (-π, -π)]

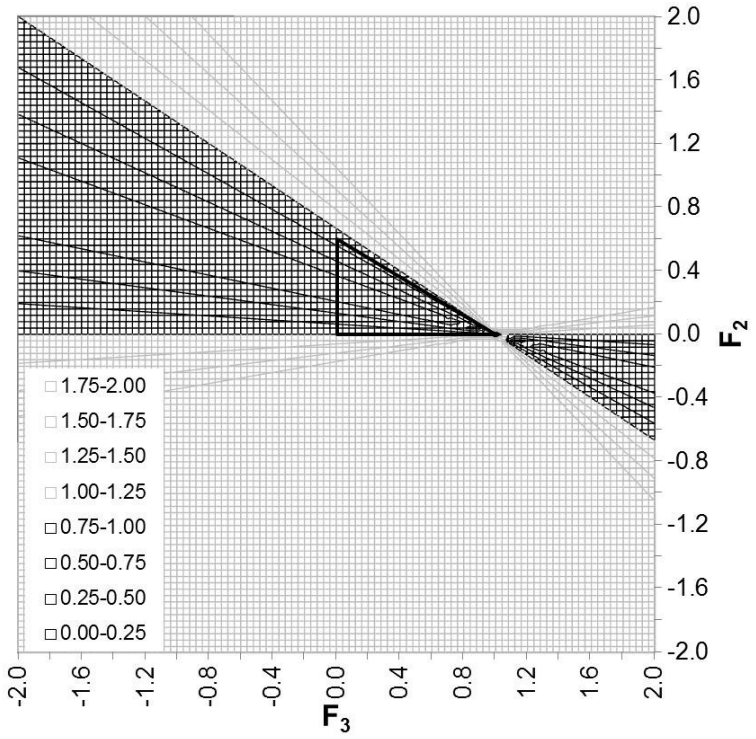

Figure D-3: Amplification factor for the pairs (β_r, β_l) = [(π, 0), (-π, 0)]

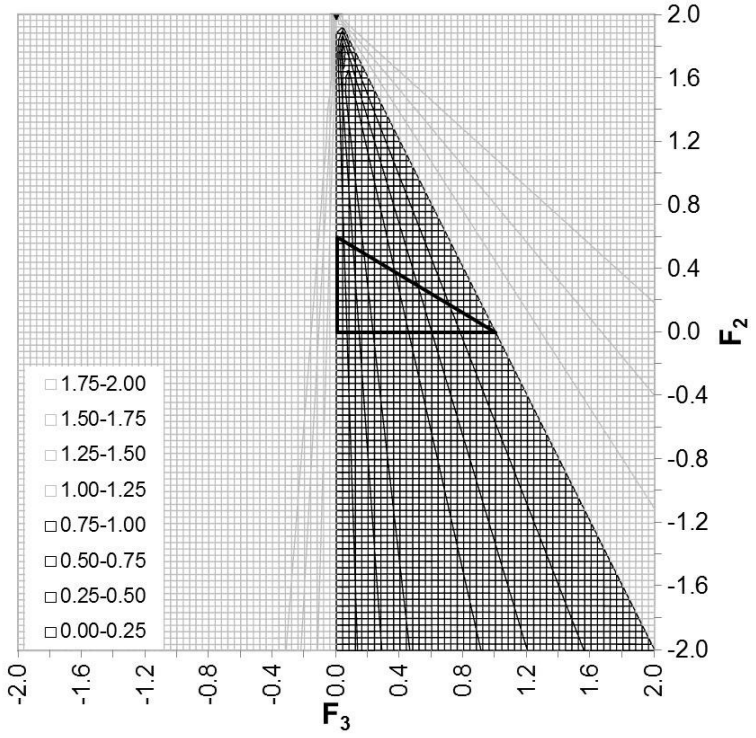

Figure D-4: Amplification factor for the pairs (β_r, β_l) = [(0,π), (0,-π)]

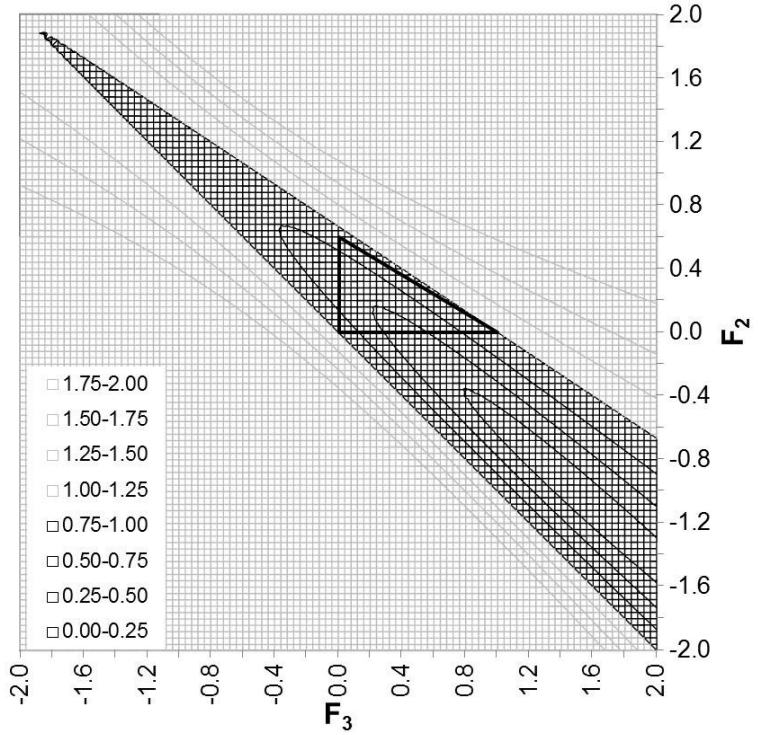

Figure D-5: Amplification factor for the pairs (β_r, β_l) = [(π/2, π/2), (-π/2,-π/2)]

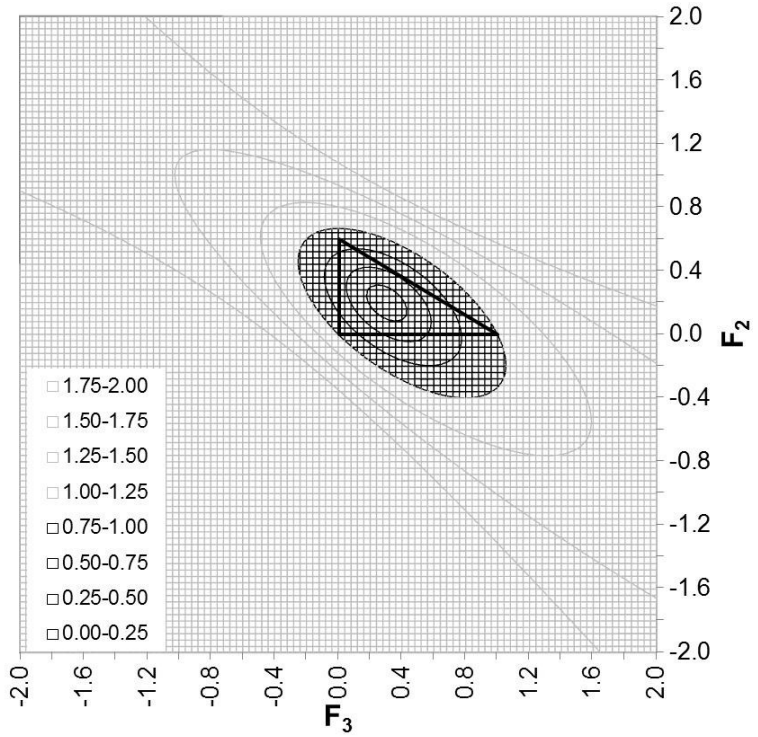

Figure D-6: Amplification factor for the pairs (β_r, β_l) = [(π/2, -π/2), (-π/2,π/2)]

It is inferred by inspection of several numerical calculations that there is a sufficient stability condition in the form of:

$$F_2 + 0.6F_3 - 0.6 \le 0 \quad for \quad F_2 > 0 \; and \; F_3 > 0 \qquad \text{(D-7)}$$

Combining equations B-4, D-3 and D-7, the stability condition in terms of time incremental, radial incremental and relevant fluid properties is obtained:

$$\Delta t\left(\frac{1}{(\Delta r)^2} + \frac{0.6}{(\Delta l)^2}\right) \le 0.6\frac{\rho c_p}{k} \qquad \text{(D-8)}$$

Since the fluid properties of equation D-8 are always positive, the stability criterion applies for all length incremental and all positive time incremental, radial incremental and radius.